

NASA Contractor Report 185239

LEWIS GRANT
IN-35
3459

Comparison of UNL Laser Imaging and Sizing System and a Phase Doppler System for Analyzing Sprays From a NASA Nozzle

(NASA-CR-185239) COMPARISON OF UNL LASER
IMAGING AND SIZING SYSTEM AND A PHASE
DOPPLER SYSTEM FOR ANALYZING SPRAYS FROM A
NASA NOZZLE Final Report (Nebraska Univ.)
134 p

N71-21485

Unclass

CSCL 14B G3/35 0003459

Dennis R. Alexander
University of Nebraska-Lincoln
Lincoln, Nebraska

March 1990

Prepared for
Lewis Research Center
Under Grant NAG3-634



National Aeronautics and
Space Administration

Contents

1	INTRODUCTION	1
2	EXPERIMENTAL APPARATUS AND PROCEDURE	3
2.1	P/DPA	3
2.2	Laser Imaging/Video Processing System	7
2.2.1	Components	7
2.2.2	Sizing Method: Segmentation	11
2.2.3	Calibration	13
2.2.4	Focus Method	15
2.2.5	Modifications	20
2.2.6	Software Updates	22
2.3	Spray Test Facility	22
2.3.1	MOD-1 Nozzle	29
2.3.2	Air and Water Supply System (AWSS)	29
2.3.3	Water Flowmeter Calibration	29
2.4	Digital Pressure Acquisition	29
2.4.1	Pressure Transducers	32
2.4.2	A/D converter board	32
2.4.3	Analog-to-Digital Conversion	32
2.4.4	Digital Pressure System Calibration	32
2.5	Experimental Procedure	32
2.5.1	Verification Tests	35
2.5.2	Spray Comparison	38
3	PRESENTATION AND DISCUSSION OF RESULTS	39
3.1	LI/VPS Calibration Results	39
3.2	Results For the MOD-1 Nozzle Comparison	47
3.2.1	Discussion of Results for Comparison - CASE I	86
3.2.2	Discussion of Results for Comparison - CASE II	86
4	CONCLUSIONS AND RECOMMENDATIONS	93
4.1	LI/VPS	93
4.2	LI/VPS and P/DPA Comparison	93
4.3	Suggestions and Recommendation for Future Work	94
5	REFERENCES	96
6	APPENDIX A: EQUIPMENT LISTING	98

7	APPENDIX B Design and Implementation of the PSP Laser Trigger	100
8	APPENDIX C.1: PSP Set-up Program	103
9	APPENDIX C.2: PSP Graphical Presentation of Results	114
10	APPENDIX C.3: MOD-1 Nozzle Input Pressure Determination	122
11	APPENDIX C.4: PSP Magnification Correction Factor Determination	124
12	APPENDIX D: Mean Diameter Calculations	126
13	APPENDIX E: Cole-Palmer Flowmeter Calibration Data	127
14	APPENDIX F: OMEGA Pressure Transducer Calibration Data	129

NOMENCLATURE

Symbol	Description
A/D	Analog to Digital
AMD	Arithmetic mean diameter
CPM	Continuous pulse mode
D(10)	Arithmetic mean diameter
D(20)	Area mean diameter
D(30)	Volume mean diameter
D(32)	Sauter mean diameter
D_d	Drop diameter
D_b	Drop diameter at background
f	Disturbance frequency
GL	Gray level
λ	Wavelength
MAGL	Measured average gray level
PBG	Particle boundary gradient
ϕ	Relative phase shift associated with P/DPA signals
PSP	Particle sizing program
q	Liquid flow-rate
SD	Standard deviation
SMD	Sauter mean diameter
SPM	Single pulse mode
T	Image threshold
T_b	Image threshold just above background
\vec{v}	Droplet velocity vector

Section 1

INTRODUCTION

Spray characterization is essential in many technologies. Improved cloud simulation for icing studies, increased efficiency for combustion technology, and design optimization of applicator nozzles for industry and agriculture are only a few areas which benefit from accurate spray measurements. The lack of a universally accepted calibration/verification standard and operating characteristics of sizing instrumentation has left the questions of accuracy and repeatability in spray measurements unanswered. Recently, various groups (e.g., ASTM Subcommittee E29.04 on Characterization of Liquid Particles, 1986 Droplet Technology Workshop, etc.) have addressed the question of accuracy and calibration in drop-size instrumentation, however no agreement has been reached with regard to methods or apparatus for standardizing drop-size measurement instruments [1]. The following work involves the evaluation of two instruments based on different drop-sizing techniques in side-by-side benchmark tests under identical operating conditions.

The non-intrusive nature of laser/optical techniques have shown the most promise in spray characterization. Of the three major types of laser/optical techniques (i.e., imaging, doppler anemometry, and laser-diffraction), the laser-diffraction method is most widely used, and probably the best known system is the Malvern instrument [2]. Doppler anemometry, however, is receiving more attention due to the recent development of Aerometric's P/DPA, which has an increased sizing range (35:1) [3,4], in comparison to the (10:1) range for visibility dependent Doppler anemometers [5]. With the use of real-time digital image processing to perform focus discrimination without correction, the University of Nebraska - Lincoln (UNL) laser imaging system [6-10] has shown the capability for true volumetric analysis. Previously, imaging systems, e.g., Weiss et al. [11], and others, have used depth of field corrections based on the maximum measured drop-size to "back-out" the number of smaller particles in a normalized volume. Processing time can be saved using this method, however the assumptions may lead to errors in obtaining accurate size characteristics. The above techniques vary in several areas; 1) sampling method (e.g., spatial vs. temporal), 2) probe volume (e.g., line of sight averaging, crossed beams, vs. focus volume), 3) instrument drop-size range and resolution, and 4) calibration and/or verification (e.g., reticles, monodisperse droplets, or polydispersions). Similarities shared by the imaging technique and the laser-diffraction method are that both are spatial sampling methods which allows for similar calibration (i.e., calibration reticle [7,12]). The similarity in probe volume of Doppler anemometers and imaging systems allow for verification and comparison with minimal correction. In this work, a P/DPA and a laser imaging system were evaluated by concurrently performing a set of baseline benchmark tests.

According to Tishkoff [13], chairman of ASTM Subcommittee E29.04 on Characterization of Liquid Particles, the four major areas of concern in spray characterization are instrumentation, sampling, data processing, and terminology. In the following work, the emphasis of the evaluation was placed on instrumentation (i.e., the setup and operation of the P/DPA, a temporal sampling

instrument in ideal conditions, and the UNL laser imaging system, a true spatial sampling instrument). The difference in data acquisition or sampling method was minimized by overlapping the probe volumes of the two systems [14] and analyzing a spray under steady-state conditions (i.e., spray characteristics remain constant with respect to time). Data processing and terminology of the two systems closely follow the standard practices established by ASTM [15]. Taking into account the above criteria, the comparison of the P/DPA and the UNL laser imaging system was accomplished with minimal reduction of drop-size data.

The comparison of the P/DPA and the UNL laser imaging system is discussed in the following order; 1) experimental apparatus including the droplet sizing instruments, 2) procedure and operating conditions for the benchmark tests, 3) results obtained from the benchmark tests, and 4) conclusions as to the operation, data representation, and comparability of the two instruments.

Section 2

EXPERIMENTAL APPARATUS AND PROCEDURE

The apparatus, used in the benchmark tests, consisted of a P/DPA [3,4], a laser imaging/video processing system (LI/VPS) [6-10], a MOD-1 nozzle [16], air and water supply systems (AWSS), and the measurement instrumentation used to monitor the operating conditions of the nozzle. Verification tests were performed using a Berglund-Liu vibrating orifice aerosol generator (VOAG) [17,18]. Operating conditions of the tested apparatus and the setup parameters for the sizing instruments are detailed.

2.1 P/DPA

Phase/Doppler Particle Analyzer theory and operation are described by Bachalo et al. in several references [3,4], therefore, only a brief description of the P/DPA components and operation follows. Setup features specific to this research are detailed with special attention given to the selection of appropriate photo-multiplier tube (PMT) gain voltage.

The P/DPA is a crossed beam laser Doppler anemometer (Fig. 2.1). The P/DPA transmitter utilizes a 10 mW He-Ne laser. The transmitter beam is split and the resulting beams are focused to a point by a convex lens. The Doppler fringes, formed at the crossed beam intersection, are relayed to the P/DPA receiver by the refracted light from a droplet passing through the crossed beam intersection. The P/DPA receiver uses a pair of convex lens to collect and focus the Doppler fringes from the passing droplet onto three PMTs, aligned parallel to the droplet's velocity vector (\vec{v}). The PMT voltages are filtered and amplified to remove the pedestal component of the burst and increase the differentiation of Doppler frequencies in the signal (Fig. 2.2). Particle size measurements are determined from the phase shift in the filtered Doppler signal.

Velocity measurements are taken identically to the laser Doppler velocimeter, but the P/DPA is very distinct in its method of particle size measurement. Bachalo et al. [4] have shown droplet size (D_d) to be dependent on the relative phase shift (ϕ) associated with a Doppler signal incident on two adjacent PMTs.

With the operating conditions of the VOAG and the MOD-1 nozzle varying, the P/DPA also required adjustment in operating parameters. The following is a brief summary of the P/DPA setup parameters (Fig. 2.3). Parameters (A) and (B) are specified for the transmitter laser supplied by the manufacturer, and do not require adjustment. Hardware parameters of the P/DPA fixed for the duration of this work, specified according to reference [19], were; (E) the focal length of the transmitter lens used, was 495 μm for a measurable size range of 1 to 300 micrometers (μm), (F) the receiver was positioned 30° off the forward axis of the transmitter for sizing water droplets, (G) the refractive index was set for water, and (T) the Direct Memory Access (DMA), which allows for the storage of approximately 16,000 concurrent raw PMT signals for processing, was switched off

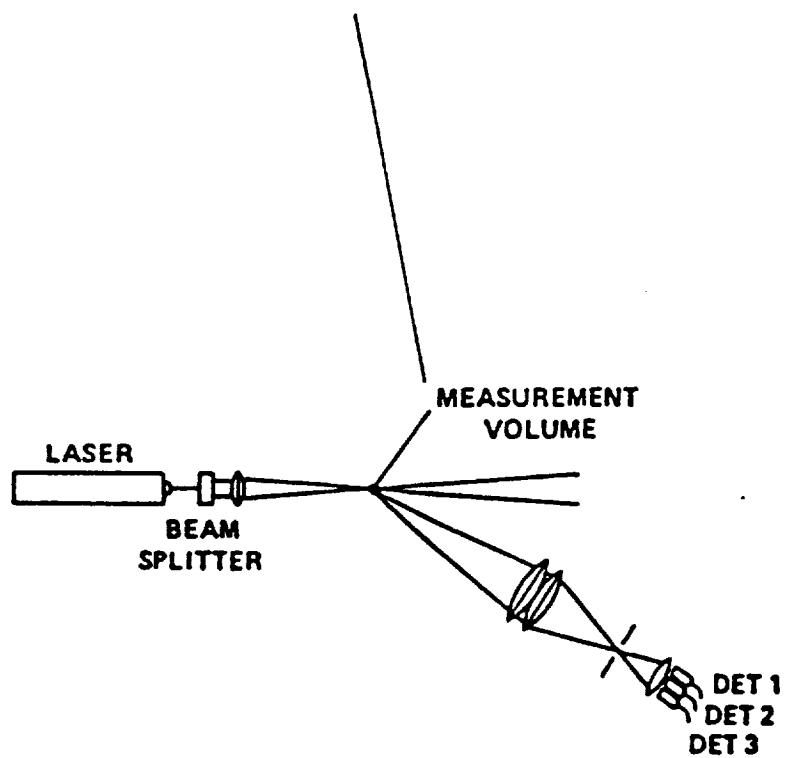
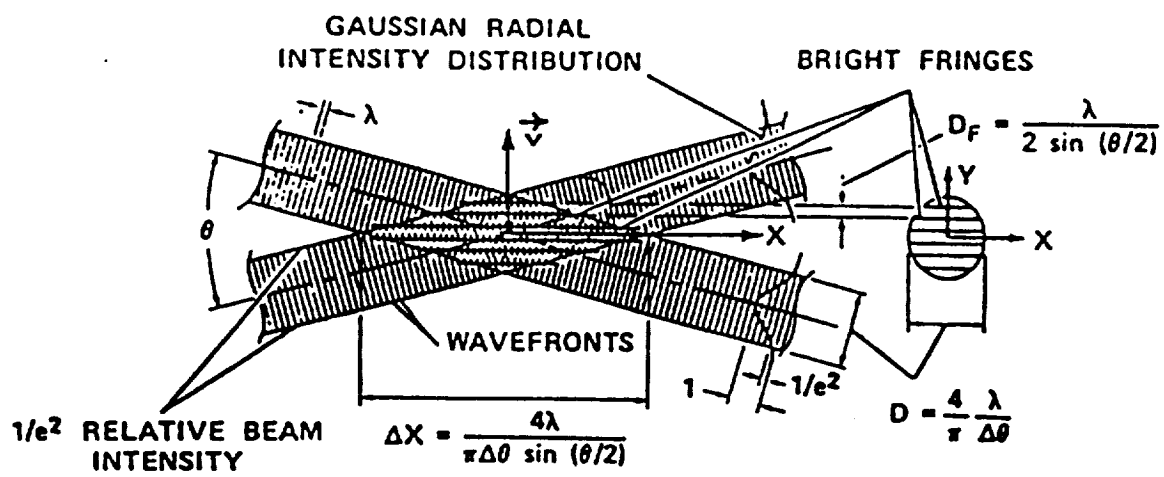
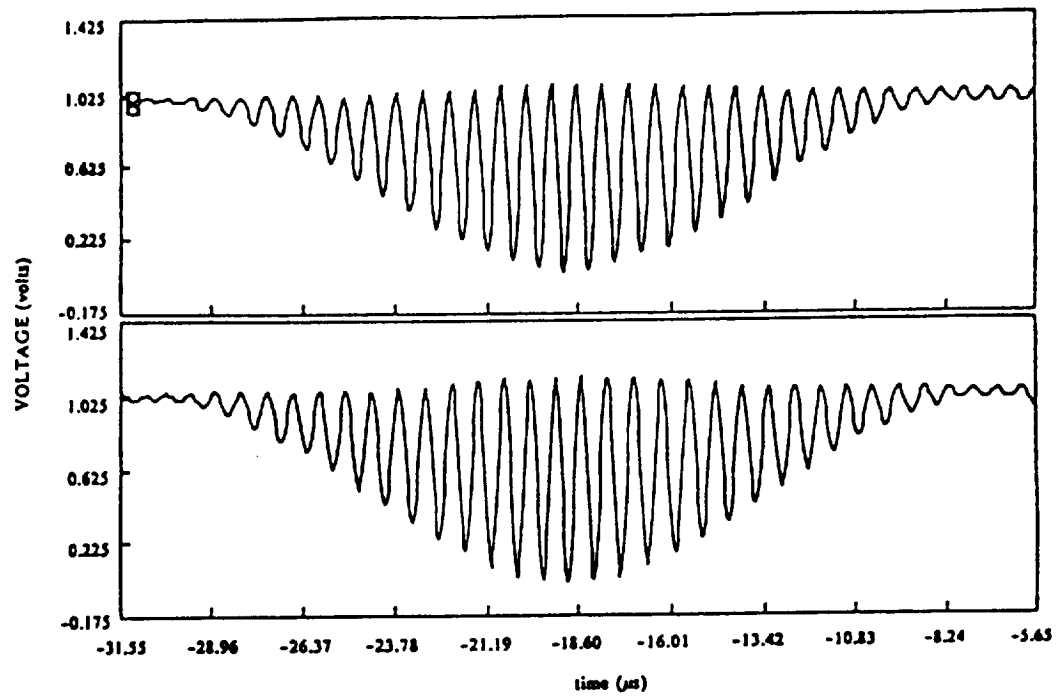
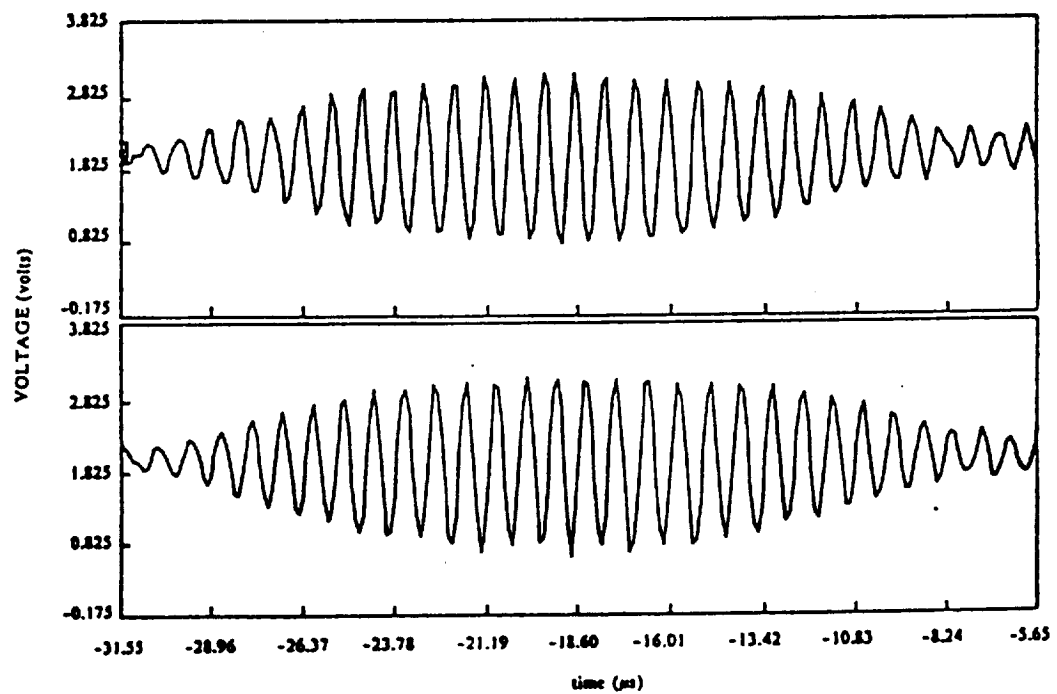


Figure 2.1: Phase Doppler/Particle Analyzer



a. - Doppler Burst Signal from First Two PMTs.



b. - Doppler Signals Filtered and Amplified.

Figure 2.2: P/DPA PMT Signals

```

(A) Wavelength= .6328 μm
(B) Beam Dia. = 2.5 mm
(D) Beam Sep. = 12.5
(E) Xmit Lens = 495 mm
(F) Coll.Angle= 30 deg
(G) Refrc Indx= 1.33
(J) Size Max = 98 μm
(Q) Velo Max = 7.7 m/s
(R) Stop Mode = Samples
(S) MaxSamples= 10000
(T) DMA = OFF
(U) Data Drive= A
(V) Filename = TEMP
(W) Filenumber= 1

(L) High Volt = 300 volts
-----
Current File = A:TEMP_01.DAT      Size Span = 2.8- 360 μm
Beam Spacing = 12.5 mm           Size Range= 2.8- 98 μm
Fringe Spacing= 25 μm
Beam Focus Dia= 159 μm
Nom Cycle Cnt = 6.3
4 < Cycles < 19
Velocity Span = 2.41 - 7.7 m/s
Velocity Range= 2.41 - 7.7 m/s

Parameter to change or <CR> to exit

```

Figure 2.3: P/DPA Setup Page

to facilitate the comparison with the LI/VPS. For this research, the beam separation, parameter (D), was alternated between 25 and 12.5 mm for the different spray size distributions generated (i.e., the beam separation and the transmitter lens' focal length specify the fringe spacing and number in the probe volume which, in turn, specifies a range of allowable drop-sizes to be measured). Other parameters, such as; (N) and (M) the high pass filter setting, (L) PMT voltage, (J) size, and (Q) velocity ranges are set according to the specific operating conditions droplet density, size distribution, etc.) of the VOAG or MOD-1 nozzle. The high pass filter allows only those Doppler signals with a frequency above a preset limit to pass on for further processing. The high pass filter setting is dependent on the average droplet velocity, and can be set by studying the count vs. velocity distribution. The selection of a high pass filter can be fine-tuned by using an oscilloscope to monitor the filtered PMTs for uniform signals with minimal distortion. The previous parameters are discussed in detail in the P/DPA operating manual.

The PMT gain voltage was to be set at a point just prior to PMT saturation. The above was accomplished by studying the saturation lights connected to each PMT. The saturation lights were to flash intermittently 50% of the time which implied approximately 1% saturation. Following the above procedure in performing an analysis on a high density spray, an inordinate number of large drops showed up in the analysis (Fig. 2.4). The large drops were determined to be false by concurrent studies by the LI/VPS and previous studies by NASA on the tested nozzle. According to Bachalo [20], the false drops were reflections or echoes in the PMTs caused by the high density of the spray, therefore, the PMT voltage should be set by stepping through the PMT voltage range (i.e., approximately 275 to 475 volts), and studying the number vs. size distribution for a point where little change occurs in the distribution shape (Fig. 2.5).

2.2 Laser Imaging/Video Processing System

The basic architecture of the LI/VPS has been described in detail by Ahlers and Alexander [8,9]. Ahlers [7] performed an analysis on static particles (e.g., polystyrene microspheres) situated in the plane of focus of the imaging optics. Further work by Wiles [10] described a technique for focus classification without depth of field corrections. The implementation of a particle sizing system capable of performing analysis on aerosol sprays has been the focus of the current research program. The following discussion is divided into sections covering: 1) components and operation, 2) drop sizing method, 3) calibration technique to minimize uncertainty due to camera tube non-linearities, 4) focus criteria, 5) modifications for dynamic measurements, and 6) software updates.

2.2.1 Components

The LI/VPS is divided into two subsystems, a laser imaging device and a video processor. The laser imaging device (Fig. 2.6) components are: a COHU camera system (control unit and camera), a Laser Energy Inc. (LEI) laser system (power supply unit and laser), a Laser Holography Inc. (LHI) control system (sync circuit and laser control unit), the imaging optics, a Panasonic NV-8950 or RCA VET650 VCR, a Panasonic TQ-2023 (A) laser/optical memory disk recorder (LDR), a Panasonic WJ-180 time/date generator, a Sony Trinitron monitor, a Sanyo monitor, and a back-up Molelectron UV Series II Model UV12 (MUV12) N₂ laser. The video processor (Fig. 2.7) consists of a Recognition Concepts Inc. (RCI) Trapix 55/32 real-time image processor, a PDP 11/73 computer for control, and the processing software. A LSI-11/03 computer is also available for utility processing.

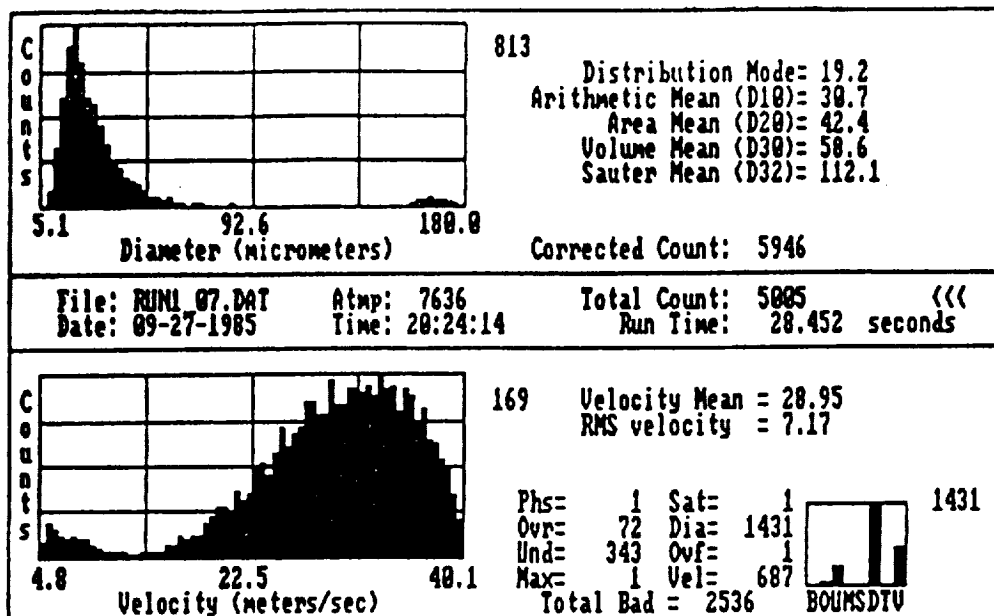


Figure 2.4: Reflections Caused by High Density Spray

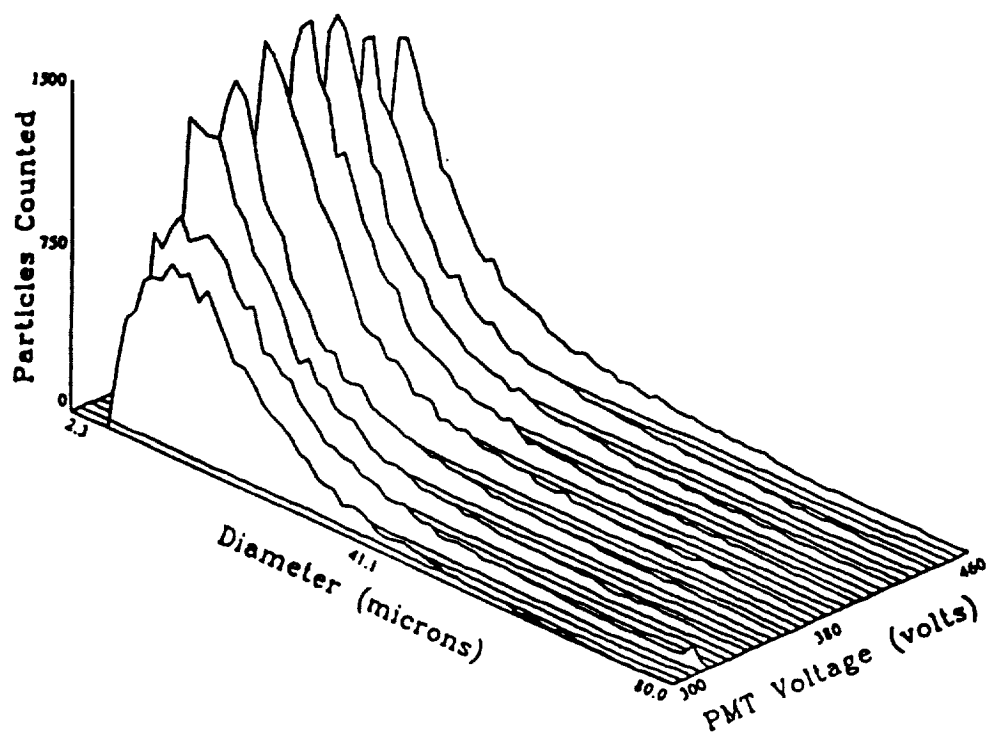


Figure 2.5: Drop Distribution Behavior with increasing PMT Voltage

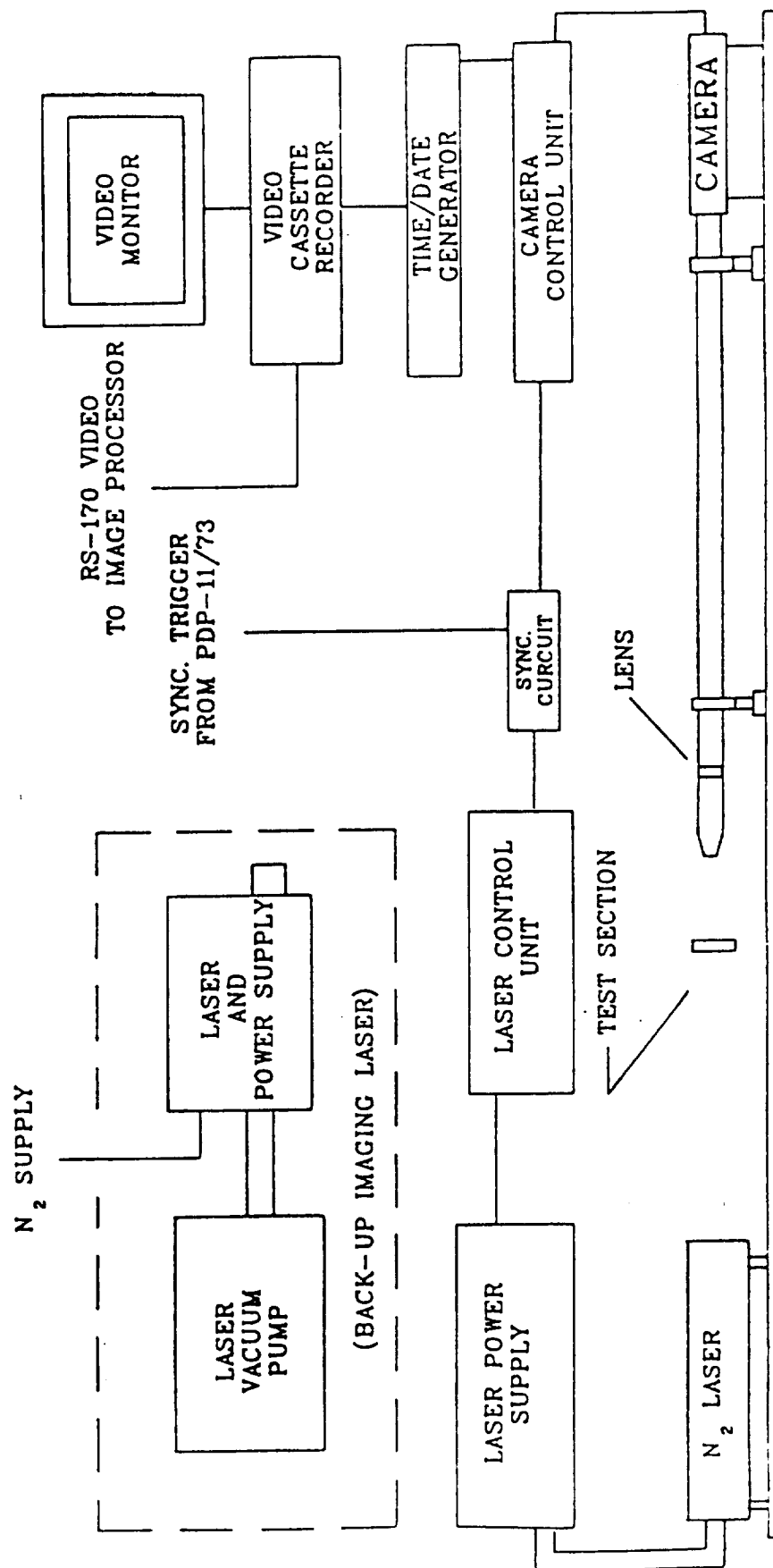


Figure 2.6: LI/VPS Laser Imaging Device

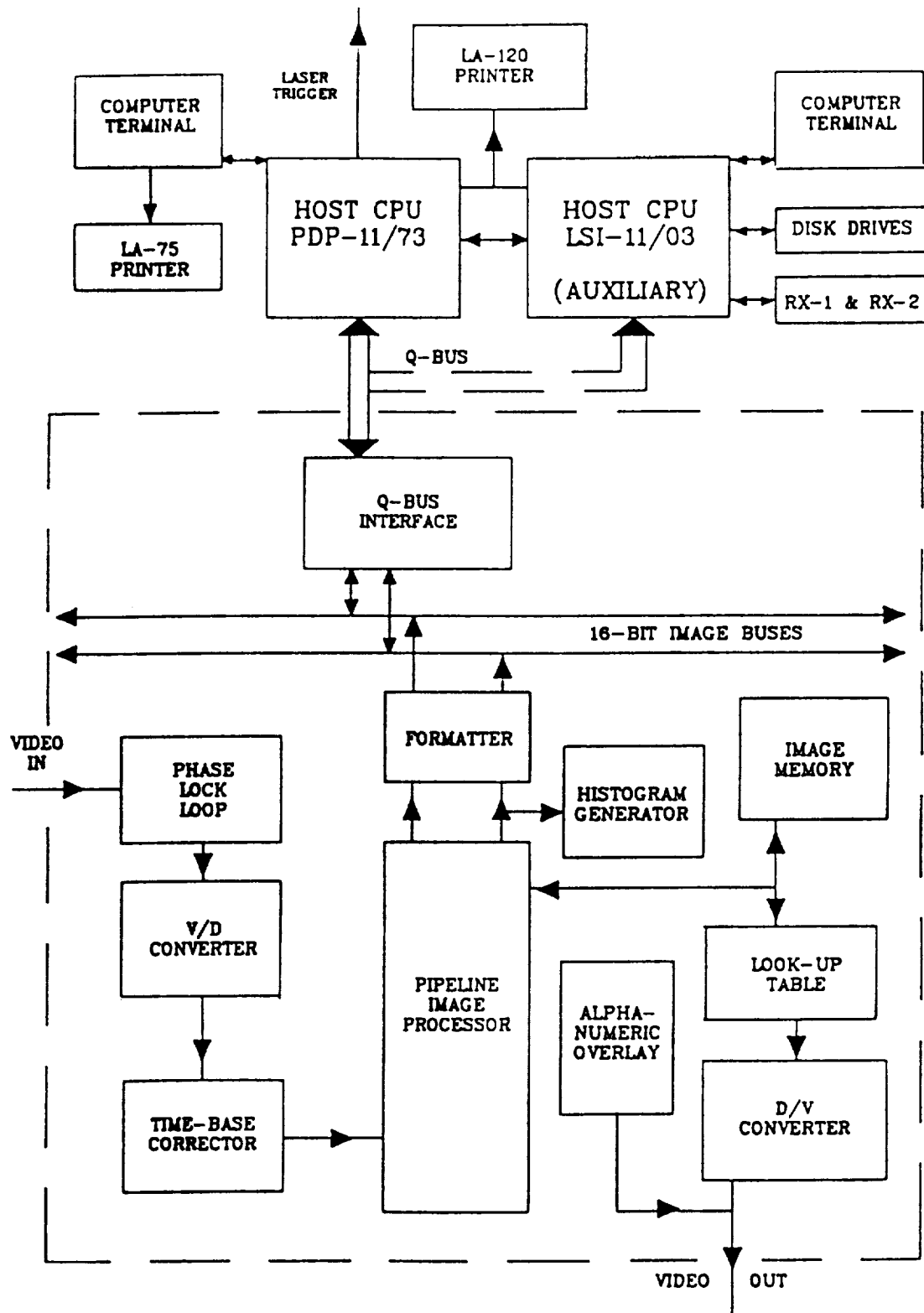


Figure 2.7: LI/VPS Video Processor Schematic

The baseline sync of the laser imaging system originates with the camera control unit (CCU). The CCU, operating on 60 Hz (line) cycle, drives the camera at video rates (i.e., one field every 16.67 milliseconds (ms) or one complete frame every 33.33 ms). The laser sync circuit (LSC); 1) receives the CCU triggering pulse, 2) uses the CCU trigger to generate a sync pulse for the laser, 3) sets the laser in sync with the camera process, and 4) sets the pulse rate of the laser to multiples of 60 Hz (e.g., 30, 15, etc.), or allows the operator to pulse the laser manually or by computer control.

The LHI laser control unit has variable power settings with an internal sync generator. The LEI laser system consists of a Model N2-50 power supply and pulsed laser ($\lambda = 337$ nm). The original system was operable within a range of 2-20 kW pulsed power and has been upgraded to 40 kW. By changing the mirrors in the laser tube, the pulse duration of the laser can be varied from either 3 nanoseconds (ns) or 10 ns. A second N₂ laser (MUV12) also contains its own internal sync generator, but the power cannot be varied. The MUV12 (laser and vacuum pump) has a peak power output of 250 kW and is limited to a pulse duration of 10 ns.

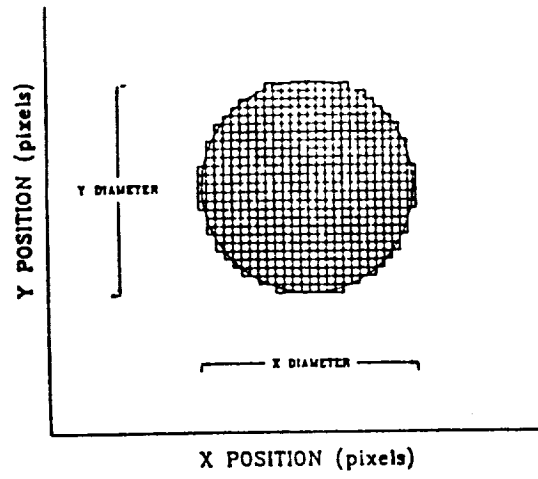
With the laser system in sync with the camera system, the object field is transferred to the camera by the imaging optics. A plano convex lens magnifies the object field before transferring the object field to the camera tube. System capabilities include a 500X and 1000X lens (i.e., 500X implies 800 by 800 micrometer (μm) field of view, and 1000X implies 400 by 400 μm field of view) for measurement. The video signal is then routed to a VCR where the images can be recorded for later viewing as a visual aid, or the images can be sent to the digital image processor. Other available options to the system are the use of the Panasonic time/date generator which overlays the time, date, and optional stopwatch capabilities on the analog video signal; and the availability of the Panasonic TQ-2023F LDR to store video frames which can provide for fast retrieval time without the tape positioning problems associated with a VCR.

The user interfaces with the LI/VPS at the PDP 11/73 console. Through the processing software, the user instructs the Trapix 55/32 to perform various logical and arithmetic operations on the images supplied by the laser imaging system. The Trapix 55/32 image processor has one megabyte of image memory which gives the processor available space to store four concurrent video frames. The PDP 11/73 computer controls the Trapix 55/32 through a parallel interface with a sub-library of control subroutines. The LSI-11/03 computer is also available for utility processing.

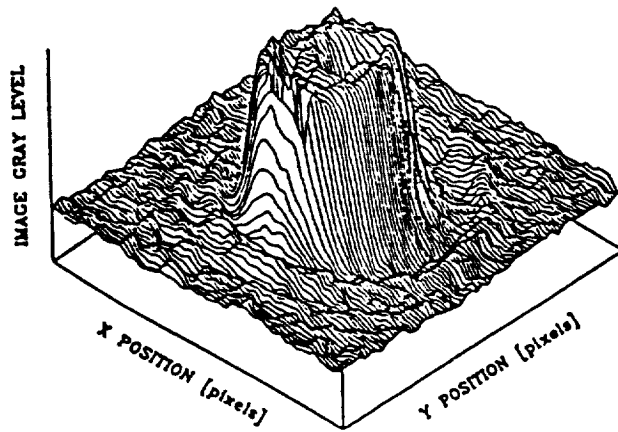
2.2.2 Sizing Method: Segmentation

The original software package developed by Ahlers [7] uses a technique called segmentation. The segmentation technique was adopted because sequential line by line processing is inherent to the camera system. The camera outputs a standard RS-170 composite video signal. The video signal is composed of 525 scan lines with interlace (i.e., odd and even scan lines interwoven into one complete frame). The segmentation technique uses the pattern recognition of the system (i.e., the conversion of the analog video signal into discrete pixels with specific intensity level and position) to analyze particles.

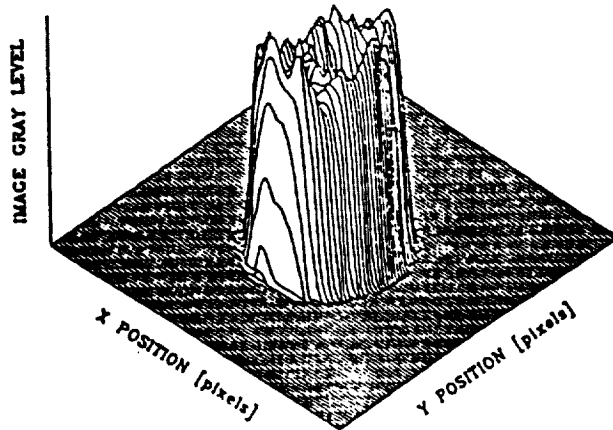
The premise of segmentation implies that discrete line segments, which lie adjacent to one another, can be summed into discrete two-dimensional objects. With the particles appearing as black disks on a white background in the digitized frame, the segmentation method finds the pixels upon which the particles reside and joins them into line segments (one pixel wide) in the line by line processing. The software matches the segments of the previous line to the current line until the objects are completely specified (Fig. 2.8(a)).



a. - Particle Characterized by Segmentation.



b. - Unthresholded Particle Image.



c. - Thresholded Particle Image.

Figure 2.8: LI/VPS Particle Representation

The Analog-to-Digital conversion is performed by the Trapix 55/32. The analog signal (i.e., video frame) is converted to a 512x512 array with array elements (i.e., pixels) that have eight bit precision (i.e., 256 grey levels). Ahlers showed the optimum threshold (T) was at a gray level of approximately 90 [7]. Figures 2.8(b) and 2.8(c), show the digitized particle before and after the thresholding process has been performed, respectively. After-which, with the subroutine, FINDTR, developed by Ahlers [7], the processor is able to find the transition which occurs at the 90 T. With the two transition points of a segment found, the program processes the remainder of the line until all segments are found. The above procedure is the basis for segmentation with program execution continuing in a line by line order.

2.2.3 Calibration

Previous work on the LI/VPS has included sections on calibration [7,10]. The initial work by Ahlers determined the qualifiers for calibration and specified an initial set of magnification correction factors (MCF). MCF qualifiers were the micron per pixel correction, the correction for non-linearities in the camera tube and the optimum value for the threshold of the image for sizing particles. The camera non-linearities initially were assumed to be dependent only on the x pixel location, this assumption required;

$$MCF = f(x). \quad (2.1)$$

Further work by Wiles showed improved accuracy by specifying MCFs with x and y dependence;

$$MCF = f(x, y). \quad (2.2)$$

In Ahlers' work, MCFs were determined by fitting experimental data points (i.e., x position, MCF) to the appropriate curve (i.e., straight line, exponential, etc.), whereas with Wiles' work, the MCFs as functions of x and y pixel position were found intuitively. In this researcher's work, calibration of the system became necessary after the COHU camera tube had to be replaced due to loss of sensitivity. Because the two-dimensional MCFs determined by Wiles were intuitive and specific to the replaced camera tube, a new method, which could be easily repeated, had to be deduced for determining the MCFs. Experimental data was discretized into 50 pixel intervals (Fig. 2.9), whereby the MCF was implied to be constant with respect to the x position in each interval;

$$MCF = \begin{cases} f1(y), & 50 \leq x < 100 \\ f2(y), & 100 \leq x < 150 \\ f3(y), & 150 \leq x < 200 \\ f4(y), & 200 \leq x < 250 \\ f5(y), & 250 \leq x < 300 \\ f6(y), & 300 \leq x < 350 \\ f7(y), & 350 \leq x < 400 \\ f8(y), & 400 \leq x < 450 \\ & \text{for } 50 \leq y < 450. \end{cases} \quad (2.3)$$

The above functions could than be found by curve- fitting the data (y position, MCF) specific to each interval. The following discussion is a description of the calibration method and procedure used.

The calibration method uses a calibration reticle (i.e., opaque disks in the form of thin metal films deposited on glass substrate) [12]. The configuration and particle size variation of the specific

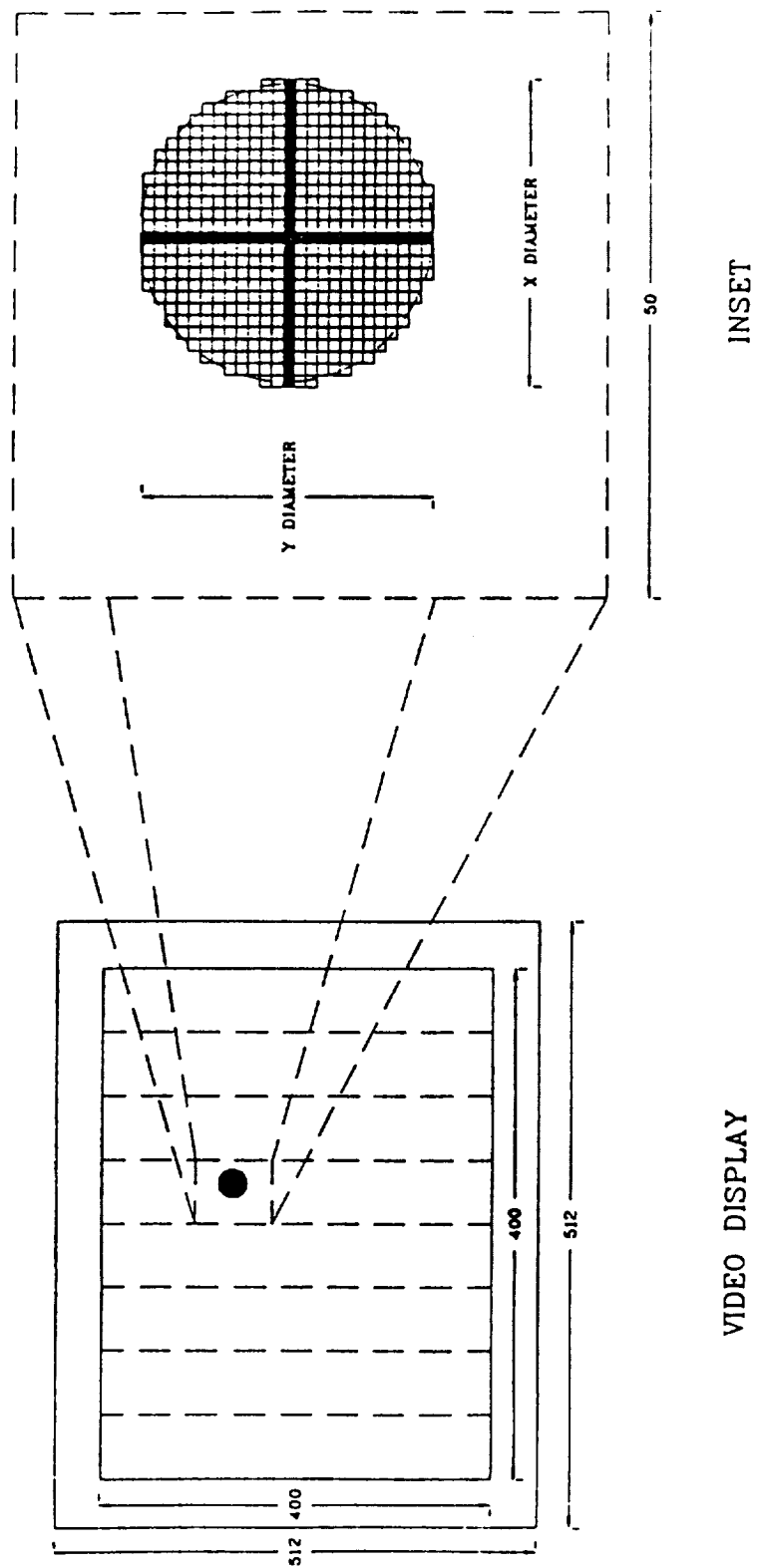


Figure 2.9: Two-Dimensional Calibration Technique

reticle (Model #RR-50-3.0-0.08-102-CF-114) used in calibration are shown in Fig. 2.10 and Table 2.1. The range in diameter of the reticle particles is $5.29\ \mu\text{m}$ to $92.75\ \mu\text{m}$. The calibration reticle is well suited for the LI/VPS because it can easily be positioned in the plane of focus of the imaging optics, eliminating the need for depth of field correction.

The calibration procedure uses a revised version of the Particle Sizing Program (PSP) developed by Ahlers [7]. The modified PSP is setup to collect data (i.e., particle position, x and y pixel diameters, etc.) for a prescribed opaque disk from the calibration reticle. With the calibration reticle in the focal plane of the imaging optics, the calibration program is started. The calibration reticle is then positioned randomly throughout plane of focus with the program storing the data simultaneously. With the known diameter, the MCFs are found by Equation (2.4);

$$MCF = \frac{\text{True diameter } (\mu\text{m})}{\text{Measured diameter (pixels)}} \quad (2.4)$$

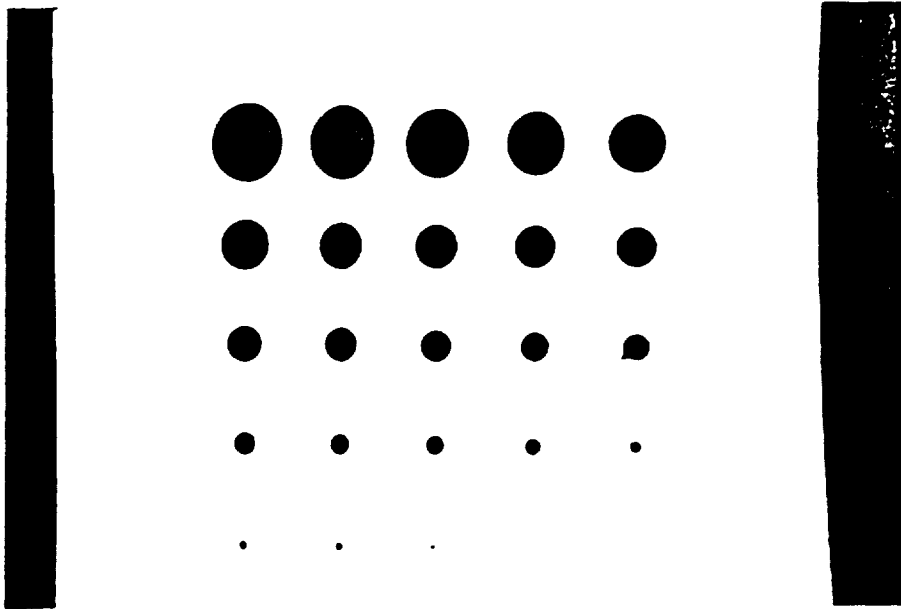
The calculated MCF is then specified according to the particle's center position. The data is then sorted into the perspective 50 vertical pixel intervals, and then each set of data (i.e., y pixel position, x MCF, and y MCF) is sorted according to y pixel position. With the correction factors specified as dependent variables of the y pixel position, the data can be set to the best fit curve. Figure 2.11 is a flow diagram of the aforementioned procedure. The above procedure was carried out for the 500X and the 1000X lens. The use of a different particle from the calibration reticle being the only change in the procedure. Because the MCFs are determined in the procedure as average values over the total diameter of the particle, the appropriate particle had to be chosen to avoid excessive overlapping of calibration intervals. Also, to avoid the edge effect (i.e., pixel elements being discrete implies pixels can be on or off depending on the position of the true particle's edge), the largest available particle should be chosen.

Preliminary work showed that approximate MCF for the 500X lens was $2.1\ \mu\text{m}/\text{pixel}$, and conversely, $0.98\ \mu\text{m}/\text{pixel}$ for the 1000X lens. As implied above for the 50 pixel intervals, a calibration particle diameter of 25 pixels would minimize interval overlap and edge effects. Therefore, for 500X lens, the #16 particle (i.e., $52.5\ \mu\text{m}$) was used, and conversely, for the 1000X lens, the #7 particle (i.e., $23.90\ \mu\text{m}$) was used. The results of the above procedure and a comparison of previous system calibrations with the present calibration is presented in Section 3.1.

2.2.4 Focus Method

Ahlers [7] performed work using polystyrene micro-spheres restrained between two glass microscope slides positioned in the plane of focus of the imaging optics. The above tests verified the methodology and calibration of the LI/VPS. As with most complex systems, development occurs in stages, therefore Ahlers constructed a particle sizing system which performed analysis on static and semi-static particles in the focal plane of the imaging optics with good accuracy. Wiles [10], in the next stage in the development of the LI/VPS, defined a method of focus classification (i.e., particles unaffected by diffraction light scatter). As Fig. 2.12 shows, with a diffraction limited system, particle focus is dependent on the particle's boundary gradient and it's relative intensity as compared to background. Because of the 8-bit precision of the video processor, the particle's intensity level with respect to background could be used as a viable criteria for focus. The particle's boundary gradient (PBG) was used as a secondary test because it rejects large out of focus particles which appear as small particles in focus by the particle intensity level test [10].

With the 256 grey level resolution and the processing capabilities of the video processor, the focus parameters are determined. The particle's intensity level or measured average grey level



a. - Video Image of Calibration Reticle.

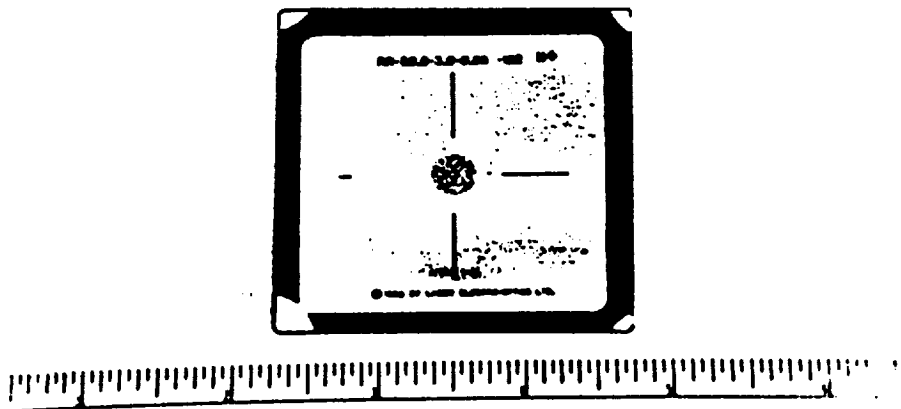


Figure 2.10: Calibration Reticle

Table 2.1: Specification Sheet for Calibration Reticle
 CALIBRATION RETICLE : RR-50-3.0-0.08-102-CF - #114
 FINAL DATA SHEET¹

	DIAMETER (μm) ²	NUMBER	AREA FRACTION	VOLUME FRACTION
1	5.29	2898	0.015	0.002
2	6.81	776	0.006	0.001
3	8.98	895	0.013	0.003
4	11.93	1171	0.030	0.009
5	17.20	1009	0.054	0.023
6	21.33	642	0.053	0.028
7	23.90	456	0.047	0.028
8	26.71	505	0.065	0.043
9	31.11	396	0.069	0.054
10	34.17	280	0.059	0.050
11	37.07	306	0.076	0.070
12	40.47	240	0.071	0.072
13	42.71	207	0.068	0.073
14	47.37	160	0.065	0.077
15	50.39	106	0.049	0.061
16	52.50	109	0.054	0.071
17	56.23	96	0.055	0.077
18	60.70	88	0.058	0.089
19	67.04	58	0.047	0.079
20	73.48	27	0.026	0.048
21	80.58	11	0.013	0.026
22	86.99	4	0.005	0.012
23	92.75	1	0.002	0.004
TOTAL		10441	1.000	1.000
D(10) = 17.81 μm D(20) = 23.04 μm D(21) = 29.73 μm				
D(30) = 27.69 μm D(31) = 34.48 μm D(32) = 40.01 μm				

¹ Reproduced from specification sheet supplied by the manufacturer.

² Diameters traceable to NBS Part. #52577,
 accurate to $\pm 2 \mu\text{m}$ ($\pm 3\%$ for $D > 70 \mu\text{m}$)

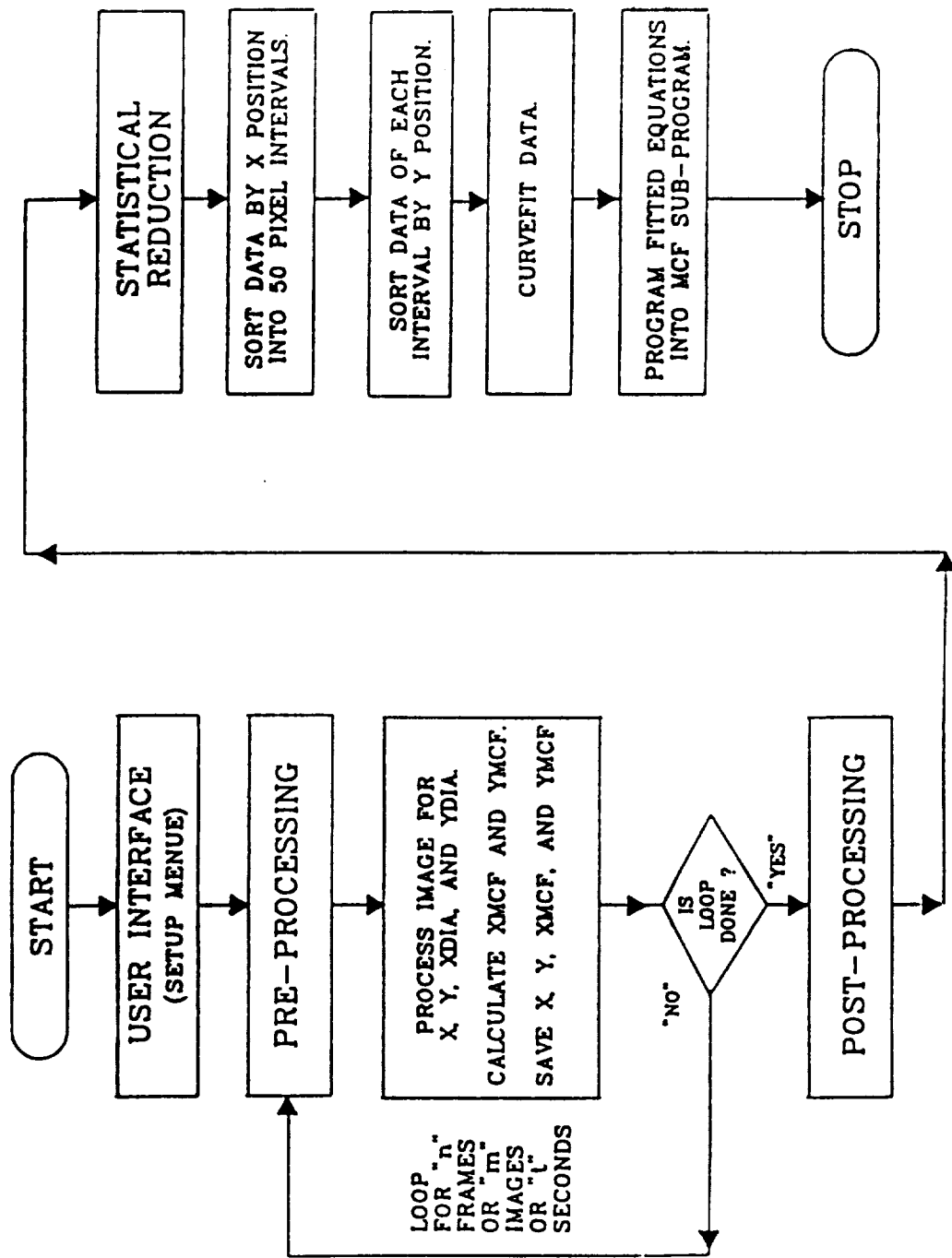
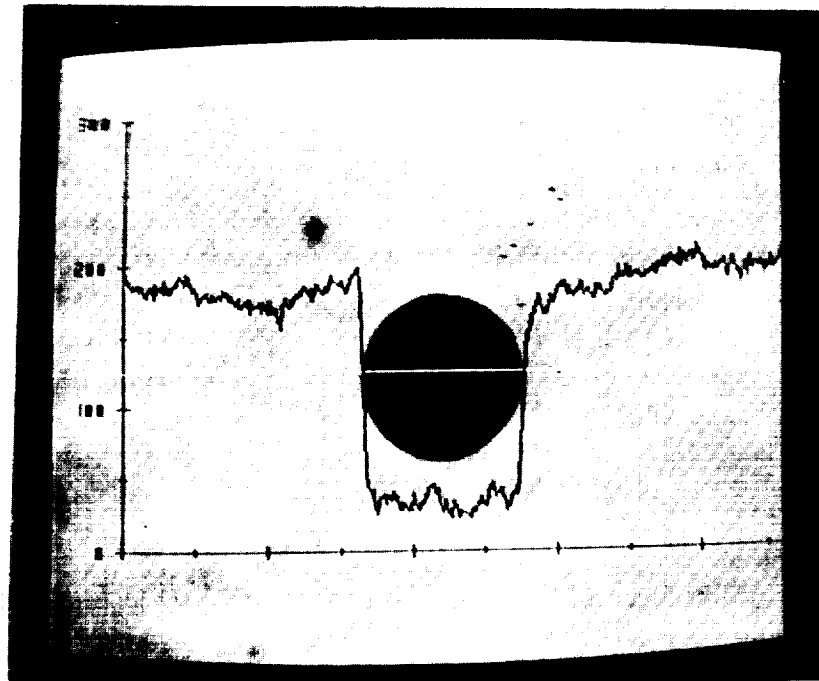


Figure 2.11: Flow Diagram for Calibration Procedure

ORIGINAL PAGE
BLACK AND WHITE PHOTOGRAPH



In-focus 92.75 μm Particle.



Out of Focus 92.75 μm Particle.

Figure 2.12: I.I/VPS Focus

(MAGL [10]) is calculated by thresholding the image at the optimum value (i.e., 90 T as specified by Ahlers), summing the pixel grey levels (GL) corresponding to specific particles as specified by segmentation, and dividing by the total number of pixels per particle (Equation 2.5).

$$MAGL = \frac{\sum_{i,j} GL(i,j)}{\sum_{i,j} Pixel(i,j)} \quad (2.5)$$

The PBG is determined by thresholding the image twice, once at 90 T, and the second, just below background (T_b). Referring to Fig. 2.12, the double threshold specifies the particle boundary gradient by:

$$PBG = D_d - D_b, \quad (2.6)$$

where D_b is the particle diameter at T_b . With the above parameters, focus was specified for a volume centered on the focal plane of the transfer lens. First, a relation, constant with respect to focal volume, was determined for the MAGL with dependence on particle diameter, and second, the PBG was specified as a constant over the range of particle diameters specified by the MAGL criteria.

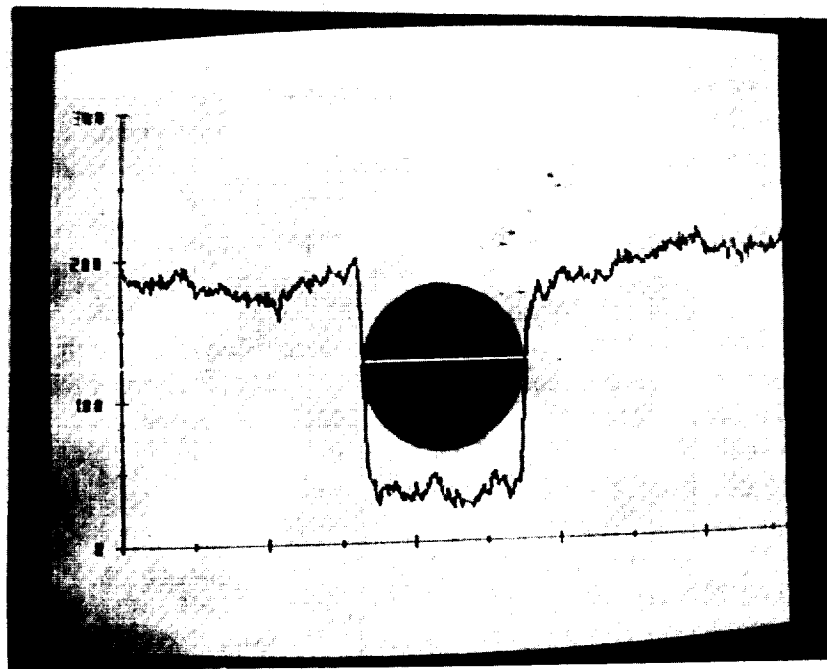
In conclusion, Wiles developed a focus criteria for the LI/VPS. In his follow-up tests, the criteria defined a depth of focus which remained fairly constant when tested with the reticle and the polystyrene spheres (i.e., 52.5 μm as specified earlier). The prescribed depth of focus was approximately 400 microns. It should be noted, Wiles' focus classification was determined and tested with the laser pulsing at 60 Hz. Thus, the focus criteria specified a depth of focus and classified particles based on grey level intensity from these operating conditions.

2.2.5 Modifications

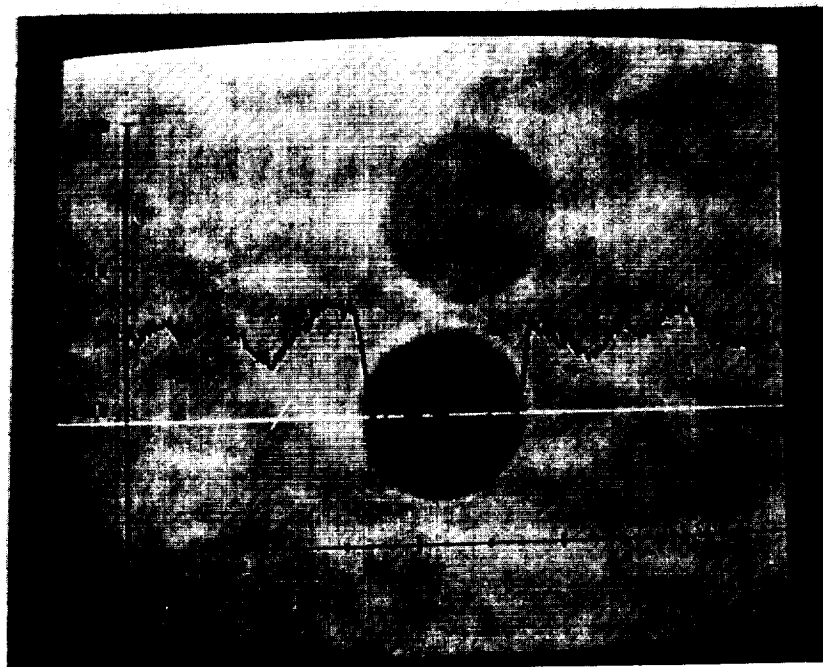
The final goal of this research was the implementation of a particle sizing system capable of performing analysis on two-phase flow (e.g., aerosol sprays). The LI/VPS has been developed in stages; (1) Ahlers' initial work, hardware and software setup, (2) Wiles' work on system focus classification, and (3) the current adaptation of the system to process truly dynamic particles in a real spray. To clarify the above statement, previous work by Ahlers and Wiles was performed with the LI/VPS operating in the continuous pulse mode (CPM), as opposed to the current work in the single pulse mode (SPM) (i.e., CPM suggests the imaging laser is pulsing at 60 Hz. in sync with the camera, and SPM implies the imaging laser is off until the video processor requires a new frame to process at which time the imaging laser is pulsed). The following discussion covers the reasoning and implementation of the SPM, and the adaptation of the previous work to function in the SPM.

All previous work on the LI/VPS was done in the CPM, therefore the system had to be converted to the SPM. The reasoning for the conversion is shown in Fig. 2.13. The two graphs were taken with the system in the CPM; the only difference being the bottom particle is dynamic whereas the top particle is stationary. As shown, there is a significant reduction in intensity for the dynamic particle as opposed to the stationary particle. The above behavior is due to the camera tube's ability to refresh between successive frames. In the CPM, the dynamic particle being frozen by the 10 ns laser pulse is present in the field of view for less than 16.67 ms (i.e., the time necessary to complete one field), but the static particle in the CPM shows greater intensity because of the cumulative effect of the particle blanking out the same area on the camera tube. The behavior being time-dependent implies the camera tube reaches a constant intensity after a sufficient amount of time. Because the software was developed for the system operating in the CPM, and all previous

ORIGINAL PAGE
BLACK AND WHITE PHOTOGRAPH



a. - Static 92.75 μm Particle in the CPM.



b. - Dynamic 92.75 μm Particle in the CPM

Figure 2.13: Static vs. Dynamic Particle Representation in CPM

work was performed on static particles (i.e., particles which have motion but appear static to the system), the system had to be adapted to size dynamic particles. Revision to the system could be achieved by either changing the system software, or changing the system hardware. Figure 2.14 shows the, MAGL vs. particle size, focus classification curves. As is shown, the 'dynamic' curve is less distinct than the 'static' curve. Because of the added ambiguities in the 'dynamic' curve, a method had to be determined to simulate the behavior of the stationary particles for the dynamic particles.

Because of the amount of work put into the development of the system software and the success of the focus criteria, a hardware modification was selected to accomplish the intensity contrast in dynamic particles. The SPM was found to exhibit the same characteristic intensity in the dynamic particles as found in static particles, in fact, the contrast between particle and background was greater. The SPM was accomplished by; (1) sending a trigger signal from the control computer to the LSC, (2) the LSC triggers the N₂ laser, (3) the laser pulses, and (4) the image processor grabs the frame just illuminated. The above procedure was accomplished by the development of a triggering circuit (APPENDIX B). The above procedure is then followed by normal program execution. The flow diagram in Fig. 2.15 shows the SPM integrated into the PSP with software modification.

The software had to be adapted to handle the SPM. As stated previously, the use of the SPM produced even greater contrast between the particle image and background. Because of the greater contrast, it was necessary to redetermine the focus criteria. Using the procedure outlined by Wiles [10] (Section 2.2.4), the MAGL curve and the PBG criteria were determined in the SPM. MAGL curves for both the CPM and the SPM are represented in Fig. 2.16. As shown in the figure, the larger particles show greater contrast whereas the smaller particles contrast is unaffected by the SPM. The focus criteria was determined for both the 500X and 1000X lens. The LI/VPS, at this point, was capable of performing size measurements in a two-phase flow.

2.2.6 Software Updates

With PSP performing analysis on two-phase flows, the software had to be updated to allow for varying conditions in the measurement analysis. Parameters, such as the sizing window specifications, output destination, etc., were queried for before processing each time the program was executed and others, such as lens magnification, were set by changing the FORTRAN code. A menu type of setup (Fig. 2.17) was adopted to minimize setup time and to aid the operator in determining the most appropriate sizing conditions (APPENDIX C.1).

In aerosol sprays, the mean diameters (APPENDIX D) determined from the count vs. drop-size data are the most common method of characterization. Characterization by mean diameters is misleading when a single mode (i.e., Gaussian distribution) is not the case, therefore the actual count vs. drop-size distribution is also used to characterize aerosol sprays. Because of the aforementioned reasoning and the unavailability of a suitable graphics package for the LI/VPS, a graphic algorithm was developed. The algorithm was coded into a FORTRAN subroutine (APPENDIX C.2) for the PSP with a DEC VT240 terminal for graphic simulation (Fig. 2.18(a)) and a DEC LA75 printer for hard-copies (Fig. 2.18(b)).

2.3 Spray Test Facility

Figure 2.19 shows the configuration of equipment for the spray characterization tests. The tests were performed in the horizontal direction due to the positioning of the sizing instrumentation.

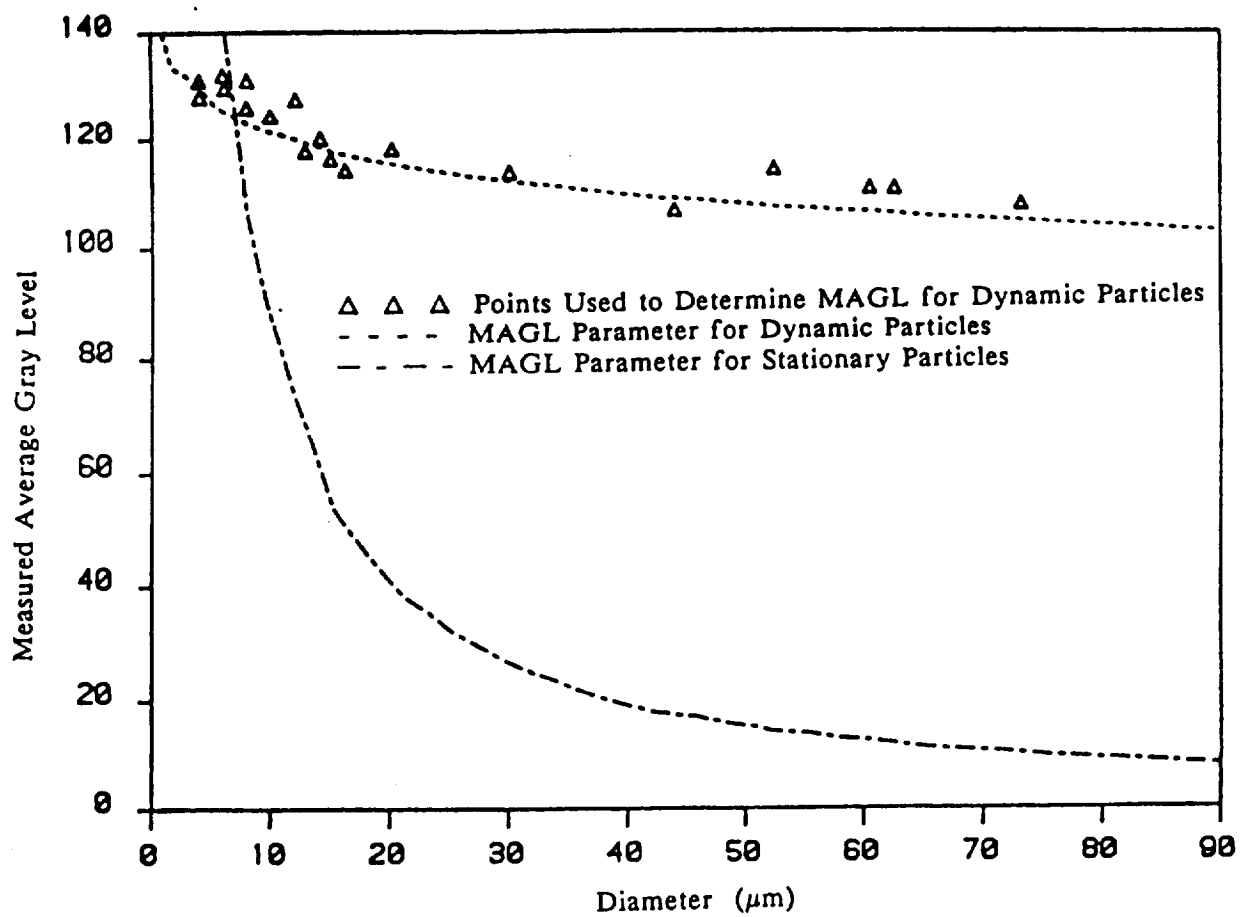


Figure 2.14: Comparison of the MAGL Parameter for Dynamic and Stationary Particles in CPM

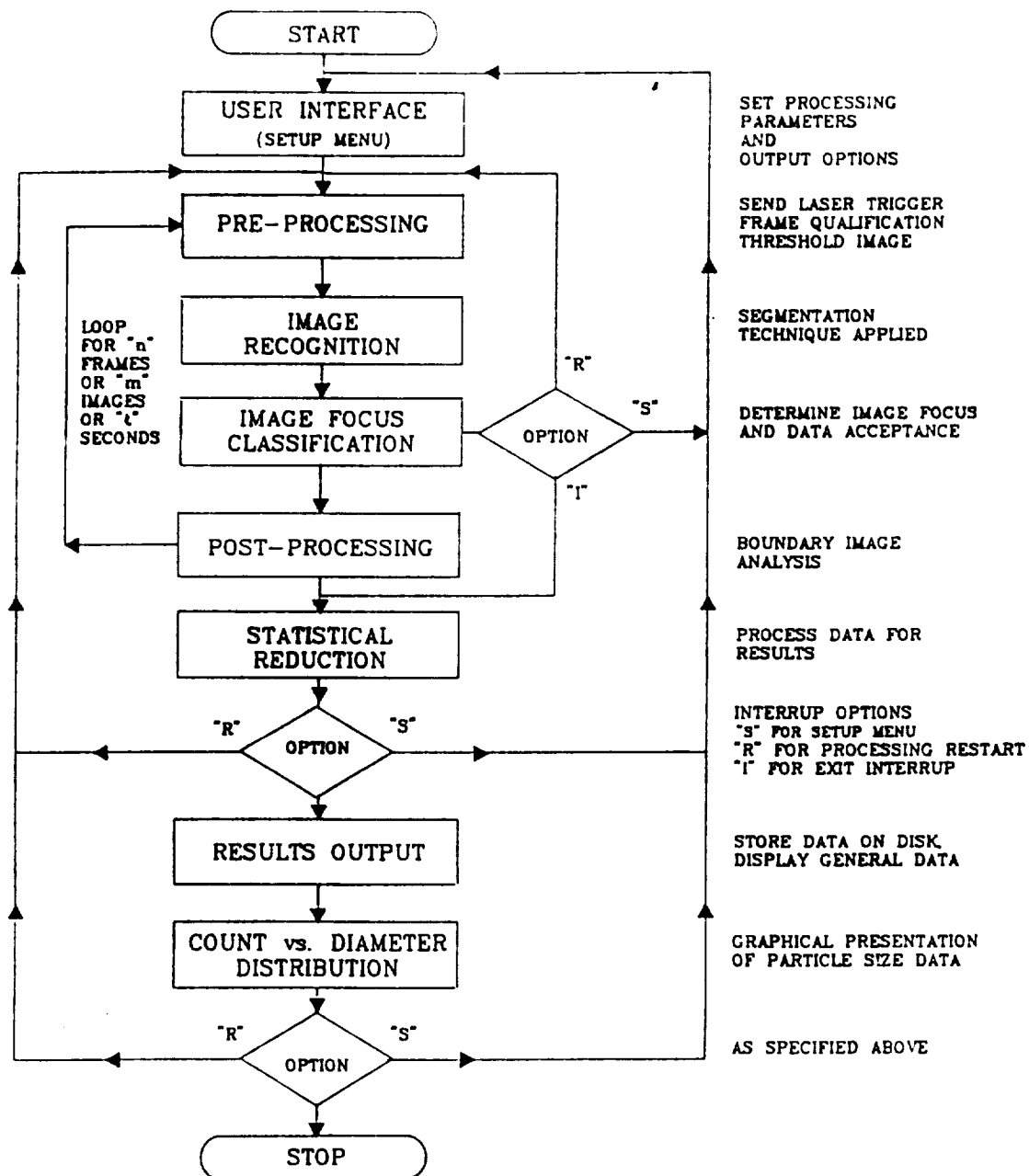


Figure 2.15: Flow Diagram for the Particle Sizing Program in SPM

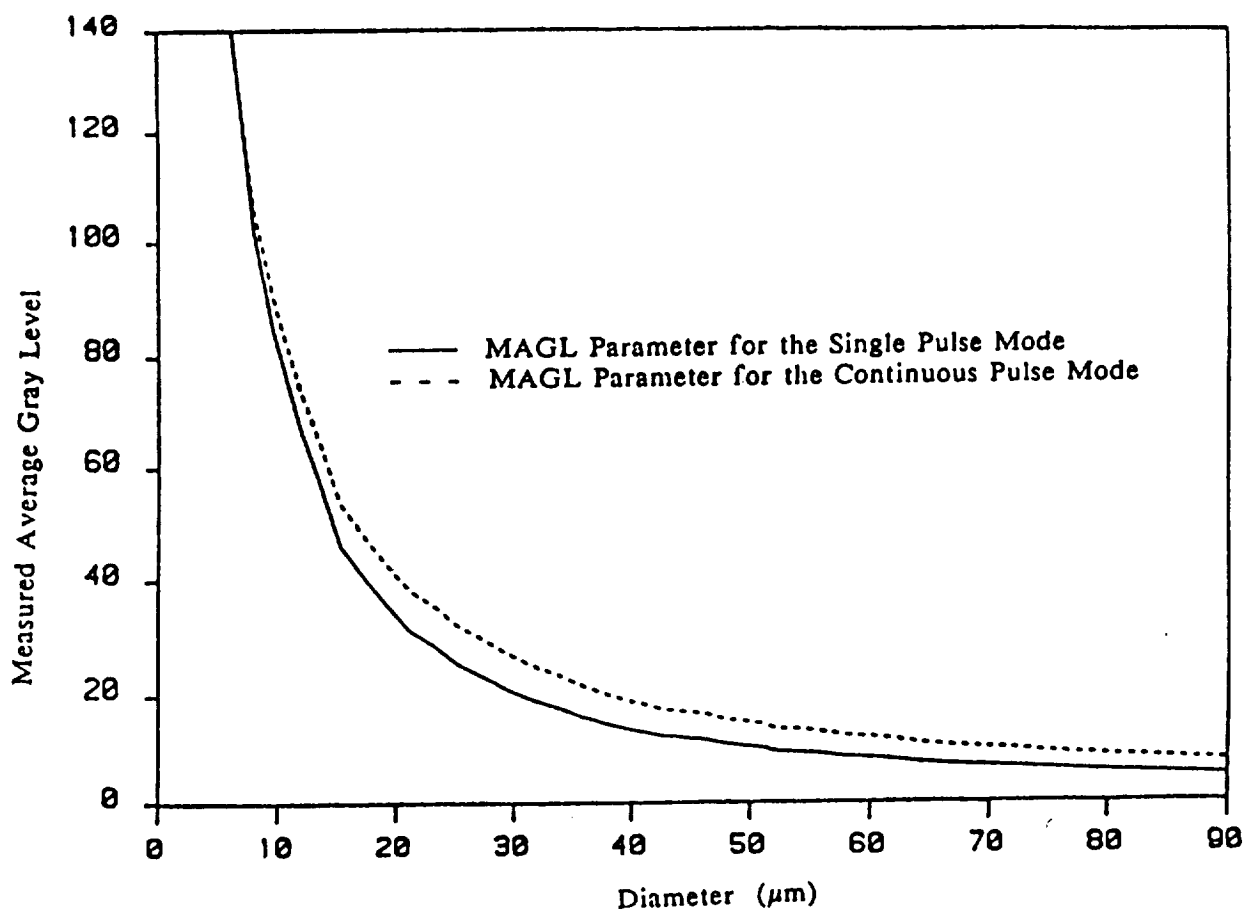


Figure 2.16: Comparison of the MAGL Parameter for SPM and CPM

SETUP
PARTICLE SIZING PROGRAM (ver. 4)

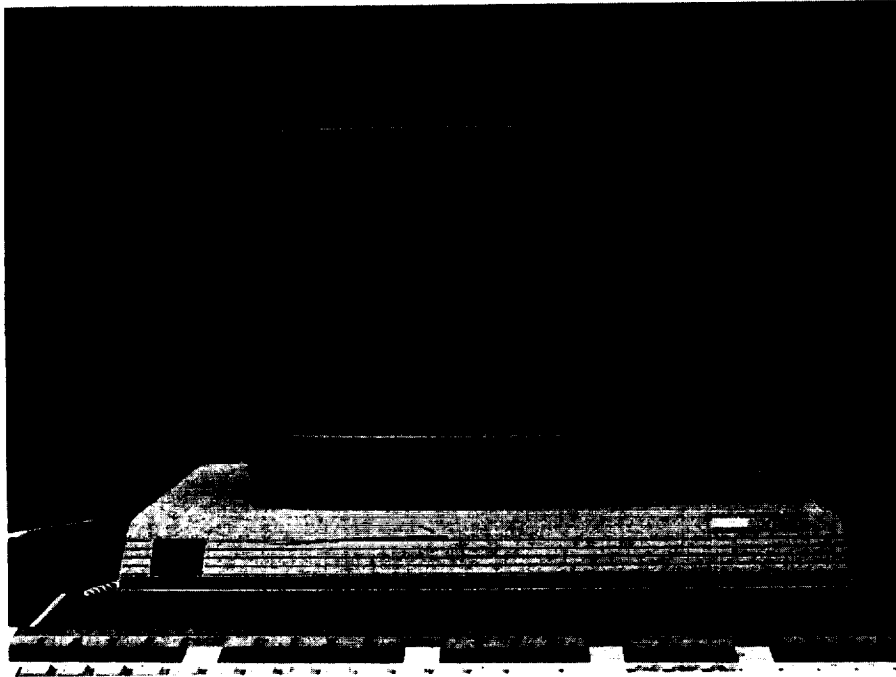
```

----- PROCESSING OPTIONS -----
(A)  DYNAMC   Type of Processing      (STATIC/DYNAMIC)
(B)  YES      Focus Criteria           (YES/NO)
(C)  AUTO     Type of Frame Advance    (AUTO/SINGLE)
(D)  PARTCL   Processing Limit         (TIME/FRAME/PARTICLE)
(E)  ( 1000)  Limiting Value           (seconds/frames/particles)
(F)  REJECT   Boundary Particles       (PROCESS/REJECT)
----- OUTPUT OPTIONS -----
(G)  YES      General Results (to PRINTER) (YES/NO)
      WRITE TO FILE (YES/NO)             (K) FILE HEADER (4 lines)
(H)  NO       Average Particle size data -- (L) FILE: (TEMP01).OUT
(I)  NO       Group Breakdown data -----/
(J)  YES      Per Frame data -----> (M) FILE: (TEMP01).DAT
----- GENERAL OPTIONS -----
(N) Group Start =( 5)  (O) Group Width =( 5.0)  (P) # of Groups =( 68)
(Q) X Window Start = ( 50)  (R) X Window Width = (450)
(S) Y Window Start = ( 50)  (T) Y Window Width = (450)
(U) Threshold = ( 90)  (V) Lens = HIGH  (W) Markers = NO (YES/NO)
-----
(X) to exit SETUP menu or (Z) to begin Partical Sizing Program ....
Enter Letter to change specific Parameter ??

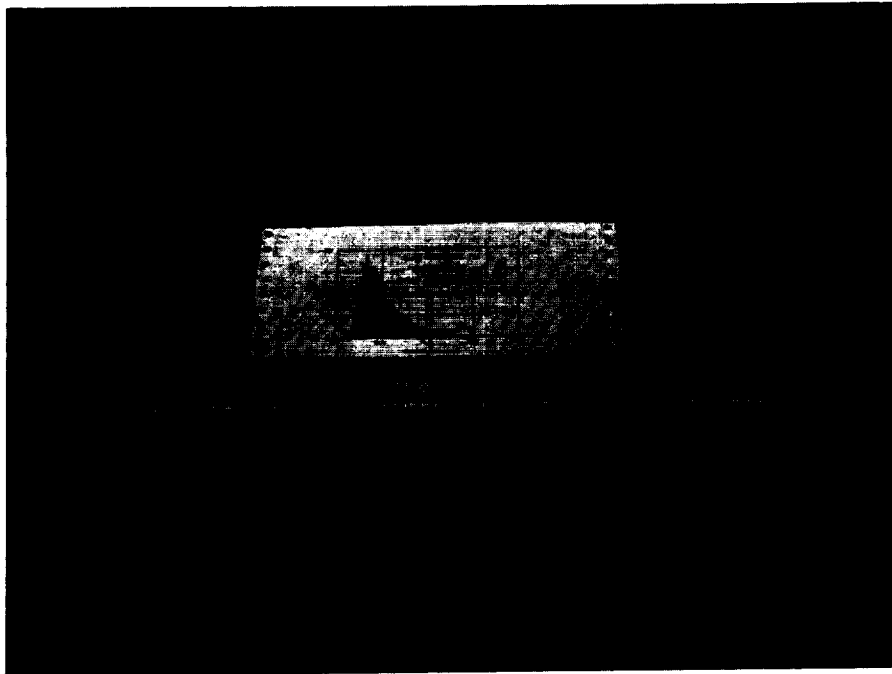
```

Figure 2.17: PSP Setup Page

ORIGINAL PAGE
BLACK AND WHITE PHOTOGRAPH



a. - DEC VT240 Terminal for Screen Emulation.



b. - DEC LA75 Printer for Hard-copys.

Figure 2.18: PSP Graphic Package

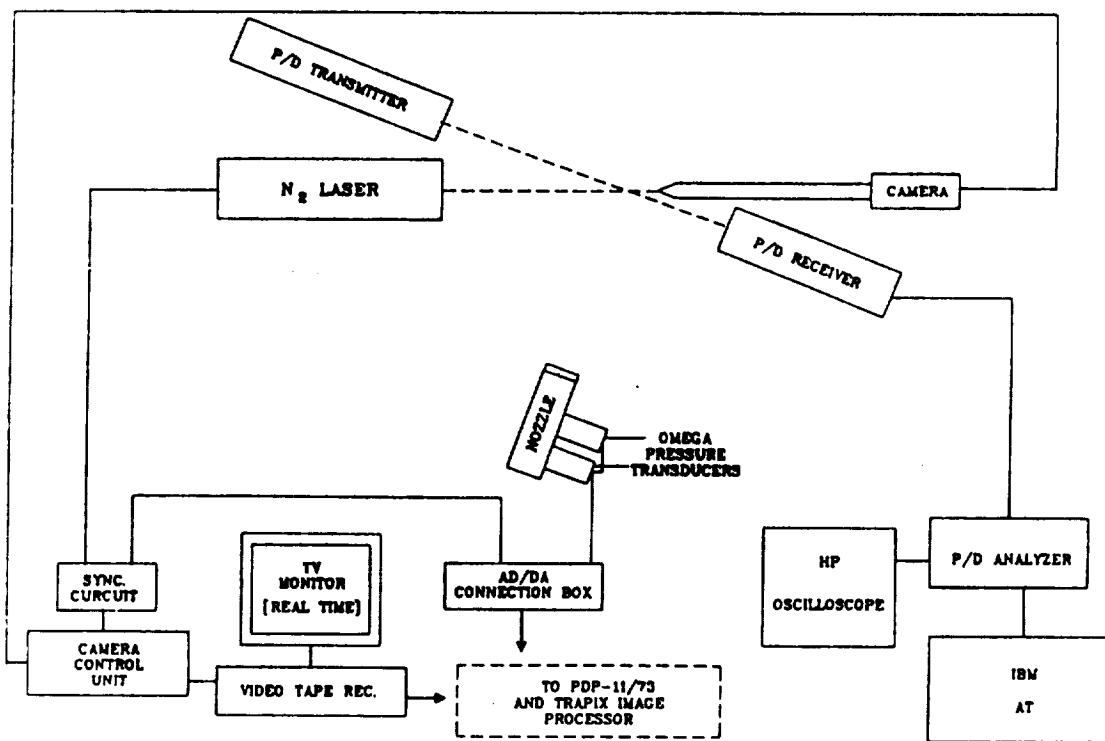


Figure 2.19: Equipment Schematic for Instrument Comparison

The experimental apparatus was situated on a Newport Research optical table equipped for isolation. The building ventilation system was used to draw off the aerosol spray after analysis. The spray characterization tests were performed on an air-assist nozzle.

2.3.1 MOD-1 Nozzle

Figure 2.20 shows the MOD-1 nozzle as supplied by NASA Lewis Research Center. The nozzle is of the atomizer type and a prototype of the nozzle proposed to be used in the NASA Altitude Wind Tunnel to simulate various cloud structures in icing studies. Variation of the drop-size in the aerosol spray produced by the nozzle is obtained by varying the input air and water pressures. The water is introduced into a 1.81 inch long by 0.368 inch diameter mixing chamber through a 0.0155 inch orifice. The air is introduced into the outer wall of the mixing chamber through twelve 0.125 inch holes. After mixing, the aerosol is expelled from the mixing chamber through a 0.125 inch orifice.

2.3.2 Air and Water Supply System (AWSS)

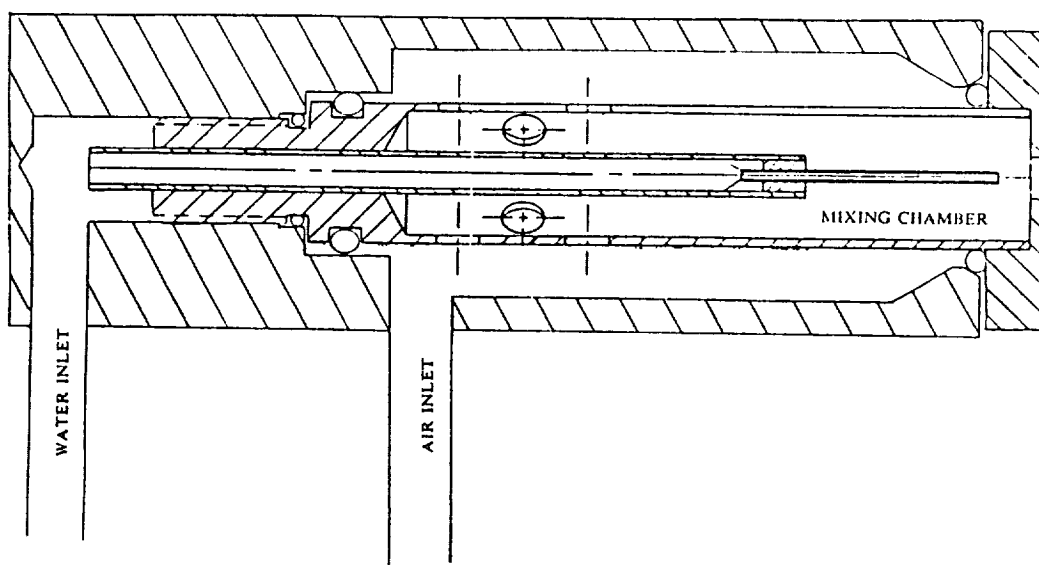
As shown in Fig. 2.21, the AWSS was constructed to supply air and water to the MOD-1 nozzle with the exception of the LI/VPS optics purge. The air for the AWSS is supplied by twin 100 hp Ingersoll-Rand turbine compressors with a delivery rate of 800 SCFM at 120 psig. Because of the high water pressure necessary for the MOD-1 nozzle, a Brunswick 20.5 liter pressure vessel was filled with water and pressurized by the supply air or for higher pressures by a regulated high pressure N₂ bottle. After pressurization, the water was filtered by an ADKIN spool filter. The nozzle air and water supply was regulated by a WATTS Model 2235 pressure regulator and a Cole-Parmer Model PR004-FM044-40G flowmeter, respectively. Connection lines in the supply system were YELLOW JACKET Model WPP0031A charging hose (500 max. psi.). The LI/VPS optics purge used a regulated high pressure N₂ bottle for a constant positive flow from the lens cover to avoid contamination.

2.3.3 Water Flowmeter Calibration

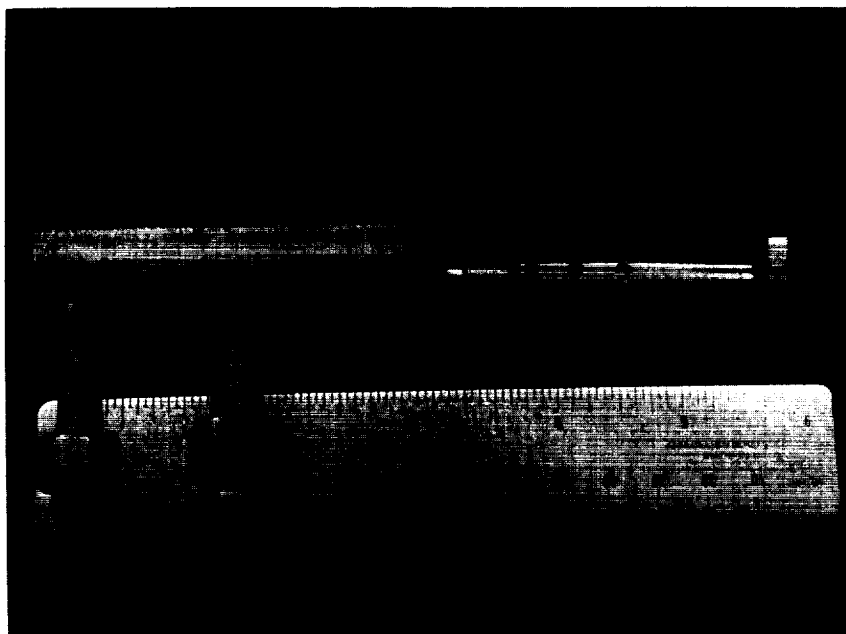
The Cole-Palmer flowmeter was factory calibrated. The calibration was verified by collecting and weighing the water passing through the flowmeter. The water was weighed on a HOWE model #3074131 balance scale. Twelve flow rates were measured with three samples collected at each flow rate. The experimental data and factory calibration data are presented in Table E13.1 with graphical representation shown in Fig. E.13.1 (APPENDIX E).

2.4 Digital Pressure Acquisition

The digital pressure system (DPS) was developed to monitor the essential input conditions of the MOD-1 nozzle. The DPS consists of two OMEGA Model PX304-150AV pressure transducers, a DEC AXV11- C analog to digital (A/D) converter board, the PDP- 11/73 micro- computer hosting the above A/D board, and a PDP RT-11 software package written to access the A/D board and store or display the resulting pressures.



a. - MOD-1 Schematic.



b. - MOD-1 Components.

Figure 2.20: MOD-1 Nozzle

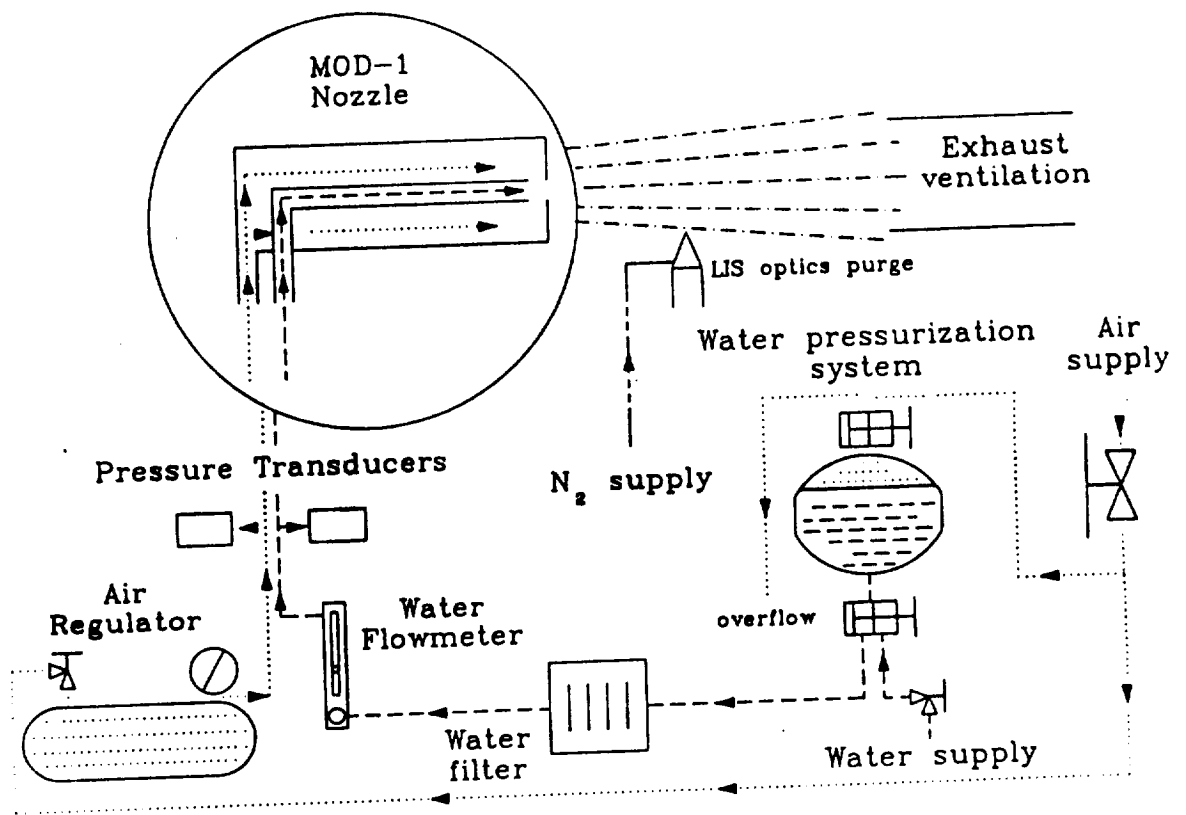


Figure 2.21: Air and Water Supply Schematic

2.4.1 Pressure Transducers

The OMEGA pressure transducers (Fig. 2.22) are bridge type strain gage transducers. The bridge excitation voltage was 10 VDC supplied by a Hewlett-Packard (Model Harrison 6200B) d.c. power supply with a bridge output of 0 to 100 mVDC. The transducers are specified to have an operating range of 0 to 150 psia with ± 0.75 psi accuracy.

2.4.2 A/D converter board

The DEC AXV11-C analog-to-digital converter board was installed in the back-plane of the PDP-11/73 microcomputer. The AXV11-C board has 12 bit digital resolution, supports up to 16 single analog input signals or 8 differential signals, A/D conversion by program, external clock, or real-time clock, and 1, 2, 4, and 8 (i.e., 10, 5, 2.5, and 1.25 volts) programmable gain settings. As recommended by the manufacturer, the 8 channel differential option was chosen to maximize analog to digital conversion, due to the 100 mV range supplied by the pressure transducers.

2.4.3 Analog-to-Digital Conversion

The transducer voltage signal is converted to a digital value available to the LI/VPS operator. An interface box (Fig. 2.23) was constructed to utilize the full capabilities of the AXV11-C board. The interface box has 8 A/D input ports and 2 D/A output ports using BNC connectors. The interface box is linked to the AXV11-C board by RS232 cable and connectors. The pressure measurements are made available to the analyst through the PDP-11/73 microcomputer. The RT-11 software package, written in FORTRAN subroutine form (APPENDIX C.3), allows for real-time pressure monitoring with storage and averaging capabilities for the duration of the main calling program. The A/D converter is programed for a gain setting of 8 (i.e., an effective analog input range of 0 to 1.25 volts) to optimize A/D conversion of the pressure transducer output range of 0 to 100 mV.

2.4.4 Digital Pressure System Calibration

The pressure transducers were calibrated for various static pressures by pressurizing the transducers and reading the A/D output after a steady equilibrium state had been attained. A laboratory grade test gage was used to measure the "standard" pressure. The test gage, with a range of 0 to 160 psig, was calibrated using an American Steam Gage Co. deadweight pressure gage tester. With the pressure transducer's specified input pressure range of 0 to 150 psia, the calibration data was taken within a range of 0 to 110 psig (14.05 to 124.05 psia). The atmospheric pressure at the time of the calibration run was measured to be 727.29 mm Hg. or 14.05 psia from a Precision Thermo & Inst Co. model #Z769 barometer. The experimental data is presented in Tables F14.1 and F14.2 with graphical representation shown in Figs. F14.1 and F14.2 (APPENDIX F).

2.5 Experimental Procedure

With system performance and verification as the basis for comparison, equivalent sampling was required. As discussed earlier, the P/DPA and the LI/VPS use different methods of particle sizing (i.e., temporal vs. spatial), but each instrument uses a probe volume for data collection. Therefore, system comparison was dependent on spray density, droplet size range, and user designation of the measurement volumes (i.e., the P/DPA's crossed-beam intersection volume, specified by

Model # - PX 304-150A V

SPECIFICATIONS

Excitation: 10 VDC

Output: 0 to 100 mV

Sensitivity: 10 mV/V $\pm 1\%$

Input Impedance: 1200 ohm

Output Impedance: 500 ohm

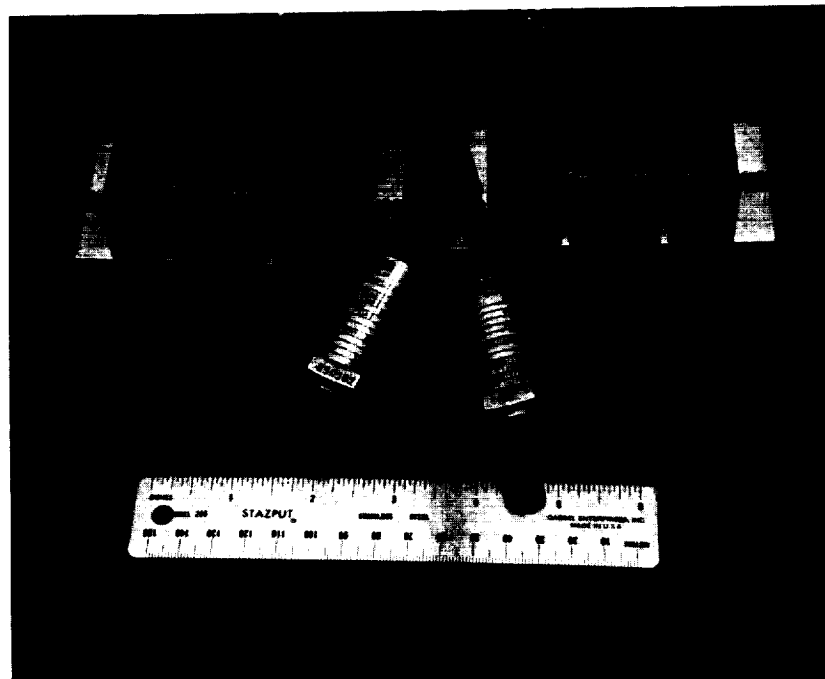
PERFORMANCE

Accuracy: $\pm 0.5\%$ full scale

Zero Balance: $\pm 2.0\%$ full scale

Operable Temperature Range:
-29 to 60° C

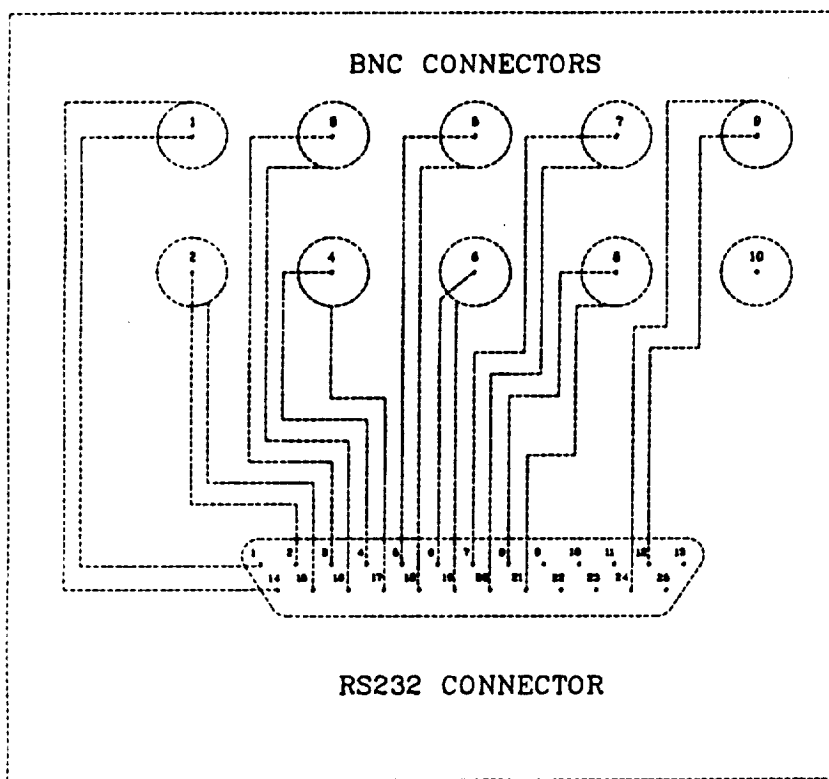
a. - OMEGA Pressure Transducer Data Sheet.



b. - OMEGA Pressure Transducers.

Figure 2.22: OMEGA Pressure Transducers

SCHEMATIC FOR AD/DA CONNECTOR BOX (For Differential Setup)



NOTE:

For further documentation refer to
PDP-11 Microcomputer Interface Handbook
page 70.

RS232	BNC
Pin 1 - CH. 1	1
Pin 2 - CH. 2	2
Pin 3 - CH. 3	3
Pin 4 - CH. 4	4
Pin 5 - CH. 5	5
Pin 6 - CH. 6	6
Pin 7 - CH. 7	7
Pin 8 - CH. 8	8
Pin 12 - DA #1	9
Pin 14 - CH. 1 Return	
Pin 15 - CH. 2 Return	
Pin 16 - CH. 3 Return	
Pin 17 - CH. 4 Return	
Pin 18 - CH. 5 Return	
Pin 19 - CH. 6 Return	
Pin 20 - CH. 7 Return	
Pin 21 - CH. 8 Return	
Pin 24 - DA #1 Return	

Figure 2.23: A/D Connector Box Schematic

the transmitter lens chosen and beam diameter, vs. the LI/VPS focus volume, specified by the imaging optics and software).

The procedure for overlapping the probe volumes is described in reference [14]. Figure 2.24 is included to show the scattered light, from drops generated by the VOAG passing through the crossed-beam intersection volume, as seen by the LI/VPS.

2.5.1 Verification Tests

The P/DPA and the LI/VPS probe volumes for the verification tests were specified as follows; the P/DPA transmitter lens with the 495 mm focal length and 25 mm beam separation formed a probe volume with an approximate 160 μm waist diameter, and for the LI/VPS, the 1000X lens specifies a 400x400x140 μm^3 volume with software selectable field of view for a 160x160x140 μm^3 volume (Fig. 2.25).

With the above configuration, the P/DPA and the LI/VPS were tested using a TSI Model 3450 Vibrating Orifice Aerosol Generator (VOAG). Operating conditions of the VOAG were varied to generate a size range of particles, 19.8 to 99.6 μm (Table 2.2).

Table 2.2: Verification Test Conditions				
TEST	ORIFICE	DISTURBANCE	WATER	THEORETICAL
(#)	DIAMETER	FREQUENCY	FEED RATE	DIAMETER
	(μm)	(Hz.)	(cm^3/min)	(μm)
1	10	330.4	0.080	19.8
2	20	100.2	0.139	35.5
3	20	79.2	0.139	39.0
4	20	62.5	0.139	41.5
5	20	51.6	0.139	44.2
6	20	41.6	0.139	47.5
7	50	30.1	0.590	85.6
8	50	25.5	0.590	90.4
9	50	19.0	0.590	99.6

Each particle size generated either in single stream form or using the dispersion cup (Fig. 2.26) to generated a spray was measured using the P/DPA and the LI/VIPS system. The TSI droplet diameter (D_d) was calculated using the TSI theoretical equation (2.7);

$$D_d = \left[\frac{6q}{\pi f} \right]^{1/3} \quad (2.7)$$

where q is the liquid flow rate and f is the disturbance frequency. Results of the tests are presented in Section 3.2.

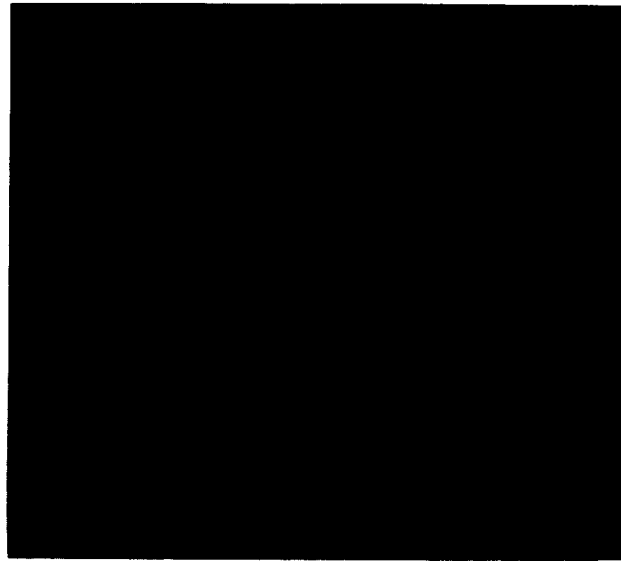


Figure 2.24: P/DPA Doppler Fringes as Seen by the LI/VPS Imaging Camera

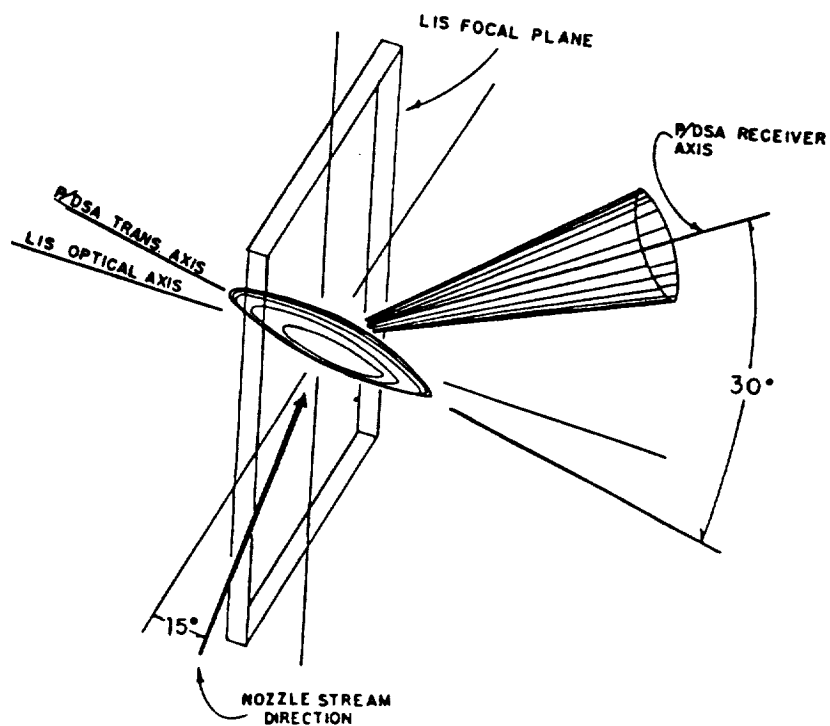
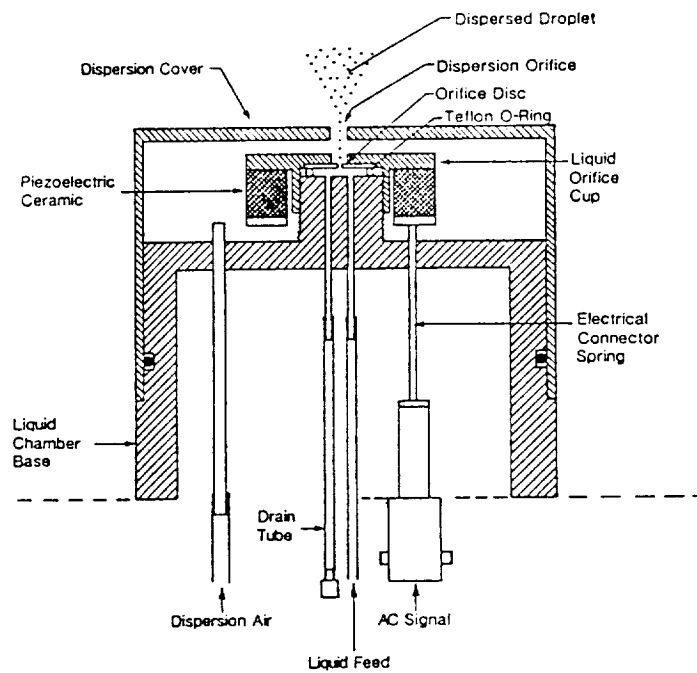
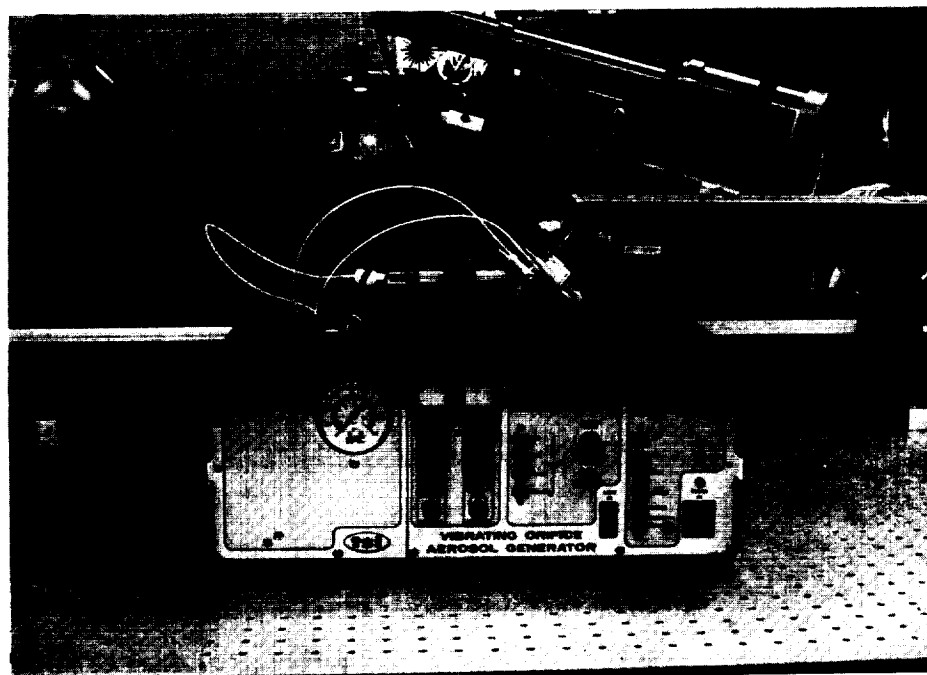


Figure 2.25: P/DPA and LI/VPS Over-lapping Probe Volumes



a. - VOAG Dispersion Cup.



b. - TSI Vibrating Orifice Aerosol Generator.

Figure 2.26: Verification Test Apparatus

2.5.2 Spray Comparison

With the spray density and particle size range depending on the nozzle conditions, the benchmark tests were performed for two specific cases. Inlet nozzle conditions are shown in Table 2.3.

Table 2.3: Comparison Test Conditions

	CASE I	CASE II
Pressure (water)	115 psia	105 psia
Pressure (air)	45 psia	65 psia

For each case, a sample was taken on centerline two feet downstream from the nozzle with succeeding samples taken radially in 0.5 inch increments to the outer edge of the spray plume.

To avoid undue comparative data reduction, the P/DPA and LI/VPS were matched in approximate probe volume size, as previously stated, and appropriate particle size range. Assuming nozzle conditions were steady state, preliminary setup of the P/DPA and the LI/VPS was performed to optimize instrument operation. The results of the analysis are presented in Section 3.3.

Section 3

PRESENTATION AND DISCUSSION OF RESULTS

This section will present the results of the LI/VPS calibration tests including a comparison with previous calibration tests, the verification tests with the VOAG, and the comparison tests using the MOD-1 nozzle. The major concern of these results is the accuracy of the sizing measurements with secondary interest in the comparability of the LI/VPS and the P/DPA.

3.1 LI/VPS Calibration Results

As was stated previously, the LI/VPS had to be recalibrated due to the replacement of the vidicon camera tube. With the new vidicon tube, the MCF became approximately $2.1 \mu\text{m}/\text{pixel}$ (i.e., for the 500X lens), as opposed to the previous factor of $1.8 \mu\text{m}/\text{pixel}$ [7,10], for the old camera tube. The new vidicon tube, therefore, reduced the LI/VPS measurement resolution. The above is mentioned to explain the increased error in determining the smaller particle sizes for the 500X lens, as well as the reasoning for the calibration of the 1000X lens. The following calibration results specify the MCFs for the 500X and the 1000X lens. Results of previous calibration tests using the calibration reticle have been compared to the new calibrations.

Using the procedure described in Section 2.2.3, the Equations (3.1) thru (3.4) represent the MCFs as functions of x and y location for the two lens;

the xMCF for the 500X lens;

$$MCF(y) = \begin{cases} 2.21 + y * 0.803E - 04 & \text{for } 50 \leq x < 100 \\ 2.20 + y * 0.290E - 04 & \text{for } 100 \leq x < 150 \\ 2.16 + y * 0.679E - 04 & \text{for } 150 \leq x < 200 \\ 2.16 + y * 0.442E - 07 & \text{for } 200 \leq x < 250 \\ 2.16 - y * 0.947E - 04 & \text{for } 250 \leq x < 300 \\ 2.11 - y * 0.306E - 07 & \text{for } 300 \leq x < 350 \\ 2.10 - y * 0.124E - 03 & \text{for } 350 \leq x < 400 \\ 2.07 - y * 0.135E - 03 & \text{for } 400 \leq x < 450, \end{cases} \quad (3.1)$$

the yMCF for the 500X lens;

$$MCF(y) = \begin{cases} 2.10 - y * 0.183E - 03 & \text{for } 50 \leq x < 100 \\ 2.11 - y * 0.240E - 03 & \text{for } 100 \leq x < 150 \\ 2.12 - y * 0.314E - 03 & \text{for } 150 \leq x < 200 \\ 2.13 - y * 0.313E - 03 & \text{for } 200 \leq x < 250 \\ 2.15 - y * 0.397E - 03 & \text{for } 250 \leq x < 300 \\ 2.18 - y * 0.484E - 03 & \text{for } 300 \leq x < 350 \\ 2.19 - y * 0.505E - 03 & \text{for } 350 \leq x < 400 \\ 2.18 - y * 0.509E - 03 & \text{for } 400 \leq x < 450, \end{cases} \quad (3.2)$$

the xMCF for the 1000X lens;

$$MCF(y) = \begin{cases} 0.977 + y * 8.09E - 05 & \text{for } 50 \leq x < 100 \\ 0.974 + y * 2.60E - 05 & \text{for } 100 \leq x < 150 \\ 0.967 - y * 8.12E - 07 & \text{for } 150 \leq x < 200 \\ 0.961 + y * 4.73E - 06 & \text{for } 200 \leq x < 250 \\ 0.961 - y * 5.46E - 05 & \text{for } 250 \leq x < 300 \\ 0.948 - y * 3.72E - 05 & \text{for } 300 \leq x < 350 \\ 0.943 - y * 6.80E - 05 & \text{for } 350 \leq x < 400 \\ 0.920 - y * 2.58E - 05 & \text{for } 400 \leq x < 450, \end{cases} \quad (3.3)$$

and the yMCF for the 1000X lens;

$$MCF(y) = \begin{cases} 0.977 - y * 9.17E - 05 & \text{for } 50 \leq x < 100 \\ 0.981 - y * 1.24E - 04 & \text{for } 100 \leq x < 150 \\ 0.981 - y * 1.19E - 04 & \text{for } 150 \leq x < 200 \\ 0.990 - y * 1.63E - 04 & \text{for } 200 \leq x < 250 \\ 1.000 - y * 1.96E - 04 & \text{for } 250 \leq x < 300 \\ 1.014 - y * 2.19E - 04 & \text{for } 300 \leq x < 350 \\ 1.027 - y * 2.63E - 04 & \text{for } 350 \leq x < 400 \\ 1.029 - y * 2.69E - 04 & \text{for } 400 \leq x < 450. \end{cases} \quad (3.4)$$

With the above equations, a software algorithm was setup in subroutine form to determine the correction factors as functions of particle location and for the magnification lens installed (APPENDIX C.4).

Figures 3.1 - 3.4 show the variation of the MCFs with respect to x and y location. The similarity in Figs. 3.1 and 3.3, as well as the similarity in Figs. 3.2 and 3.4 show the MCFs' variation is mainly due to the geometric non-linearities in the vidicon tube. The procedure developed to determine the MCFs as functions of both x and y screen location is easy to use, straight-forward, and not time consuming. The implementation of the MCFs in PSP is easily facilitated by the use of the FORTRAN subroutine format.

The following comparison represents LI/VPS accuracy studies by this investigator and the previous investigators [7,10]. The basis for the comparison was the utilization of the calibration reticle with the 500X lens. Table 3.1 shows the results for the 500X lens by this investigator. Table 3.2 represents the equivalent results for the 1000X lens under similar test conditions.

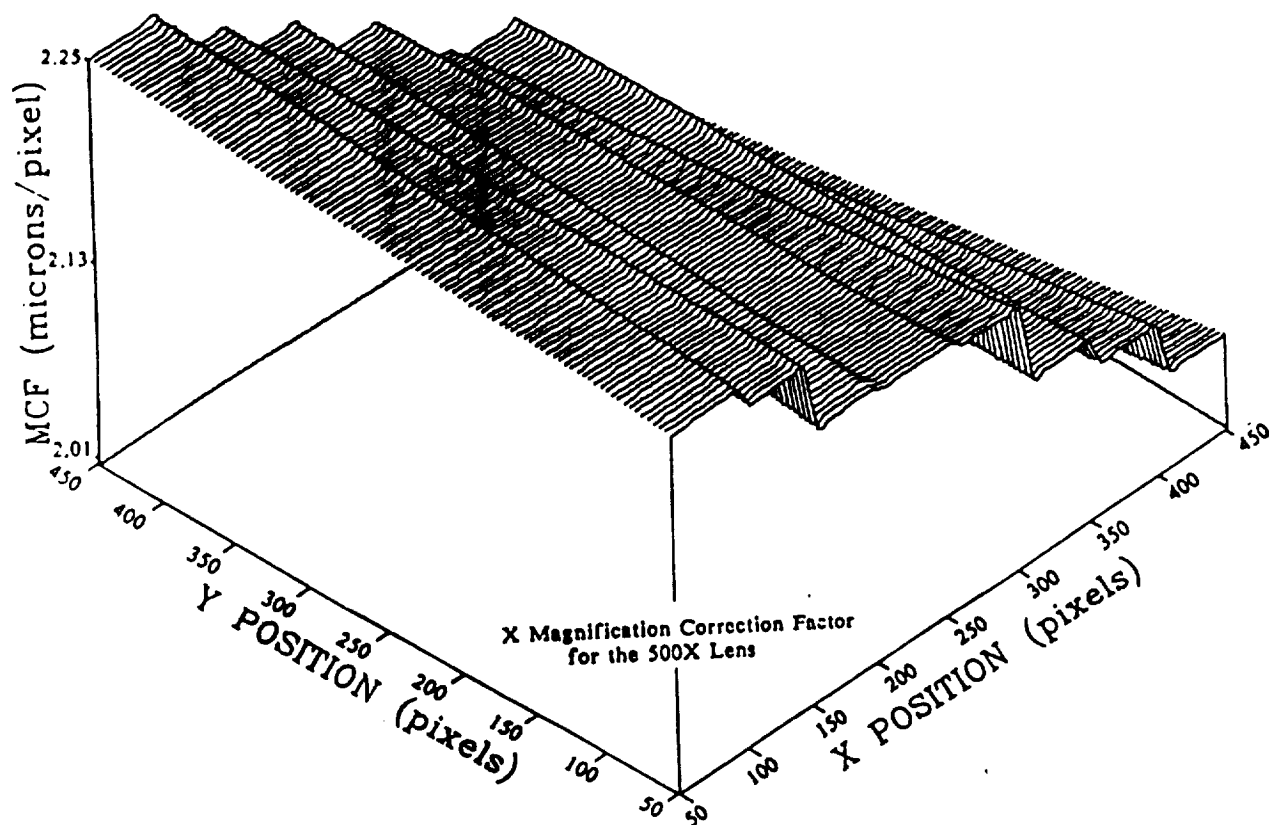


Figure 3.1: Magnification Correction Factor Behavior

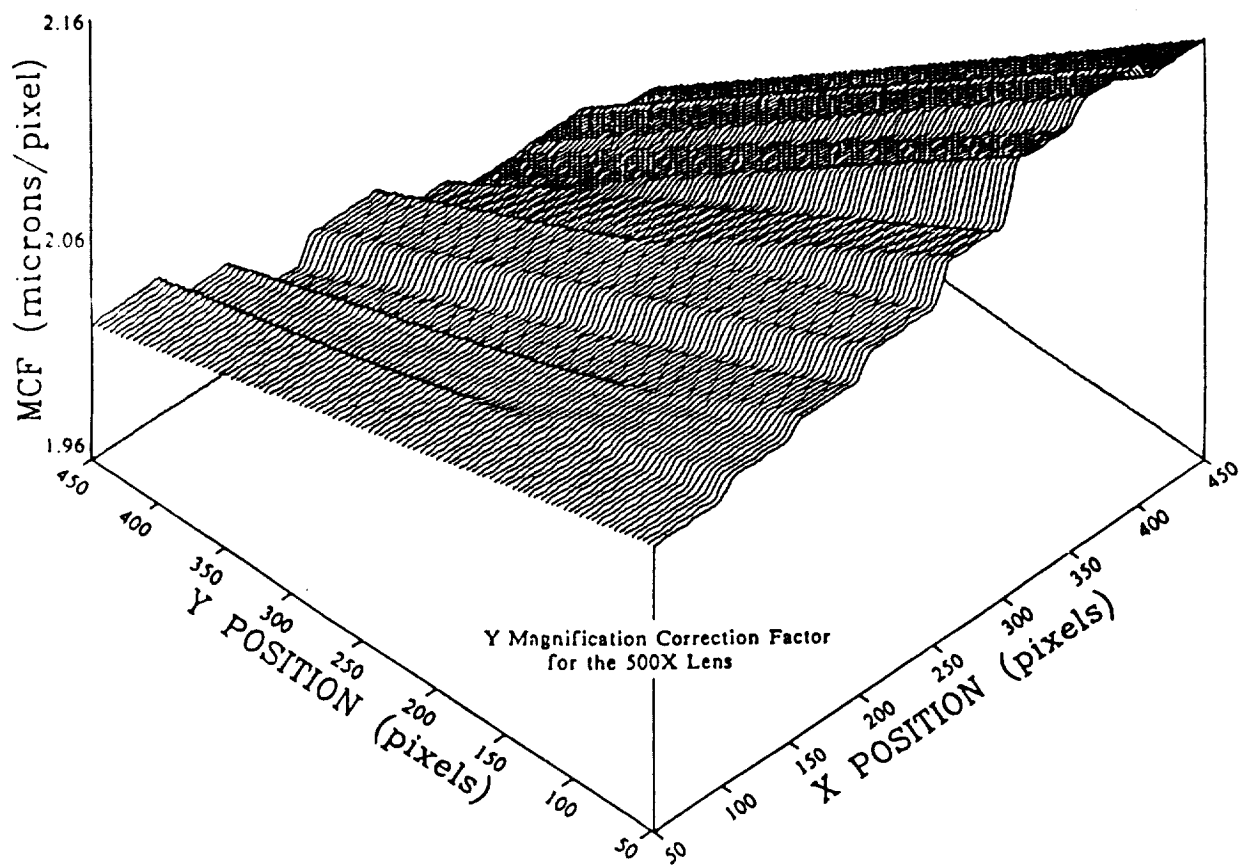


Figure 3.2: Magnification Correction Factor Behavior

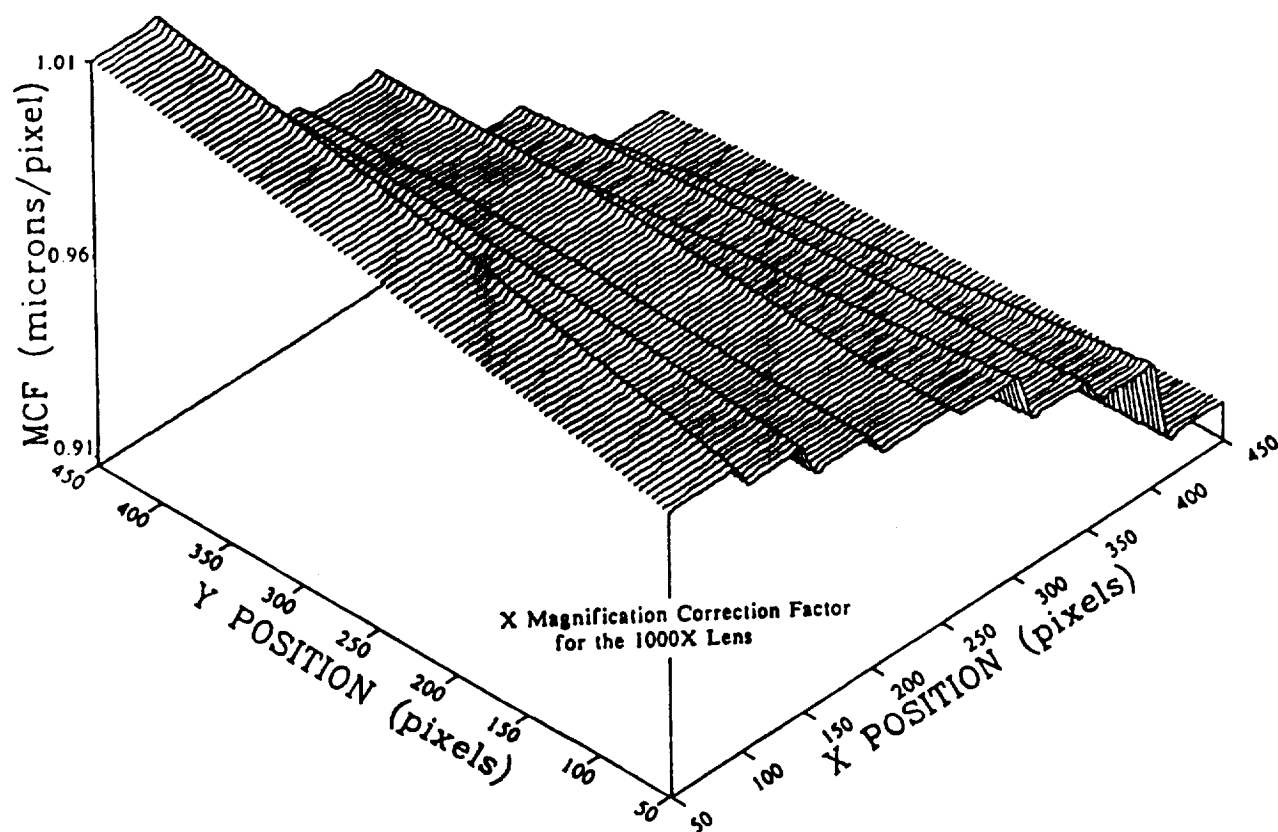


Figure 3.3: Magnification Correction Factor Behavior

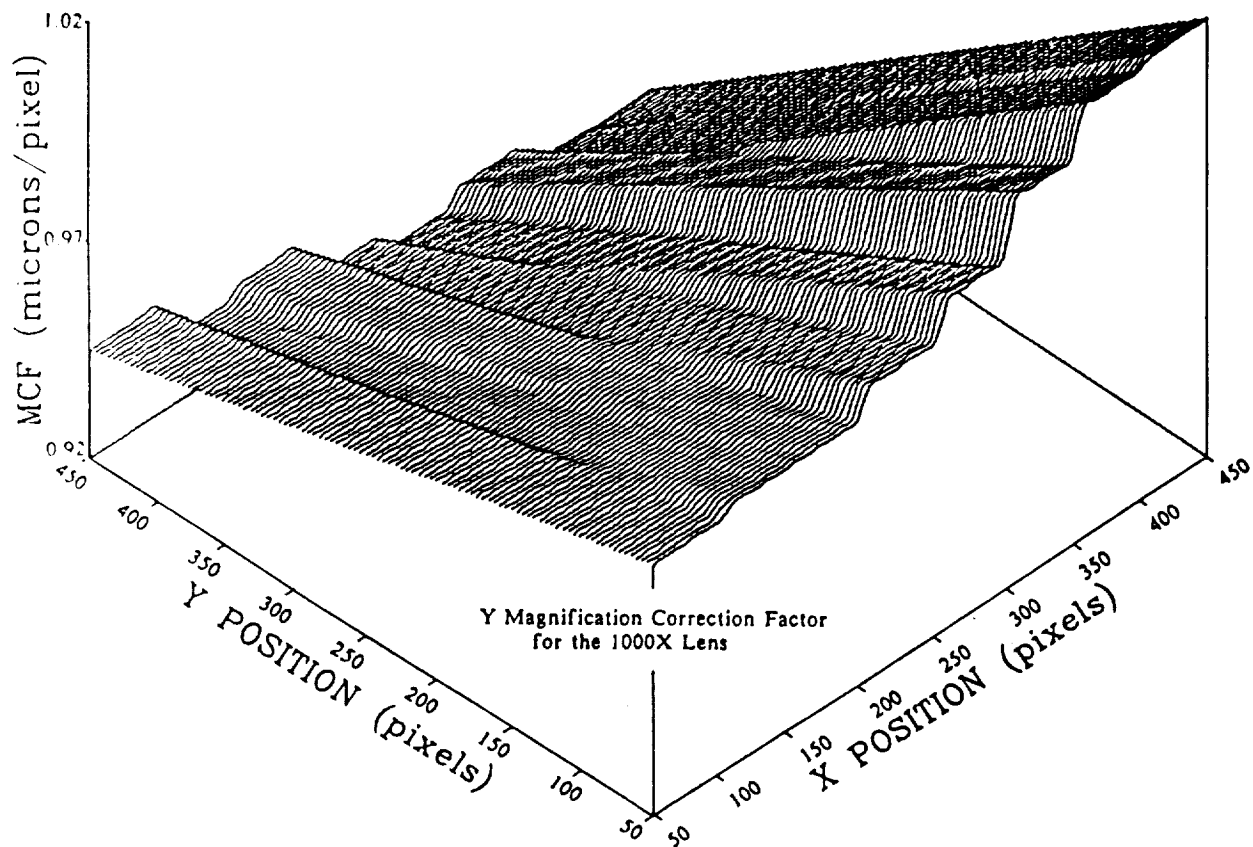


Figure 3.4: Magnification Correction Factor Behavior

#114 CALIBRATION RETICLE
 CALIBRATION FOR THE 500X LENS
 DATA TAKEN: 26-MAR-86 19:36:22
 CONSTANT THRESHOLD LEVEL = 90

Number of Frames in Analysis: 30					Particles Counted: 660				
Particle Count (#)	Actual Dia. (#)	Average Dia. (#)	Std. Dev. (#)	Diameter Size Range (#)	Average Error (#)	Error Std. Dev. (#)	Avg. % Error		
1	5.29	0.00	0.00	0.0 - 0.0	0.00	0.00	0.00 %		
2	6.81	5.45	0.81	4.2 - 7.9	1.81	0.51	26.58 %		
3	8.98	8.80	0.58	7.7 - 9.8	0.78	0.58	8.68 %		
4	11.93	10.03	0.33	10.4 - 11.9	0.33	0.43	2.77 %		
5	17.20	16.40	0.79	15.7 - 17.0	1.79	0.78	10.41 %		
6	21.33	20.46	0.45	20.0 - 21.2	1.23	0.45	5.77 %		
7	23.90	23.51	0.90	22.9 - 24.1	1.34	0.59	5.61 %		
8	26.71	27.18	0.71	26.3 - 27.8	0.81	0.61	3.03 %		
9	31.11	29.81	0.45	29.0 - 30.6	0.65	0.92	2.09 %		
10	34.17	35.51	0.37	34.2 - 35.9	0.67	0.47	1.86 %		
11	37.07	36.75	0.57	36.0 - 37.7	0.52	0.57	1.40 %		
12	40.47	40.01	0.67	39.3 - 41.1	0.67	0.47	1.66 %		
13	42.71	43.91	0.71	40.9 - 42.7	0.51	0.61	1.19 %		
14	47.37	48.31	0.56	47.3 - 49.8	0.69	0.66	1.41 %		
15	50.39	50.28	0.39	48.9 - 51.0	0.39	0.56	0.77 %		
16	52.50	51.98	0.50	49.8 - 52.8	0.54	0.34	1.03 %		
17	56.23	56.25	0.23	55.0 - 57.1	0.25	0.29	0.44 %		
18	60.70	60.85	0.70	60.0 - 63.5	0.63	0.57	1.04 %		
19	67.04	67.24	0.84	65.3 - 70.0	0.44	0.54	0.66 %		
20	73.45	73.35	0.38	71.4 - 76.1	2.82	0.36	3.84 %		
21	80.58	80.69	0.48	79.0 - 82.2	3.45	0.48	4.28 %		
22	86.99	87.10	0.57	86.2 - 88.3	1.57	0.37	1.80 %		
23	92.75	93.26	0.65	90.8 - 95.3	0.65	0.65	0.70 %		
Averages:				0.57	1.02	0.53	3.96 %		

Table 3.1: Calibration Accuracy Test

#114 CALIBRATION RETICLE
CALIBRATION FOR THE 1000X LENS
DATA TAKEN: 29-MAR-86 04:15:24
CONSTANT THRESHOLD LEVEL = 90

Number of Frames in Analysis: 30					Particles Counted: 690			
Particle (#)	Counts (#)	Actual Dia.	Average Dia.	Std. Dev.	Diameter Size Range	Average Error	Error Std. Dev.	Avg. % Error
1	30	5.29	4.93	0.89	3.3 - 7.2	1.78	1.03	33.65 %
2	30	6.81	8.76	0.81	4.2 - 7.8	1.21	0.31	17.77 %
3	30	8.98	8.67	0.58	7.7 - 9.9	0.38	0.28	4.23 %
4	30	11.93	11.40	0.33	9.9 - 13.1	0.63	0.33	5.28 %
5	30	17.20	16.67	0.29	15.5 - 19.4	0.79	0.58	4.59 %
6	30	21.33	21.03	0.15	19.7 - 23.2	0.83	0.25	3.89 %
7	30	23.90	23.69	0.24	21.3 - 24.6	0.74	0.19	3.10 %
8	30	26.71	26.78	0.32	25.8 - 27.3	1.11	0.31	4.16 %
9	30	31.11	30.67	0.27	28.7 - 33.7	1.02	0.42	3.28 %
10	30	34.17	34.33	0.29	31.4 - 36.5	0.77	0.42	2.25 %
11	30	37.07	37.02	0.50	36.0 - 39.3	0.57	0.17	1.54 %
12	30	40.47	39.78	0.27	38.4 - 42.9	0.67	0.57	4.13 %
13	30	42.71	41.87	0.31	40.3 - 43.6	0.45	0.41	3.39 %
14	30	47.37	47.77	0.22	46.3 - 50.2	0.37	0.23	0.78 %
15	30	50.39	49.89	0.30	47.9 - 51.2	0.76	0.36	1.51 %
16	30	52.50	52.78	0.17	50.2 - 53.5	0.34	0.32	0.65 %
17	30	56.23	56.02	0.23	54.5 - 57.2	1.25	0.21	2.22 %
18	30	60.70	61.01	0.15	59.0 - 63.3	1.96	0.45	3.23 %
19	30	67.04	67.33	0.13	65.2 - 71.4	0.40	0.42	0.60 %
20	30	73.45	73.38	0.18	72.1 - 77.3	0.34	0.32	0.46 %
21	30	80.58	79.88	0.28	78.3 - 83.7	0.43	0.40	0.53 %
22	30	86.99	87.21	0.31	85.8 - 89.3	1.23	0.39	1.14 %
23	30	92.75	92.78	0.25	90.2 - 97.3	0.35	0.28	0.38 %
Averages:						1.02	0.38	4.48 %

Table 3.2: Calibration Accuracy Test

Table 3.3 shows the average percent error for the above calibration accuracy tests with the previous work of Ahlers [7] and Wiles [10]. A comparison of the average % error for the three accuracy tests performed on the 500X lens shows a decrease in the % error from the one-dimensional MCF test (i.e., 4.04% error) to the two-dimensional MCF tests (i.e., for Wiles - 2.73% error and for this work - 3.96% error). The % error values for the test performed on the 1000X lens show an increase in LI/VPS accuracy for all the particles measured by the 500X lens tests. The inclusion of the 5.29 μm particle in the analysis shows an increased sizing range, as opposed to previous tests.

The following results represent the initial method used to compare the P/DPA and the LI/VPS. As specified earlier, the probe volumes of the two instruments were overlapped, and due to the steady state operation of the VOAG, samples by both instruments were assumed to be nearly identical. Two separate cases were performed to verify instrument operation and accuracy. The first case was performed with the VOAG producing a steady single stream of drops which passed through the concurrent probe volumes, and secondly, the dispersion cup (Fig. 2.26) was utilized to produce a spray of monodisperse droplets which randomly pass through the concurrent probe volumes. Nine separate tests were performed for each case with the instrument results represented in Figs. 3.5 thru 3.13 for the case without the dispersion cup, and Figs. 3.14 thru 3.22 for the case with the dispersion cup. Figures 3.23 and 3.24 show the TSI theoretical diameter, and the arithmetic mean diameters from the LI/VPS and the P/DPA distributions as functions of test number. Data in Table 3.4 has been plotted in Fig. 3.23 and 3.24 with the standard deviation (SD) also shown. The arithmetic mean diameters of the LI/VPS and the P/DPA agree, on the most part, with each other and the theoretical expected diameter within $\pm 2.6 \mu\text{m}$. The SD of the samples is shown to illustrate the monodisperse behavior of the VOAG and the ability of the LI/VPS and the P/DPA to measure the monodisperse aerosol spray. The highest SD (i.e., 1.109 μm) determined for the LI/VPS is shown in CASE II - Test 5, and for the P/DPA, the highest SD (i.e., 2.073 μm) is shown in CASE I - Test 1.

Referring to Table 3.4, the first test in both cases show the maximum SD for P/DPA. The arithmetic mean diameters, 20.5 μm for CASE I and 21.5 μm for CASE II, are within 2.0 μm of the expected diameter, 19.8 μm . The SD of the samples may be higher than the rest, due to the high density of drops passing through the P/DPA probe volume. This phenomena was especially noticeable in CASE II test runs where the dispersion cup was used. As was expected, the SD for most of the tests increased from CASE I to CASE II. The above behavior was expected, due to the increase in number of drops passing through the edges of the probe volumes.

3.2 Results For the MOD-1 Nozzle Comparison

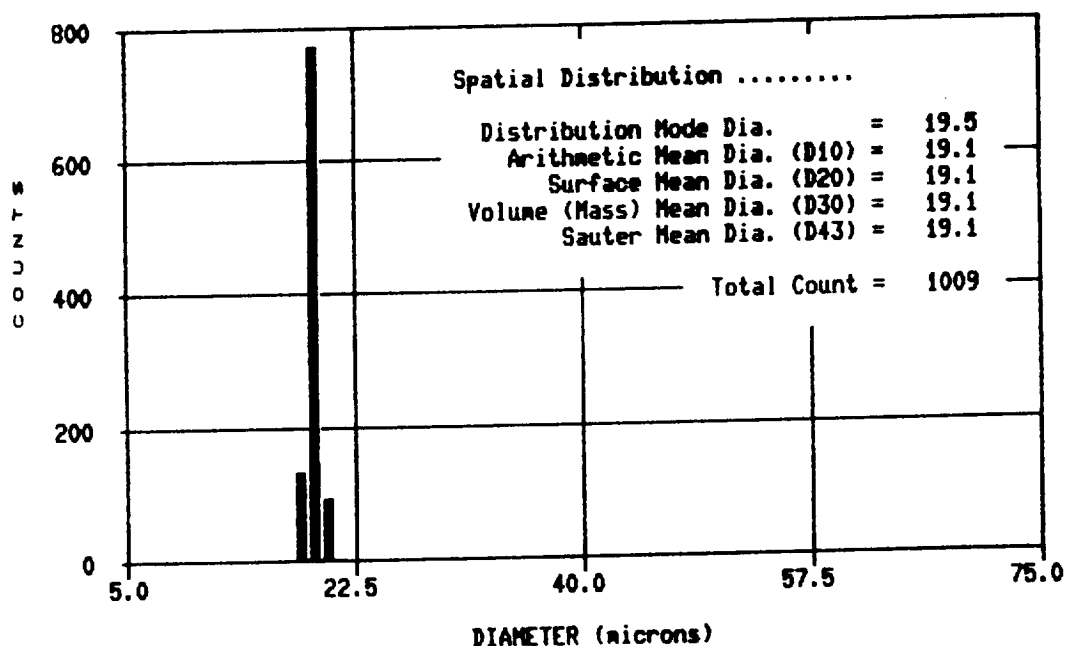
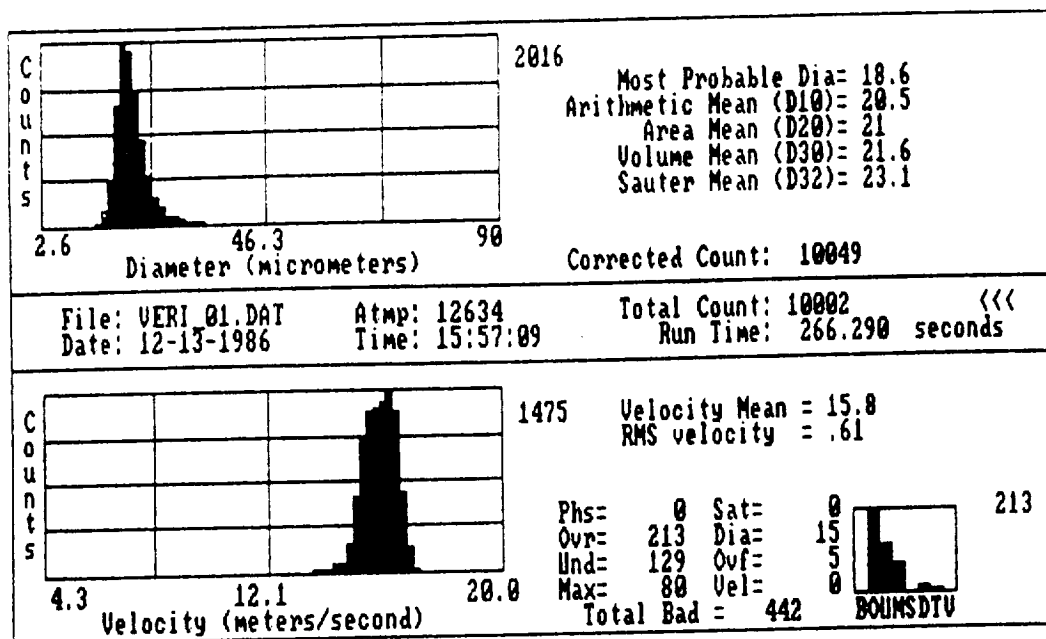
The following results represent a comparison of the LI/VPS and the P/DPA in side-by-side benchmark tests performed on a NASA MOD-1 atomizing nozzle. As previously stated, two cases (i.e., variation in the operating conditions of the nozzle) were studied. For each case, eight data runs (i.e., a data run was performed on the centerline, two feet down-stream from the nozzle with succeeding data runs performed at one-half inch increments radially outward to the edge of the dispersion) were performed by the LI/VPS and the P/DPA using a procedure similar to the VOAG analysis. Figures 3.25 - 3.32 and Figs. 3.33 - 3.40 are the results from the P/DPA and the LI/VPS for CASE I (i.e., nozzle conditions: Air pressure = 65 psia and Water pressure = 105 psia.) and CASE II (i.e., nozzle conditions: Air pressure = 45 psia and Water pressure = 115 psia), respectively.

Table 3.2: Calibration Accuracy Test

CALIBRATION RETICLE : RR-50-3.0-0.08-102-CF - #114

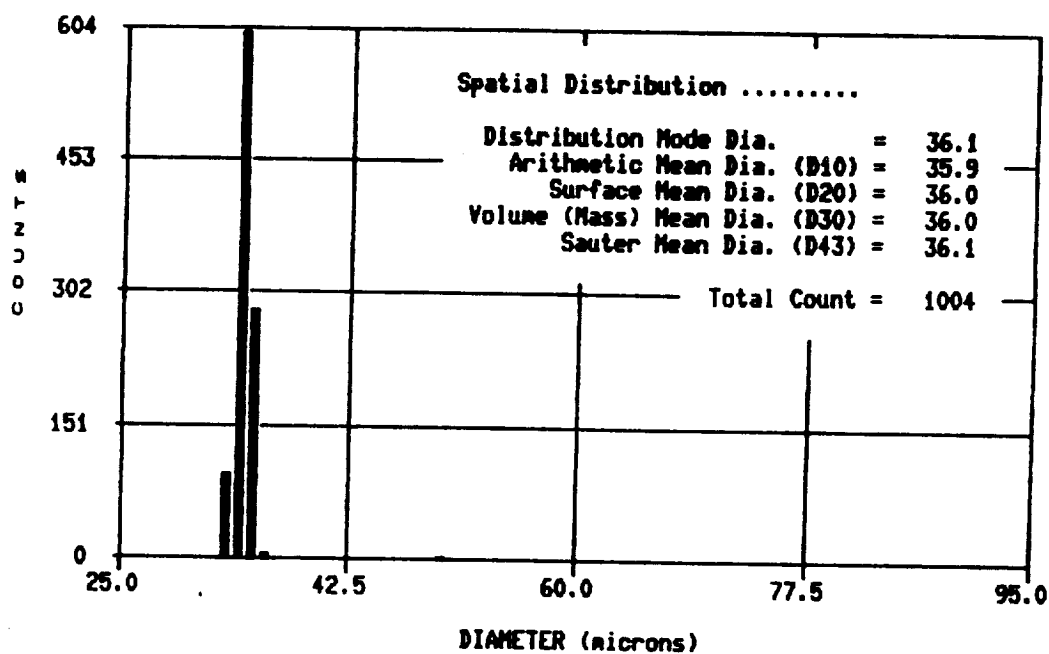
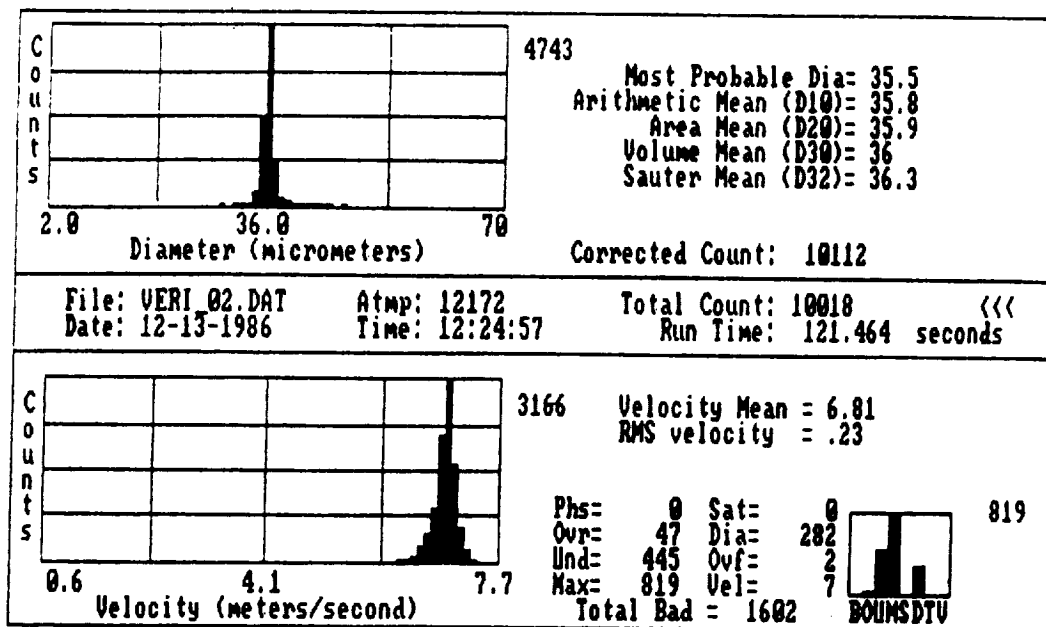
PART. (#)	DIAMETER (μm) ¹	<u>For the 500X Lens.</u>		<u>For the 1000X Lens.</u>	
		Ahlers' TEST [7] Avg. % Error	Wiles' TEST [10] Avg. % Error	Current TEST Avg. % Error	Current TEST Avg. % Error
1	5.29	0.00	0.00	0.00	33.65
2	6.81	17.75	16.06	26.58	17.77
3	8.98	7.66	7.40	8.69	4.23
4	11.93	12.12	7.53	2.77	5.28
5	17.20	3.64	1.52	10.41	4.59
6	21.33	3.33	2.04	5.77	3.89
7	23.90	2.05	2.19	5.61	3.10
8	26.71	3.01	3.89	3.03	4.16
9	31.11	5.06	1.66	2.09	3.28
10	34.17	3.27	1.66	3.43	2.25
11	37.07	2.34	1.21	1.79	1.54
12	40.47	1.04	1.91	1.66	4.13
13	42.71	1.50	2.50	1.19	3.39
14	47.37	3.96	1.52	1.41	0.78
15	50.39	3.44	0.94	0.77	1.51
16	52.50	2.06	1.21	1.03	0.65
17	56.23	1.35	1.09	0.44	2.22
18	60.70	0.91	1.33	1.04	3.23
19	67.04	4.50	0.83	0.66	0.60
20	73.48	3.02	1.25	3.84	0.46
21	80.58	2.50	0.76	4.28	0.53
22	86.99	1.45	0.88	1.80	1.41
23	92.75	0.92	0.67	0.70	0.38
AVERAGES:		4.04	2.73	3.96	4.48

¹ Diameters traceable to NBS Part. #52577,
accurate to $\pm 2 \mu\text{m}$ ($\pm 3\%$ for $D > 70 \mu\text{m}$)



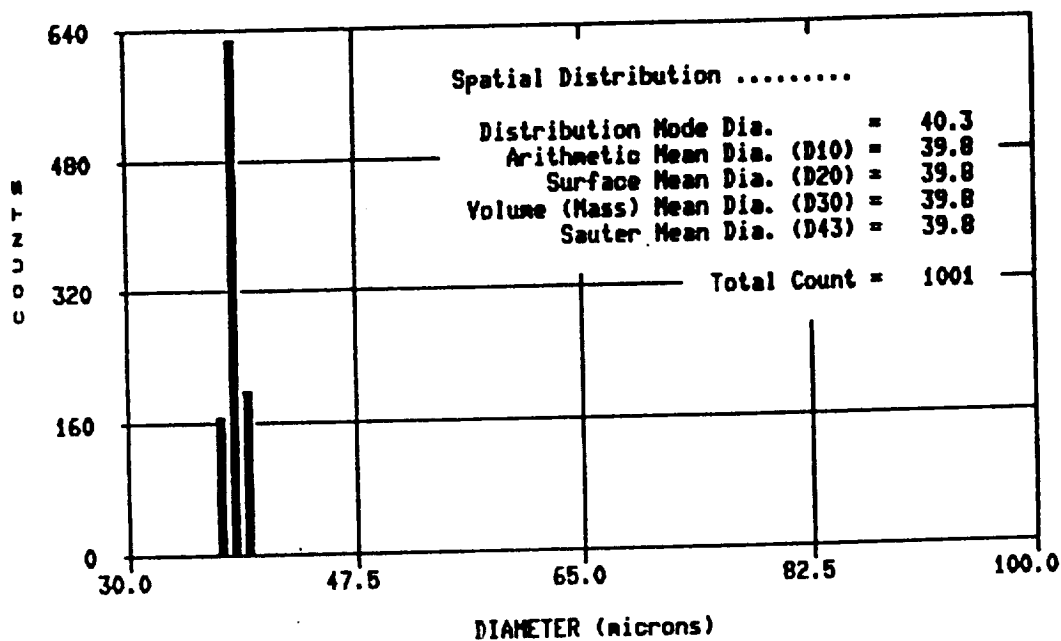
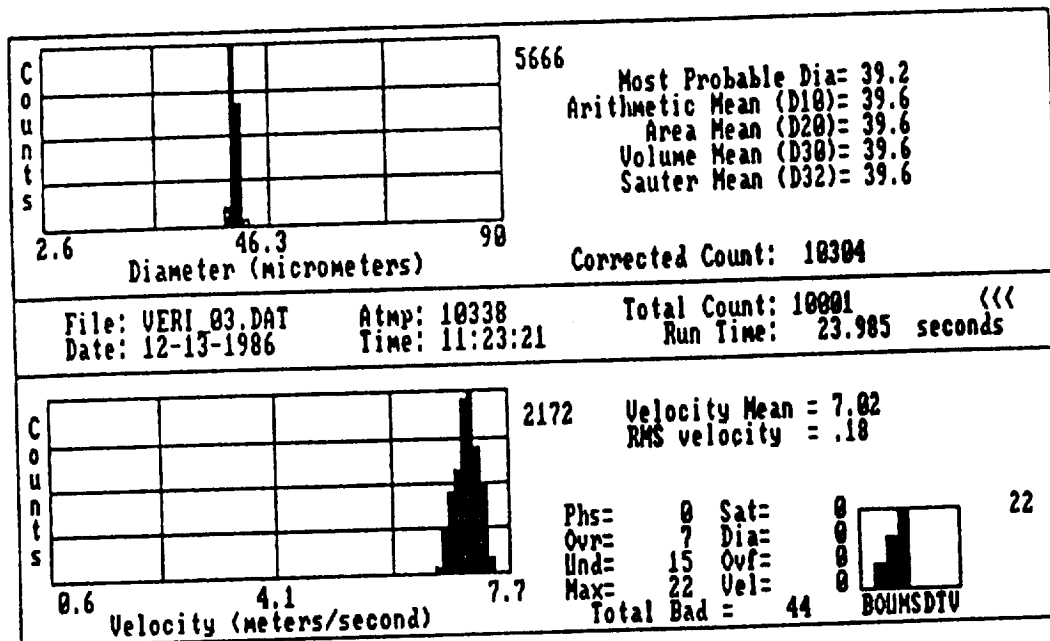
Theoretical Diameter = 19.8 μm
 Diameter of Orifice = 10 μm
 Liquid Feedrate = 0.08 cm^3/min .
 Vibration Frequency = 330.4 kHz

Figure 3.5: VOAG Verification w/o Dispersion Cup



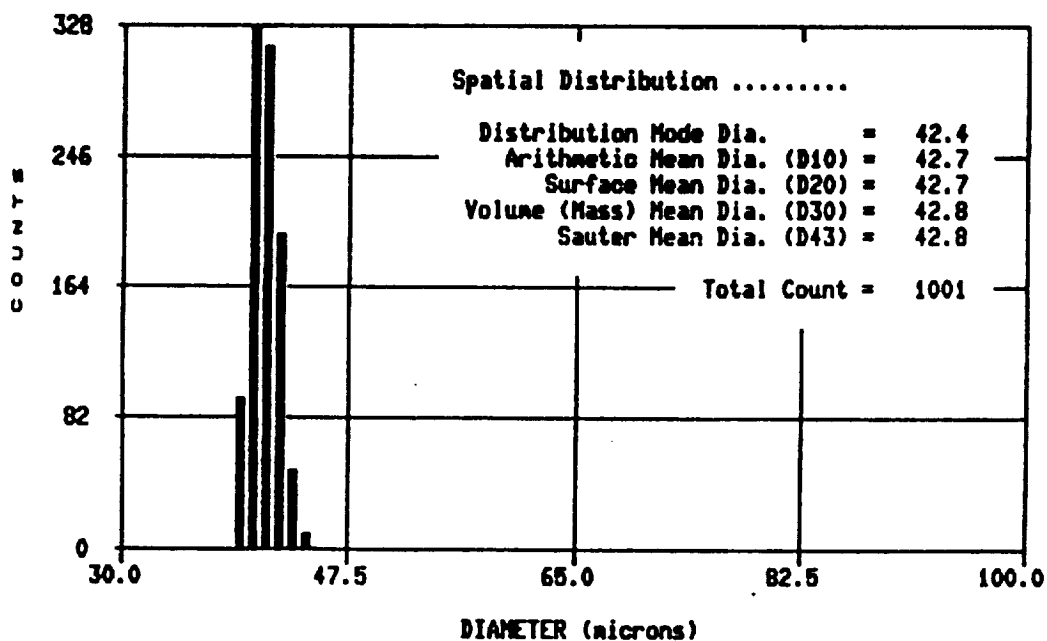
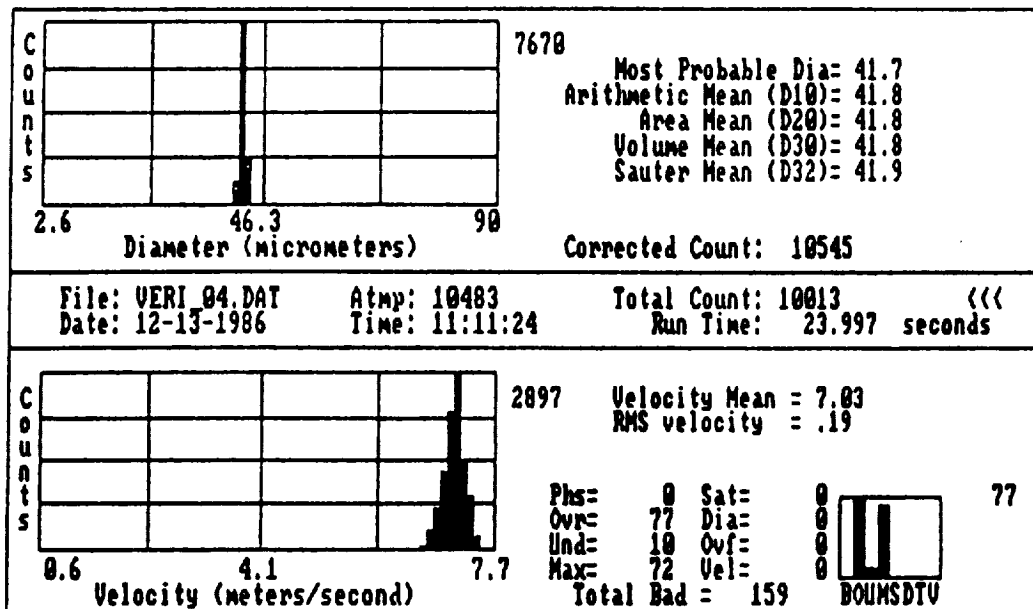
Theoretical Diameter = 35.5 μm
 Diameter of Orifice = 20 μm
 Liquid Feedrate = 0.139 cm^3/min .
 Vibration Frequency = 100.2 kHz

Figure 3.6: VOAG Verification w/o Dispersion Cup



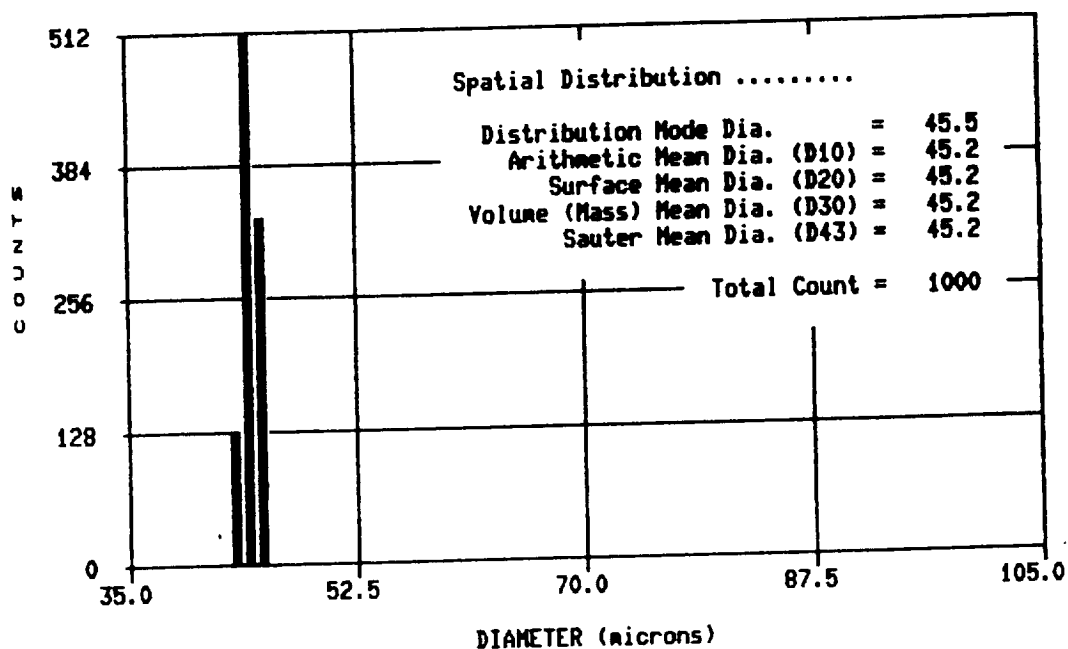
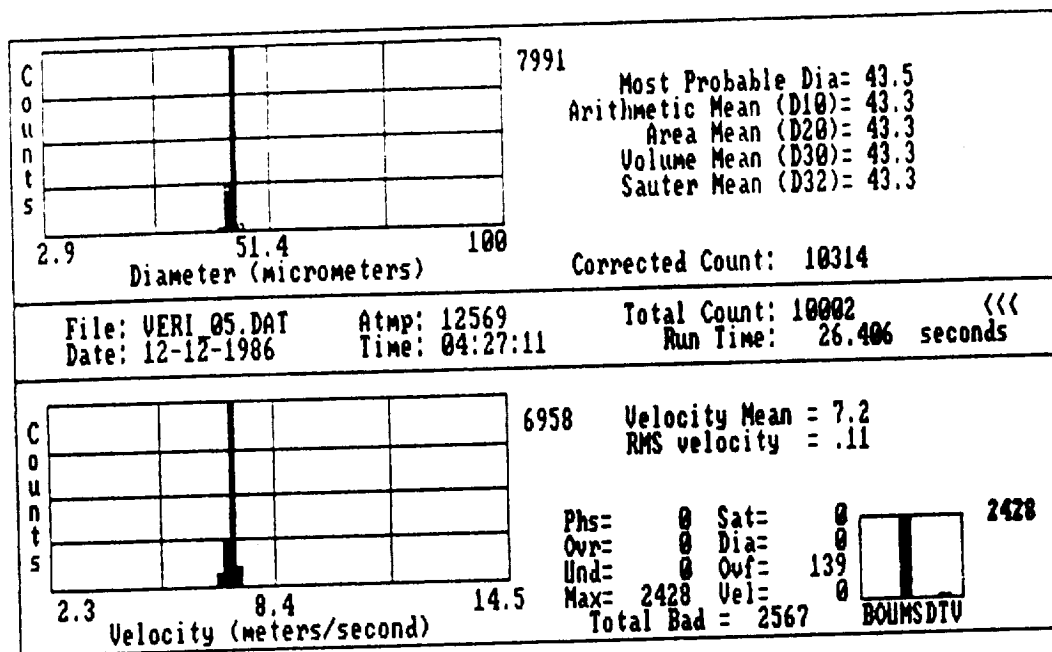
Theoretical Diameter = 39.0 μm
 Diameter of Orifice = 20 μm
 Liquid Feedrate = 0.139 cm^3/min .
 Vibration Frequency = 79.2 kHz

Figure 3.7: VOAG Verification w/o Dispersion Cup



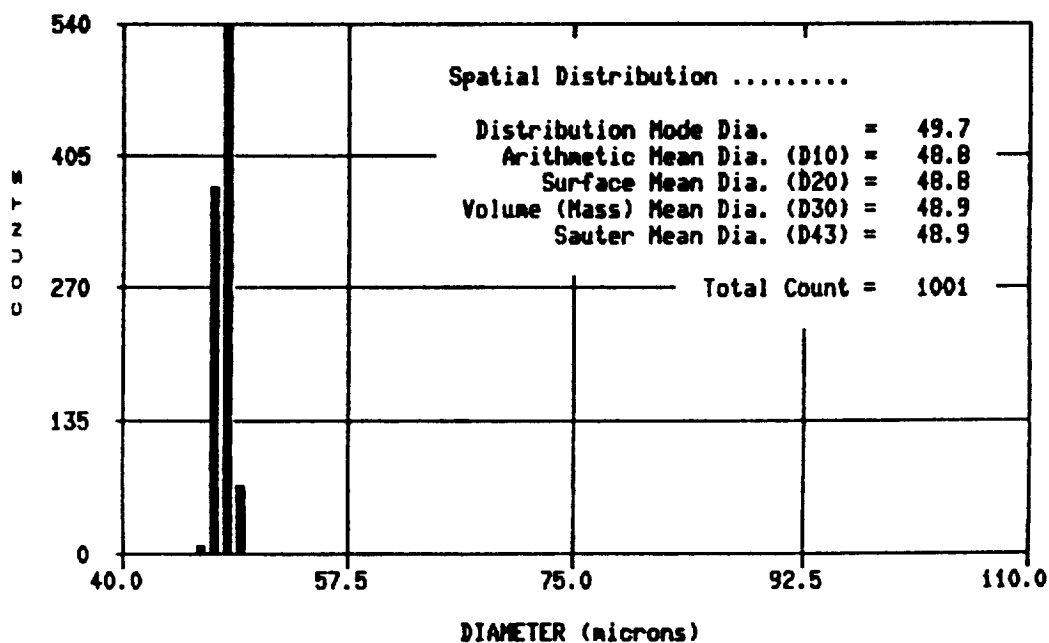
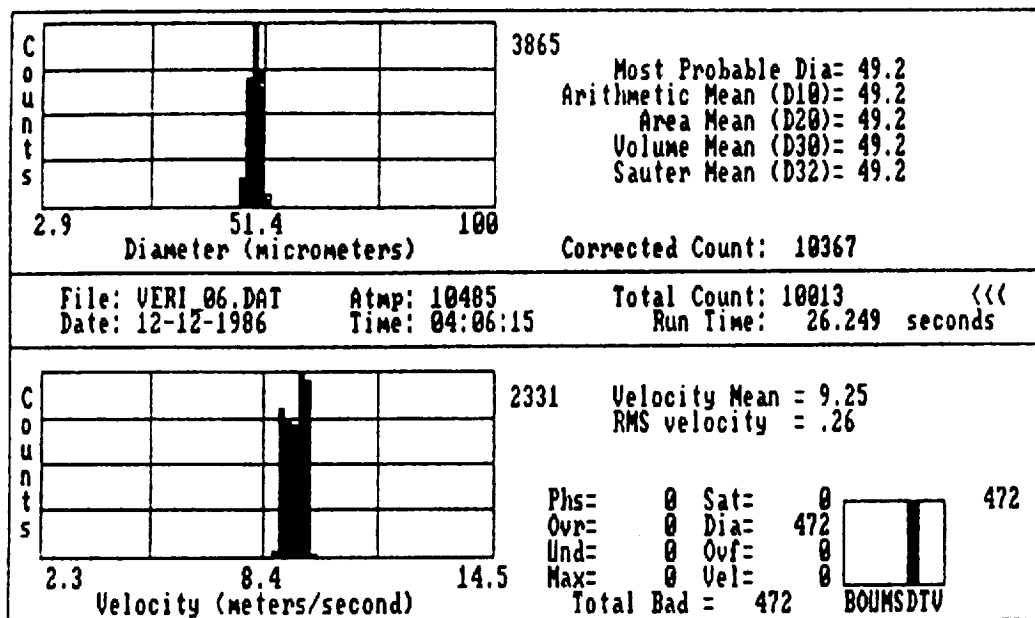
Theoretical Diameter = 41.5 μm
 Diameter of Orifice = 20 μm
 Liquid Feedrate = 0.139 $\text{cm}^3/\text{min.}$
 Vibration Frequency = 62.5 kHz

Figure 3.8: VOAG Verification w/o Dispersion Cup



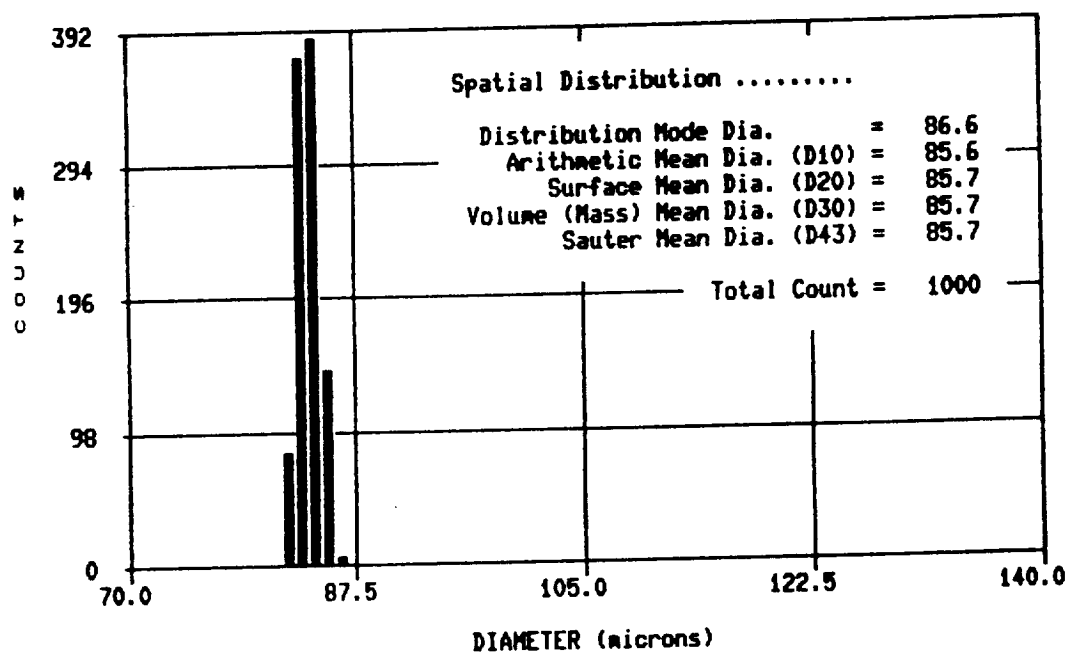
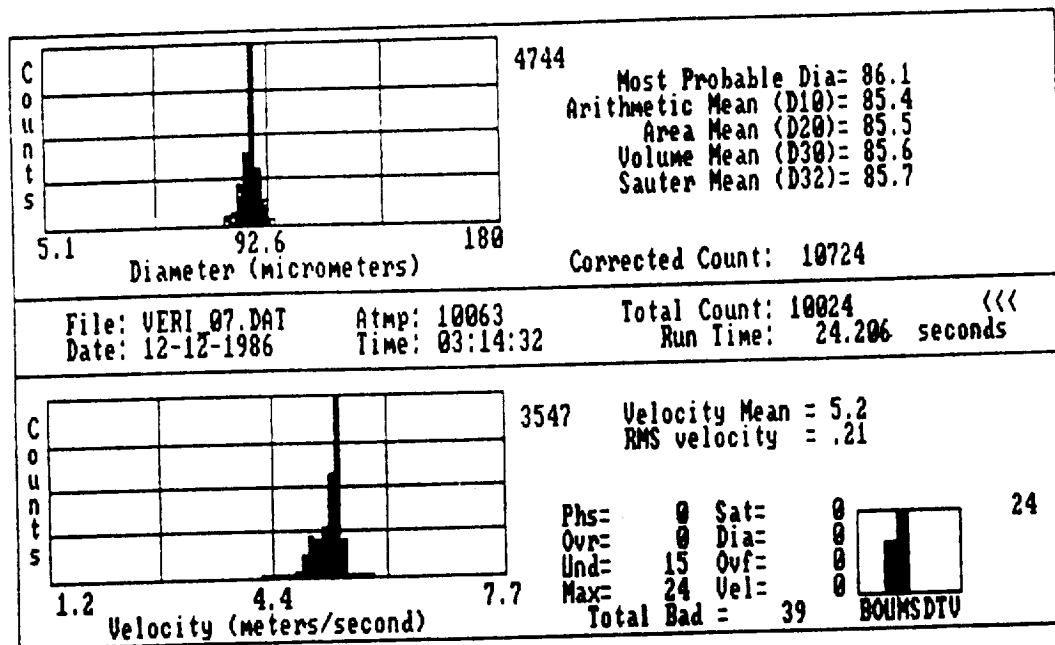
Theoretical Diameter = 44.2 μm
 Diameter of Orifice = 20 μm
 Liquid Feedrate = 0.139 $\text{cm}^3/\text{min.}$
 Vibration Frequency = 51.6 kHz

Figure 3.9: VOAG Verification w/o Dispersion Cup



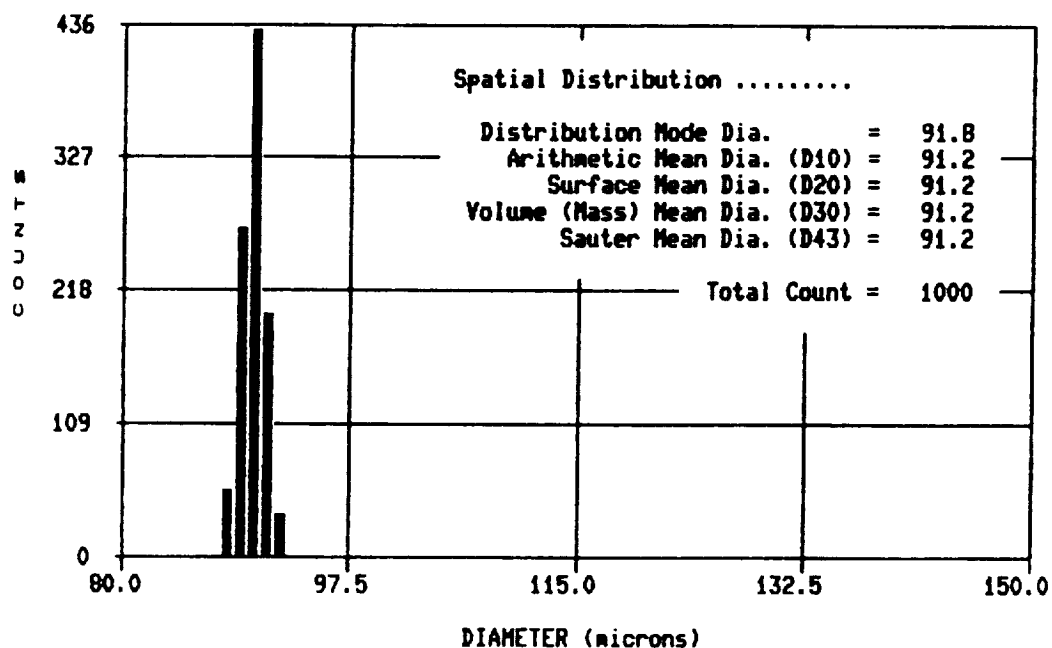
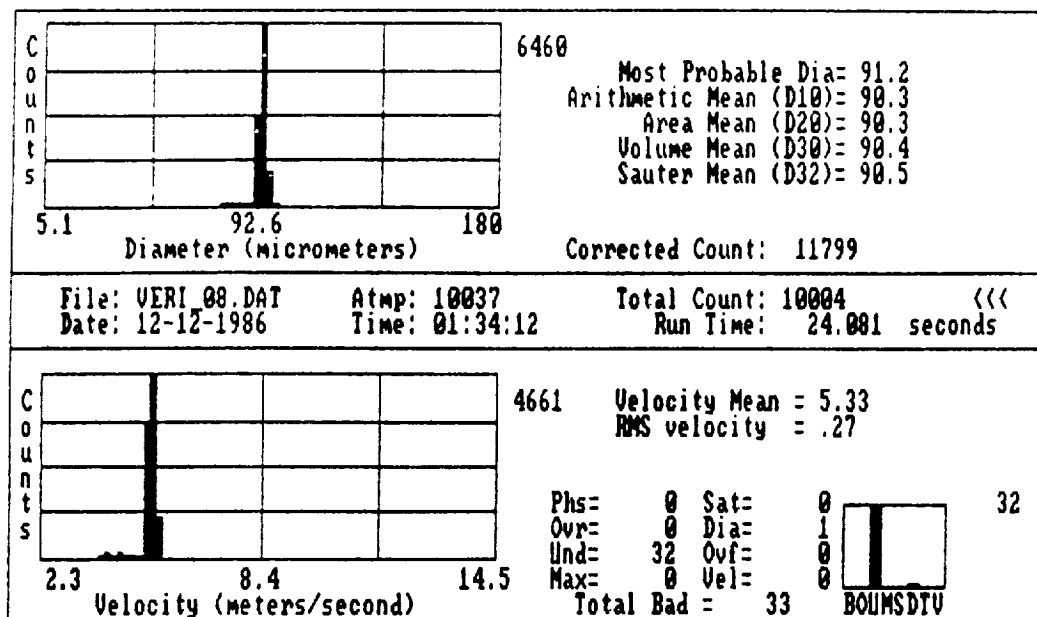
Theoretical Diameter = 47.5 μm
 Diameter of Orifice = 20 μm
 Liquid Feedrate = 0.139 cm^3/min .
 Vibration Frequency = 41.6 kHz

Figure 3.10: VOAG Verification w/o Dispersion Cup



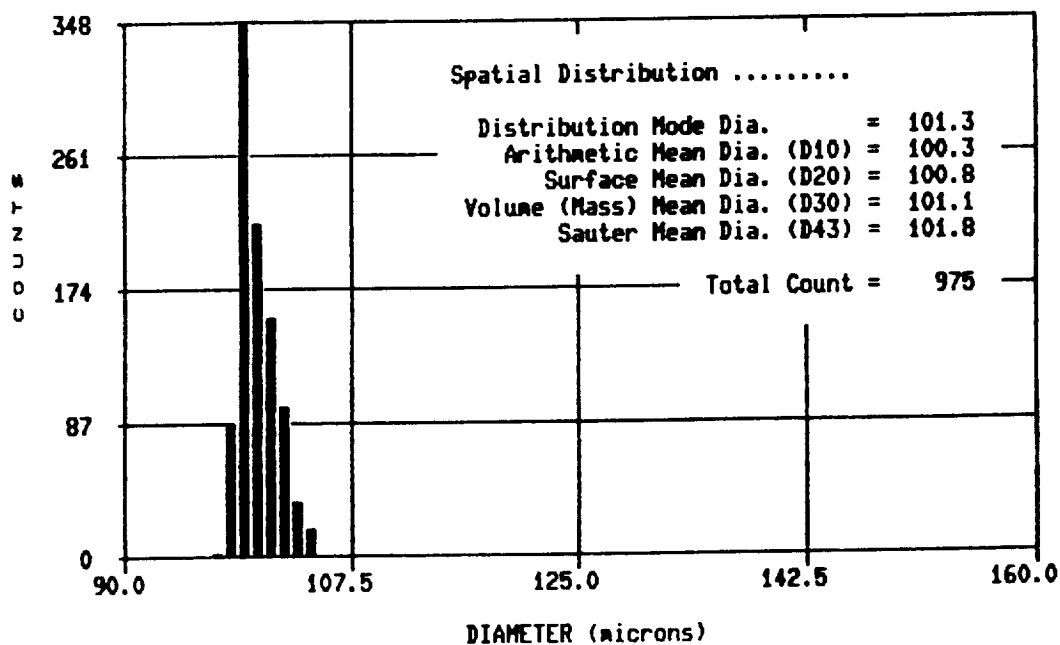
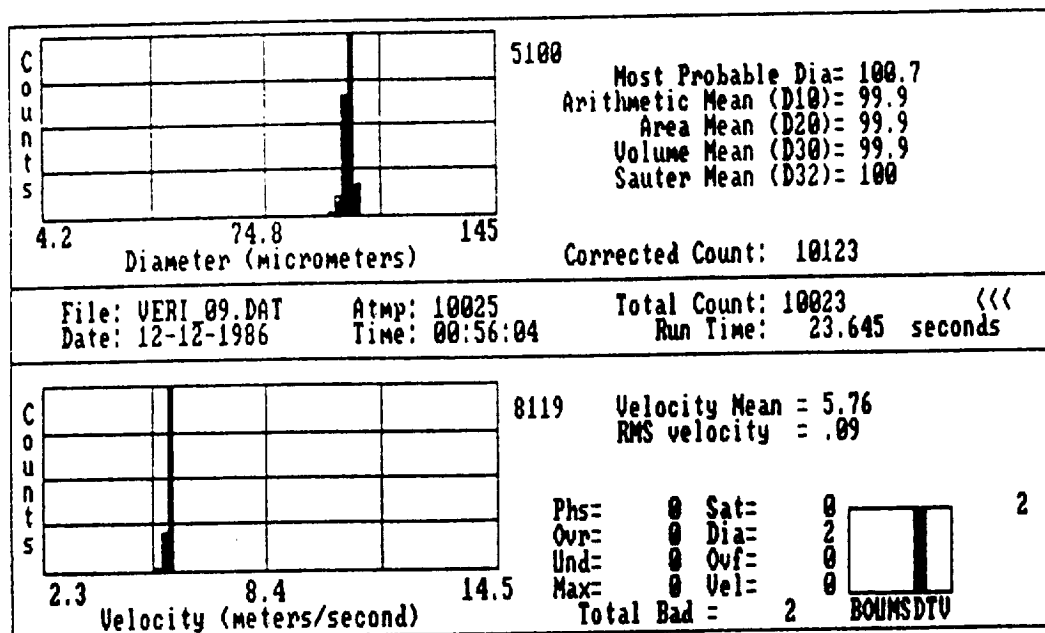
Theoretical Diameter = 85.6 μm
 Diameter of Orifice = 50 μm
 Liquid Feedrate = 0.59 cm^3/min .
 Vibration Frequency = 30.1 kHz

Figure 3.11: VOAG Verification w/o Dispersion Cup



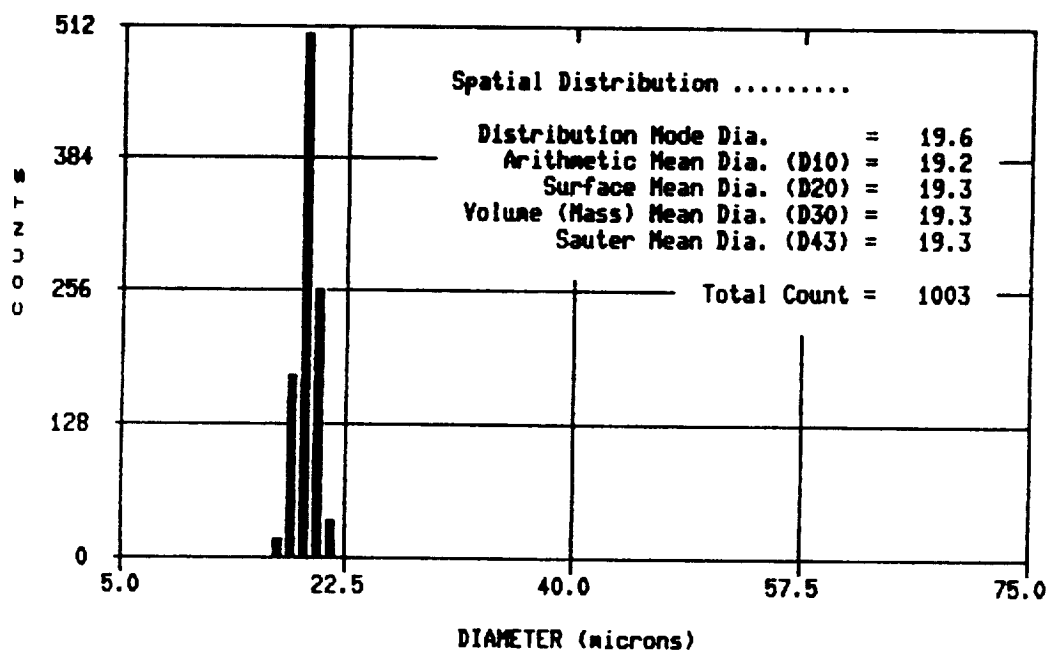
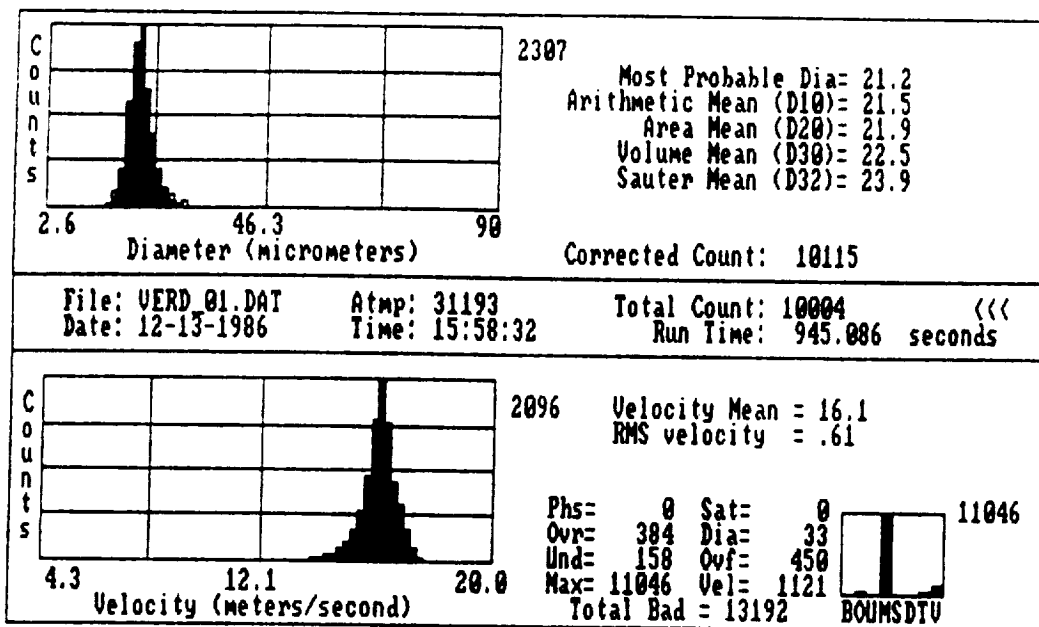
Theoretical Diameter = 90.4 μm
 Diameter of Orifice = 50 μm
 Liquid Feedrate = 0.59 cm^3/min .
 Vibration Frequency = 25.5 kHz

Figure 3.12: VOAG Verification w/o Dispersion Cup



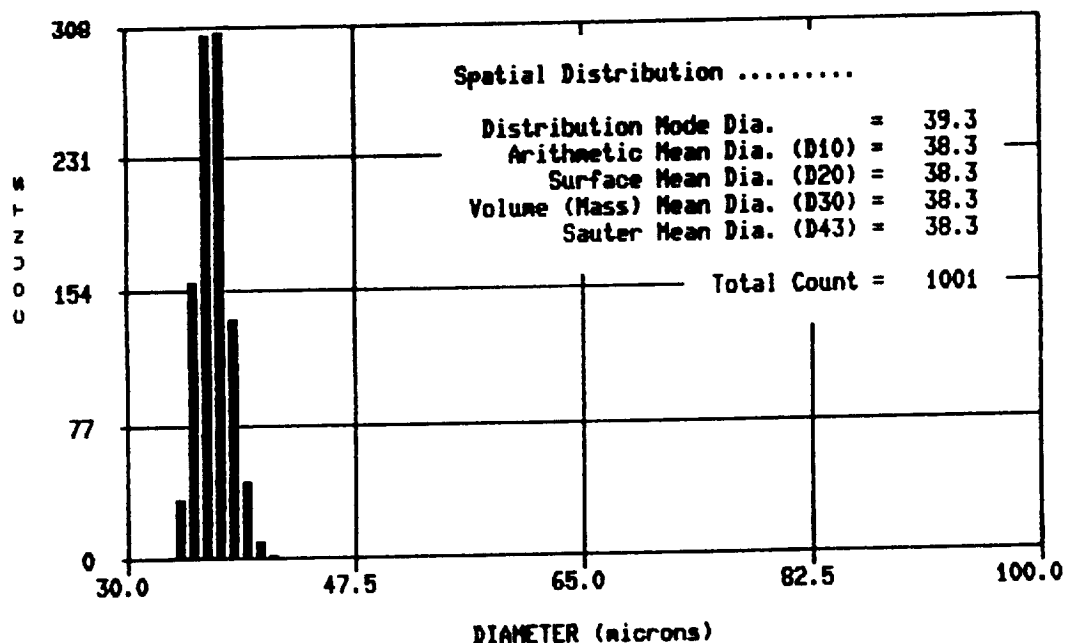
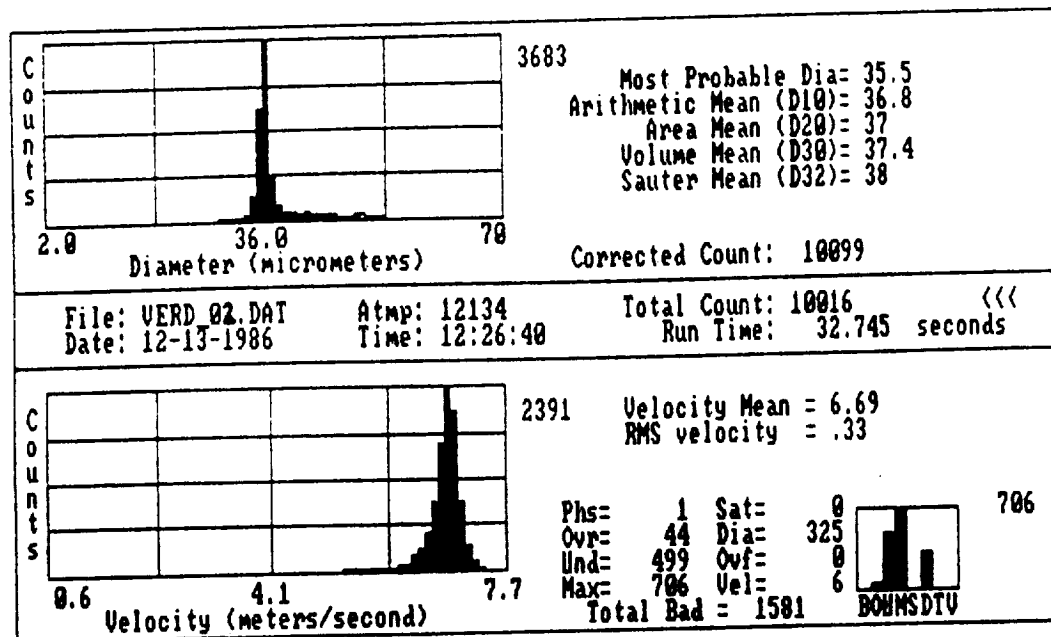
Theoretical Diameter = 99.6 μm
 Diameter of Orifice = 50 μm
 Liquid Feedrate = 0.59 $\text{cm}^3/\text{min.}$
 Vibration Frequency = 19.0 kHz

Figure 3.13: VOAG Verification w/o Dispersion Cup



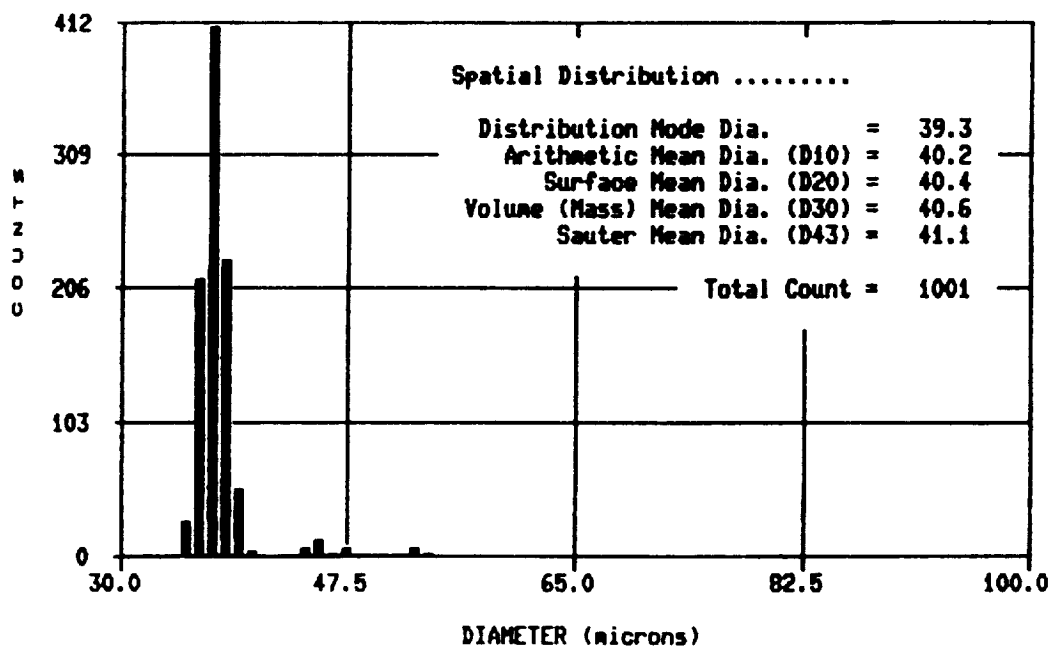
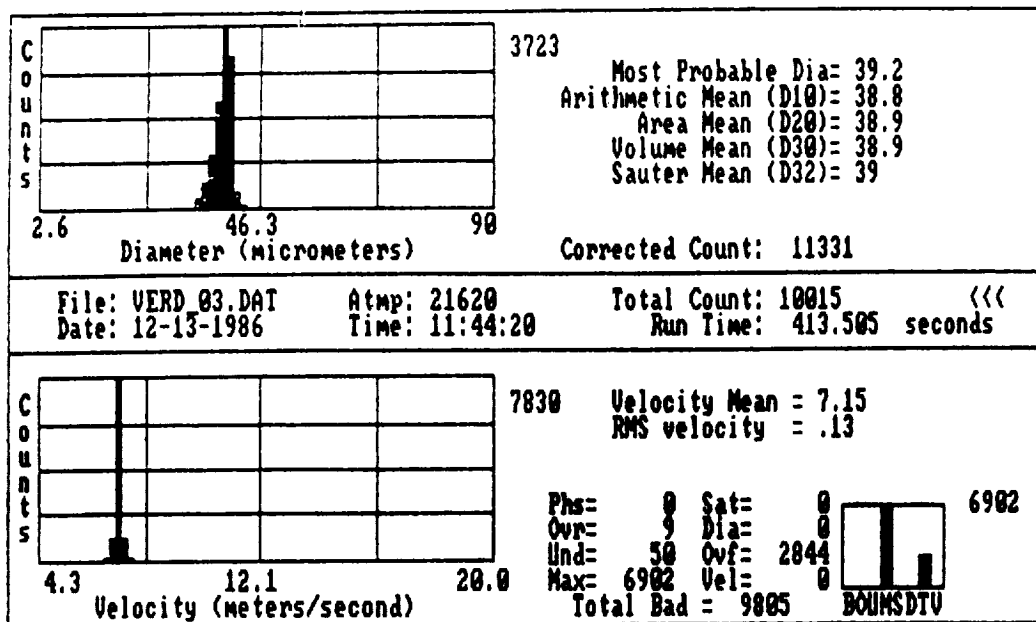
Theoretical Diameter = 19.8 μm
 Diameter of Orifice = 10 μm
 Liquid Feedrate = 0.08 cm^3/min .
 Vibration Frequency = 330.4 kHz

Figure 3.14: VOAG Verification w/ Dispersion Cup



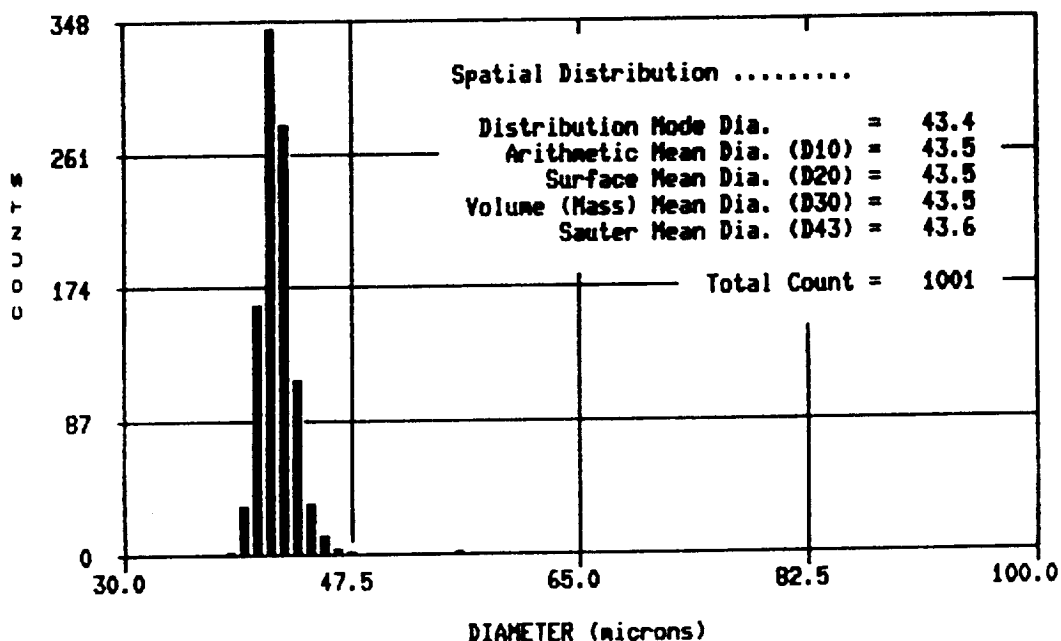
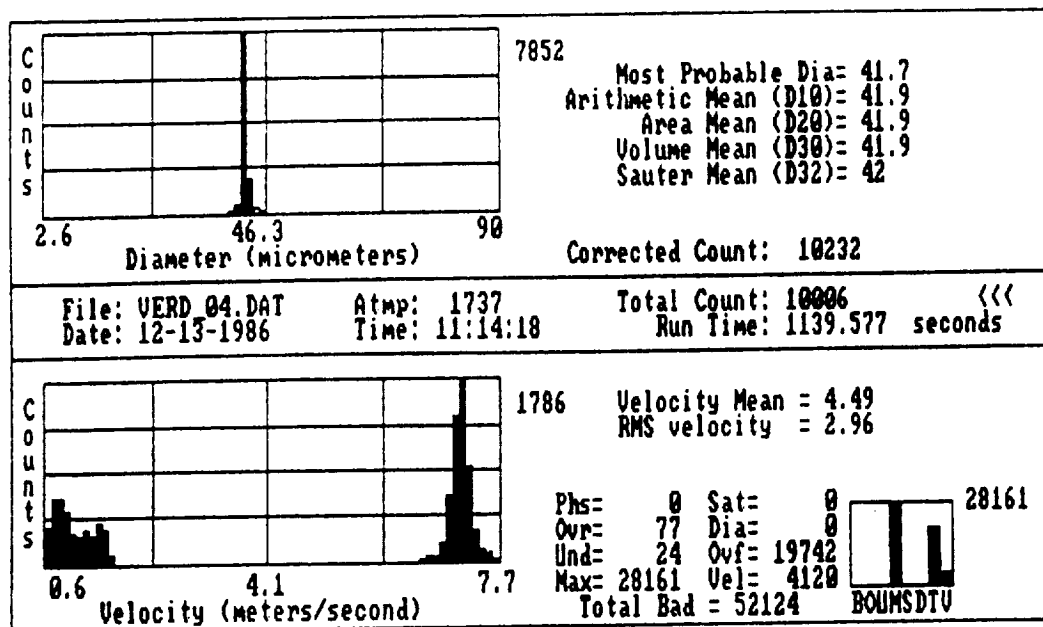
Theoretical Diameter = 35.5 μm
 Diameter of Orifice = 20 μm
 Liquid Feedrate = 0.139 $\text{cm}^3/\text{min.}$
 Vibration Frequency = 100.2 kHz

Figure 3.15: VOAG Verification w/ Dispersion Cup



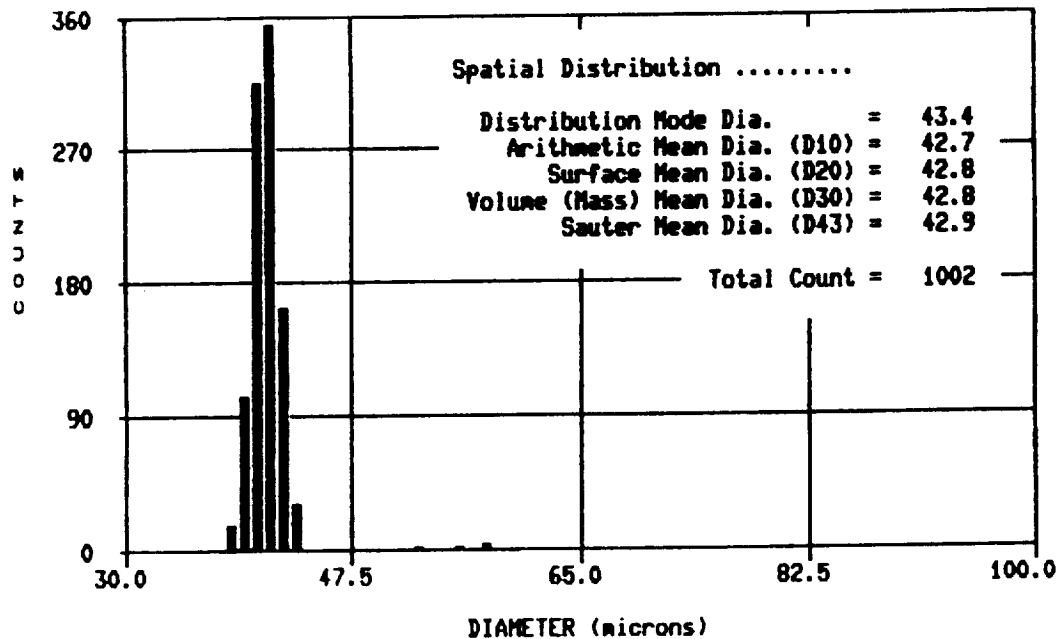
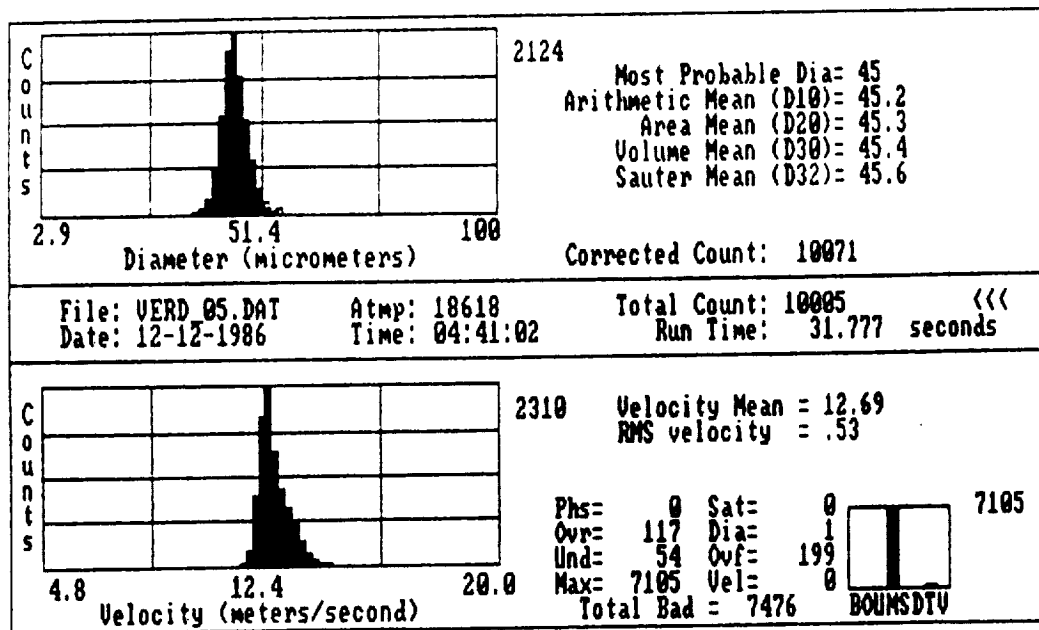
Theoretical Diameter = 39.0 μm
 Diameter of Orifice = 20 μm
 Liquid Feedrate = 0.139 cm^3/min .
 Vibration Frequency = 79.2 kHz

Figure 3.16: VOAG Verification w/ Dispersion Cup



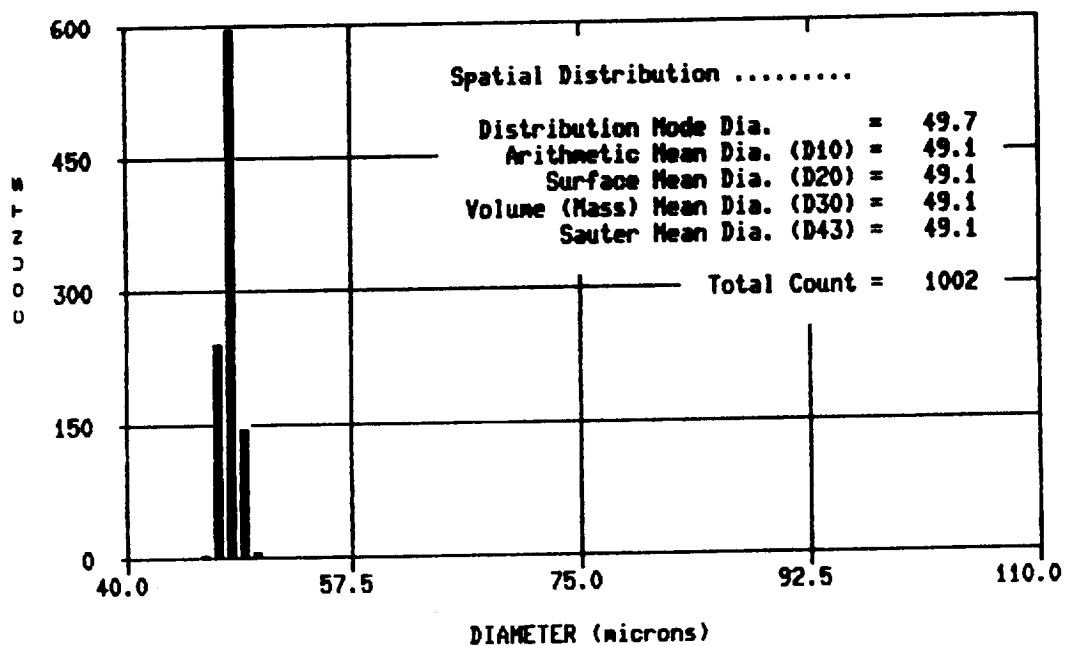
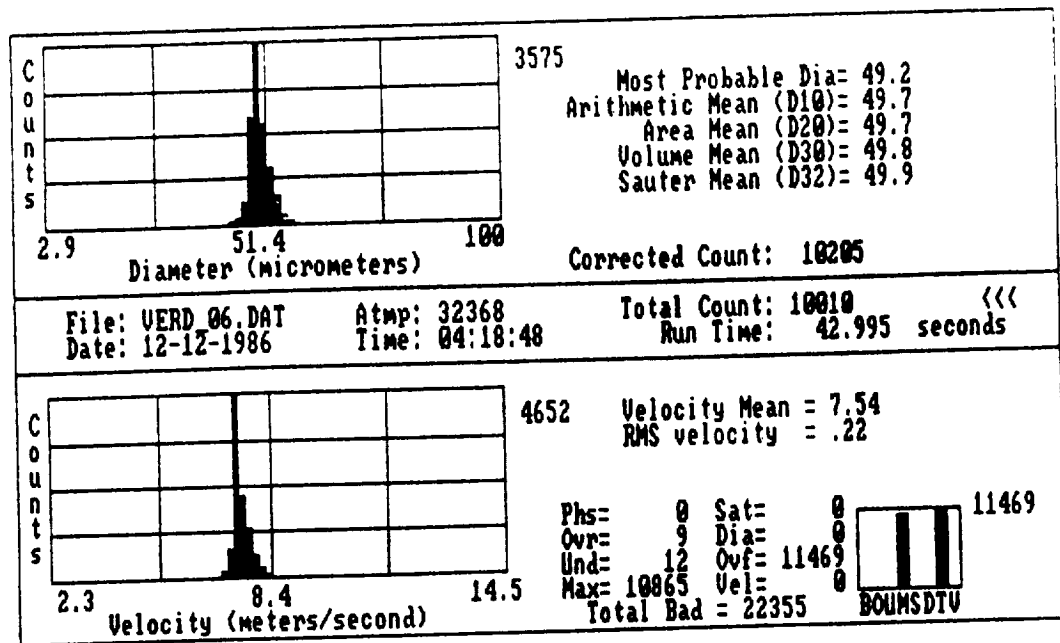
Theoretical Diameter = 41.5 μm
 Diameter of Orifice = 20 μm
 Liquid Feedrate = 0.139 $\text{cm}^3/\text{min.}$
 Vibration Frequency = 62.5 kHz

Figure 3.17: VOAG Verification w/ Dispersion Cup



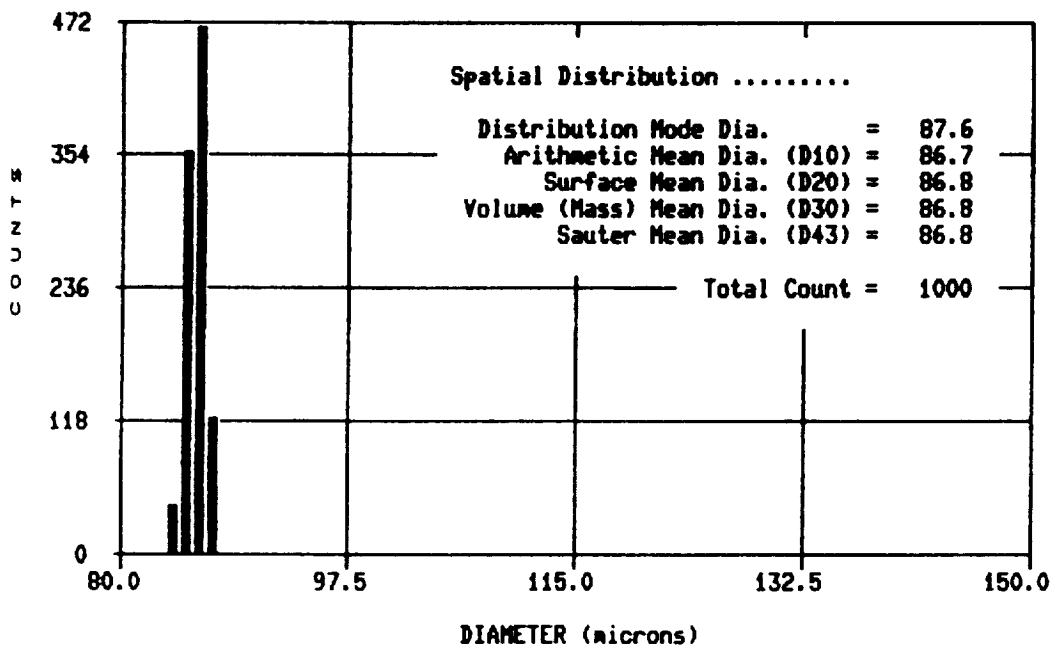
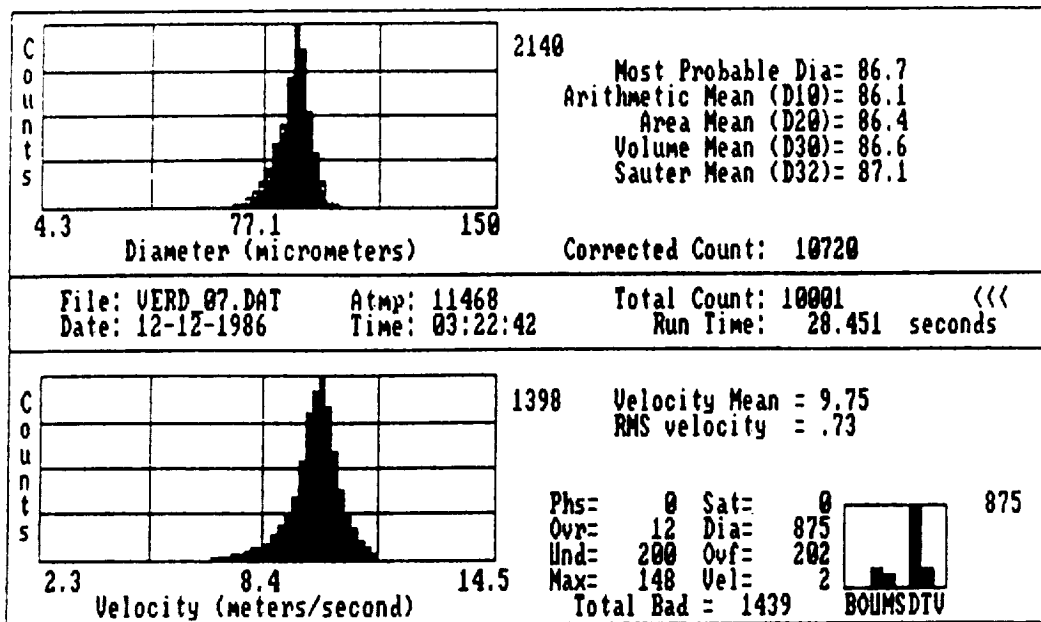
Theoretical Diameter = 44.2 μm
 Diameter of Orifice = 20 μm
 Liquid Feedrate = 0.139 cm^3/min .
 Vibration Frequency = 51.6 kHz

Figure 3.18: VOAG Verification w/ Dispersion Cup



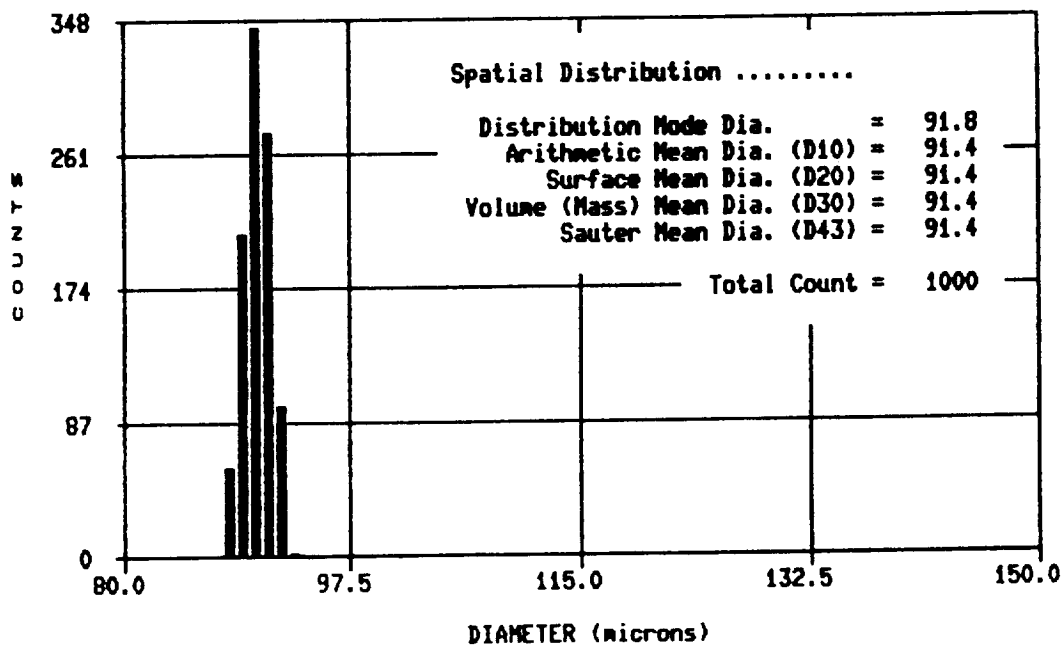
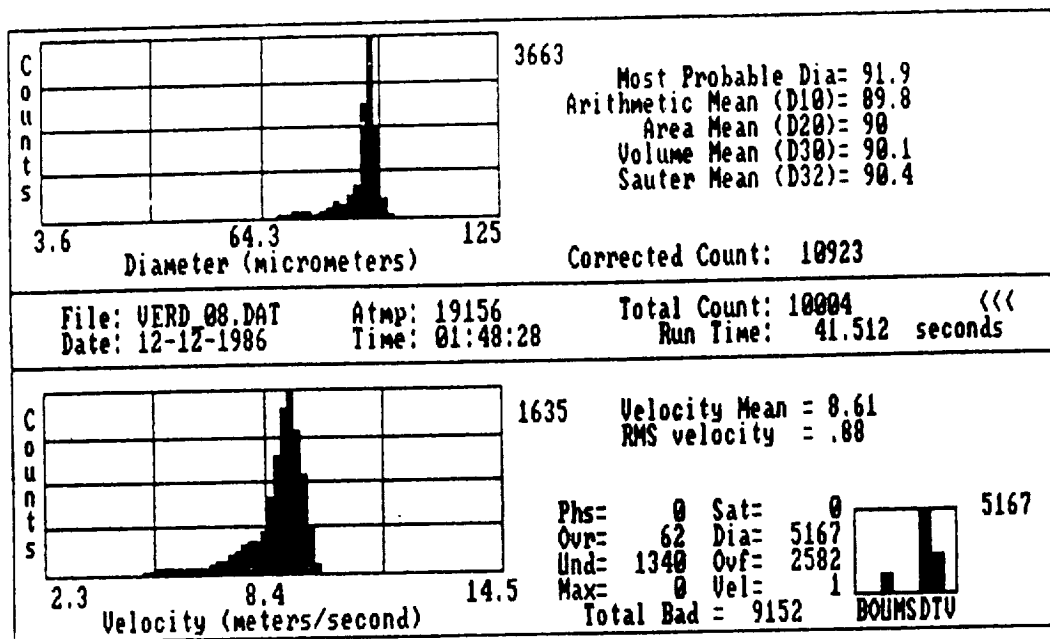
Theoretical Diameter = 47.5 μm
 Diameter of Orifice = 20 μm
 Liquid Feedrate = 0.139 cm^3/min .
 Vibration Frequency = 41.6 kHz

Figure 3.19: VOAG Verification w/ Dispersion Cup



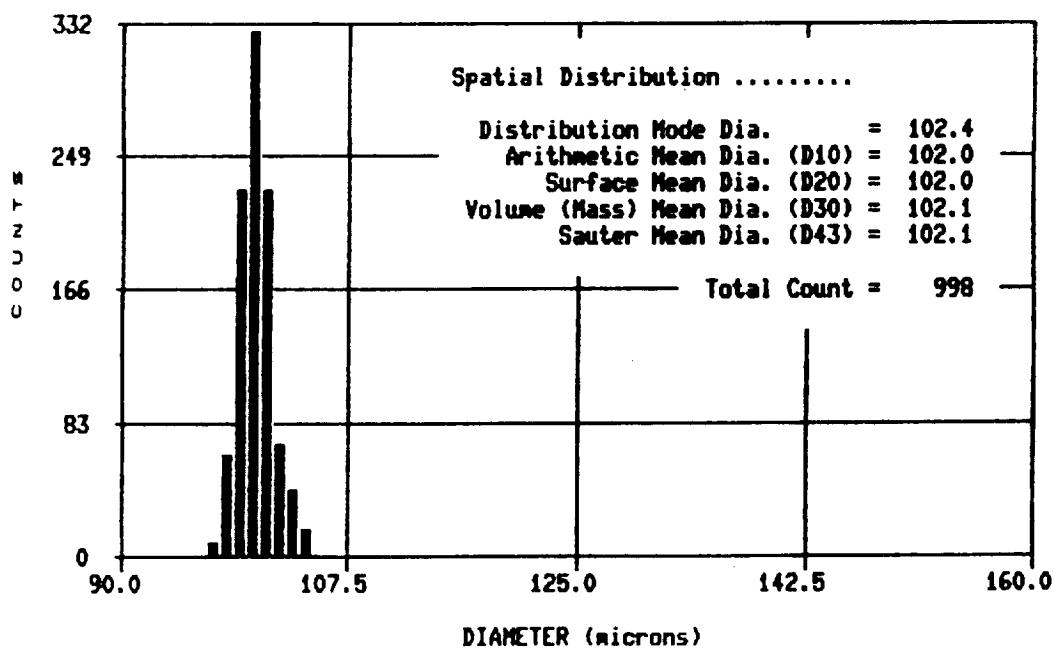
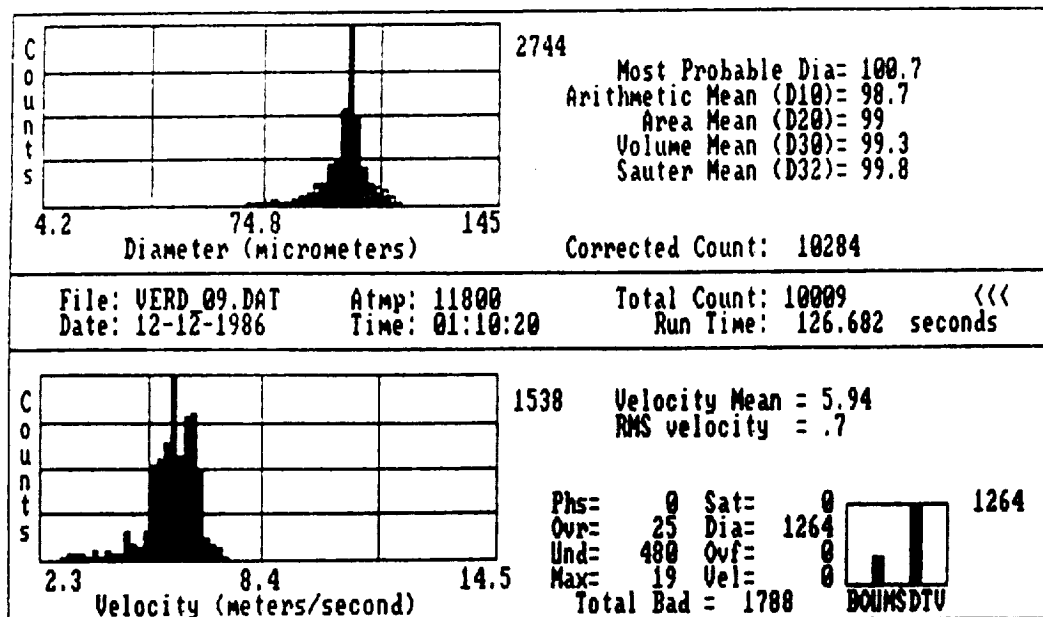
Theoretical Diameter = 85.6 μm
 Diameter of Orifice = 50 μm
 Liquid Feedrate = 0.59 cm^3/min .
 Vibration Frequency = 30.1 kHz

Figure 3.20: VOAG Verification w/ Dispersion Cup



Theoretical Diameter = 90.4 μm
 Diameter of Orifice = 50 μm
 Liquid Feedrate = 0.59 $\text{cm}^3/\text{min.}$
 Vibration Frequency = 25.5 kHz

Figure 3.21: VOAG Verification w/ Dispersion Cup



Theoretical Diameter = 99.6 μm
 Diameter of Orifice = 50 μm
 Liquid Feedrate = 0.59 cm^3/min .
 Vibration Frequency = 19.0 kHz

Figure 3.22: VOAG Verification w/ Dispersion Cup

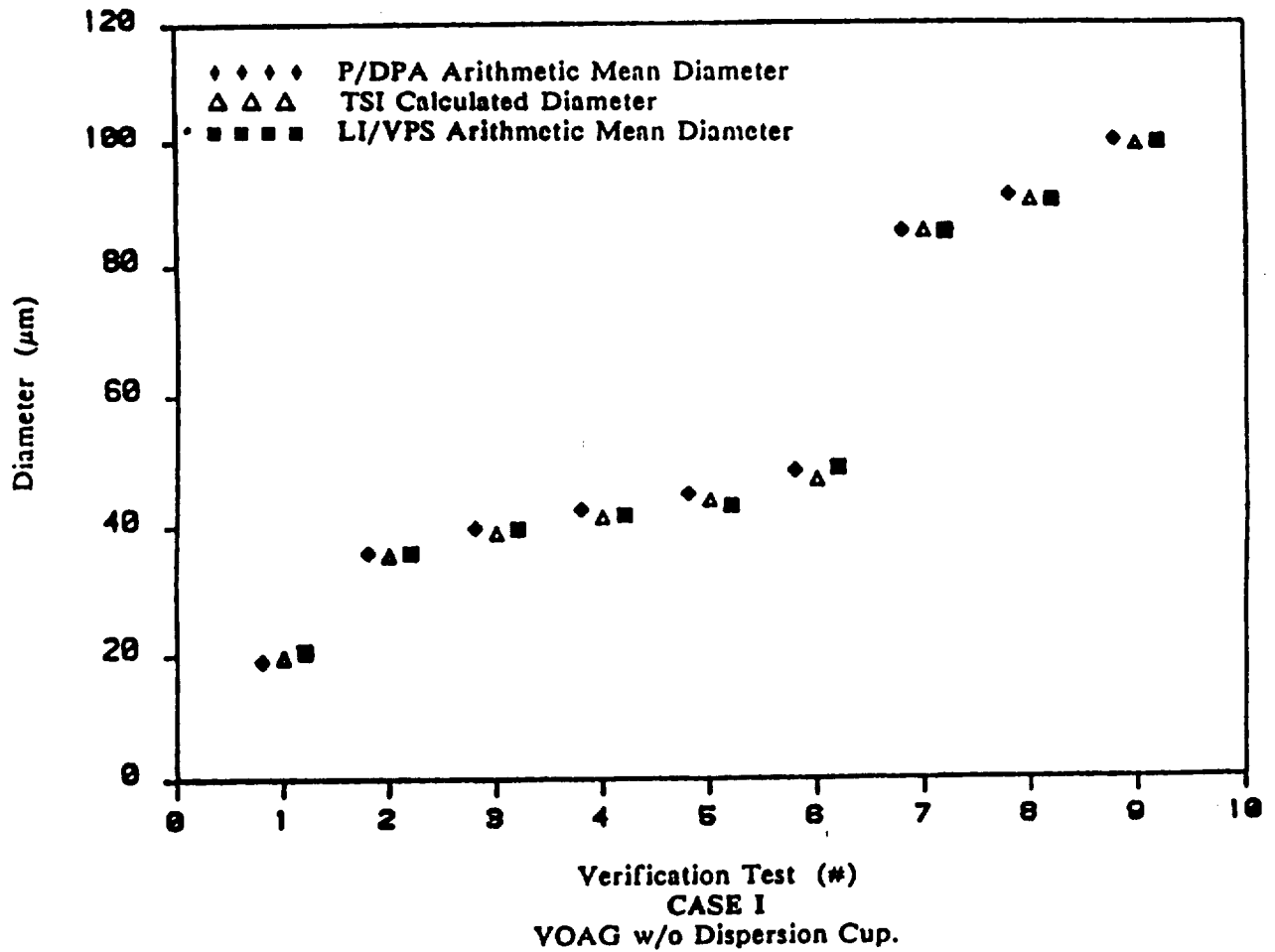


Figure 3.23: Comparison of Arithmetic Mean Diameters for CASE I VOAG Verification w/o Dispersion Cup Results

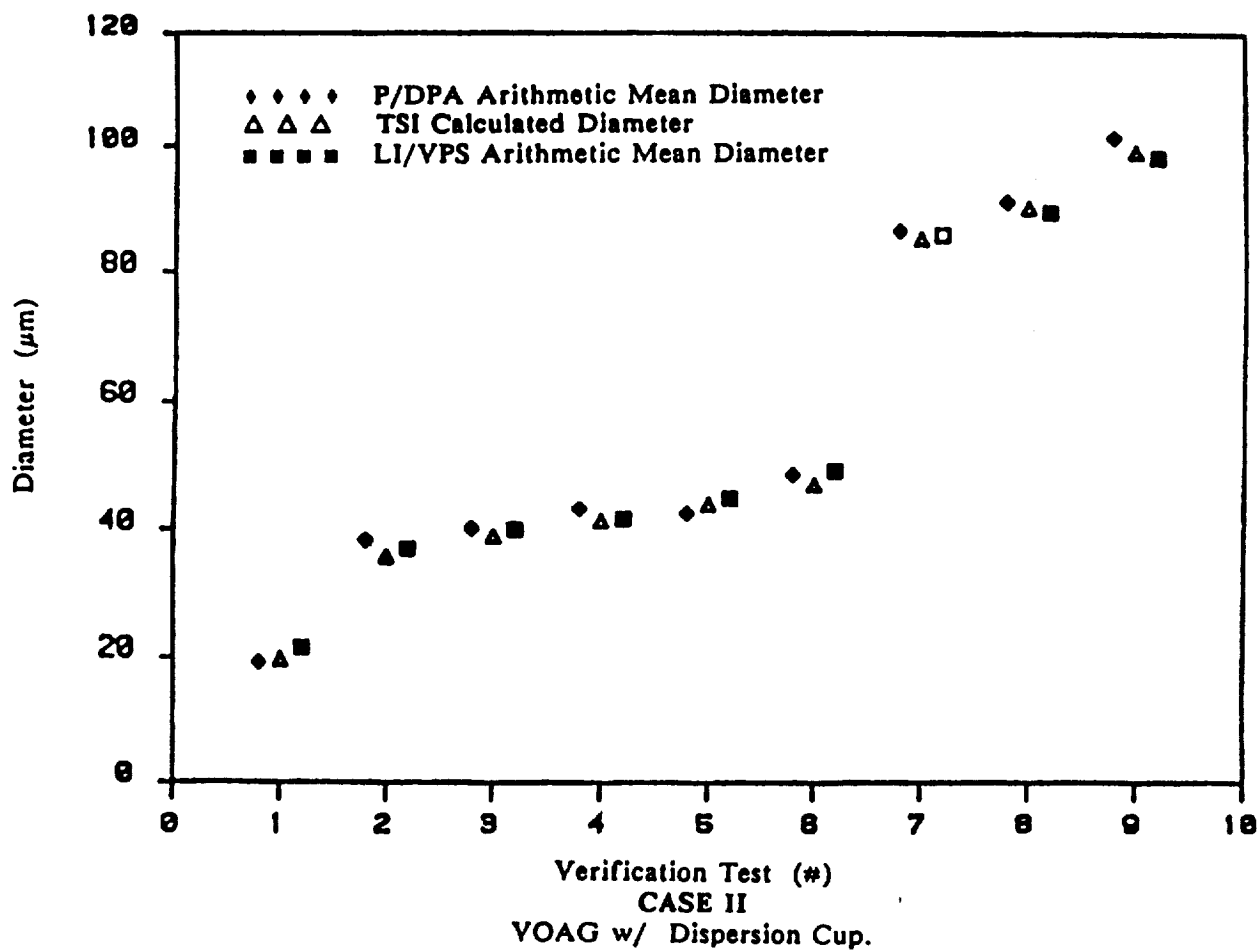


Figure 3.24: Comparison of Arithmetic Mean Diameters for CASE II VOAG Verification w/ Dispersion Cup Results

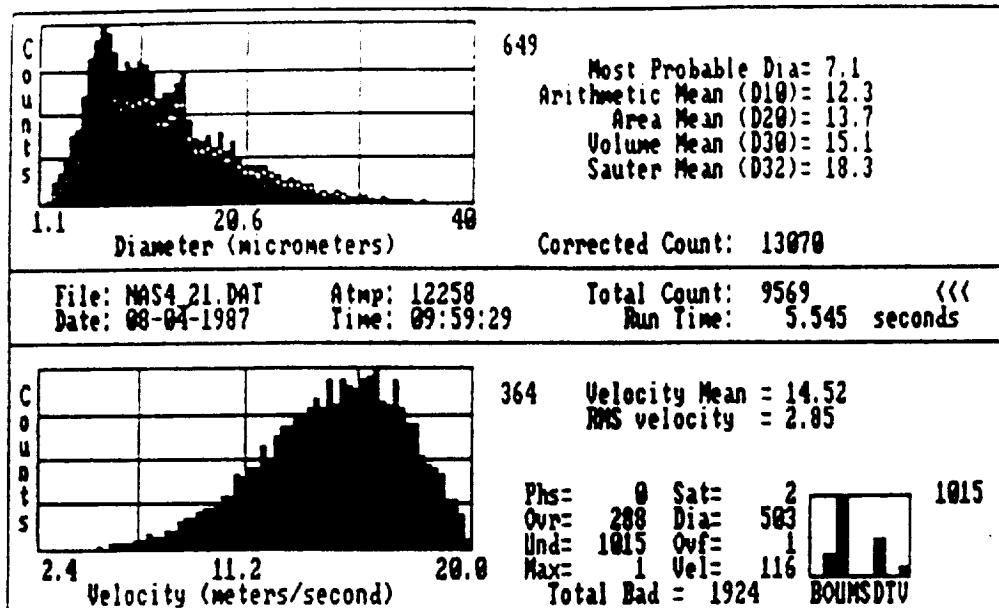
Table 3.4: VOAG Verification Results

CASE I

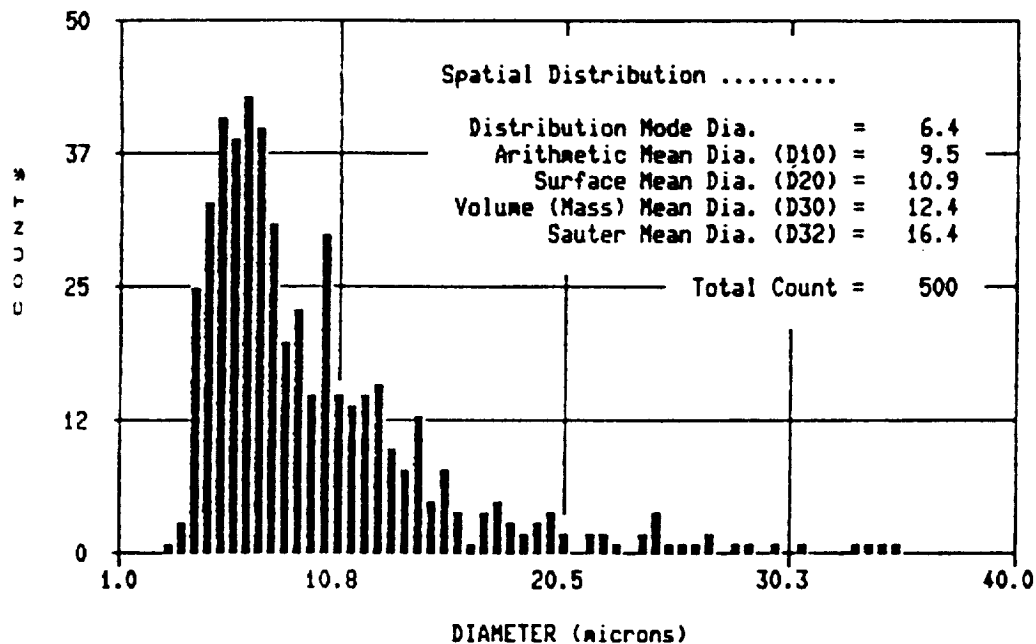
Vibrating Orifice Aerosol Generator w/o Dispersion Cup.					
TEST (#)	TSI DIAMETER (μm)	LI/VPS Results		P/DPA Results	
		ARITHMETIC MEAN DIAMETER (μm)	STANDARD DEVIATION (μm)	ARITHMETIC MEAN DIAMETER (μm)	STANDARD DEVIATION (μm)
1	19.8	19.1	0.101	20.5	2.073
2	35.5	35.9	0.818	35.8	1.020
3	39.0	39.8	0.047	39.6	0.060
4	41.5	42.7	0.176	41.8	0.128
5	44.2	45.2	0.150	43.3	0.045
6	47.5	48.8	0.153	49.2	0.076
7	85.6	85.6	0.108	89.4	0.270
8	90.4	91.2	0.142	90.3	0.399
9	99.6	100.3	0.340	99.9	0.436

CASE II

Vibrating Orifice Aerosol Generator with Dispersion Cup.					
TEST (#)	TSI DIAMETER (μm)	LI/VPS Results		P/DPA Results	
		ARITHMETIC MEAN DIAMETER (μm)	STANDARD DEVIATION (μm)	ARITHMETIC MEAN DIAMETER (μm)	STANDARD DEVIATION (μm)
1	19.8	19.2	0.325	21.5	2.063
2	35.5	38.3	0.432	36.8	1.560
3	39.0	40.2	1.355	40.0	0.566
4	41.5	43.5	1.063	41.9	0.120
5	44.2	42.7	1.109	45.5	0.379
6	47.5	49.1	0.541	49.7	0.275
7	85.6	86.7	0.139	86.1	2.080
8	90.4	91.4	0.175	89.8	0.844
9	99.6	102.0	0.420	98.7	0.155



a. P/DPA Results



b. LI/VPS Results

(CASE I)

Test Conditions: Radial Position = C_L

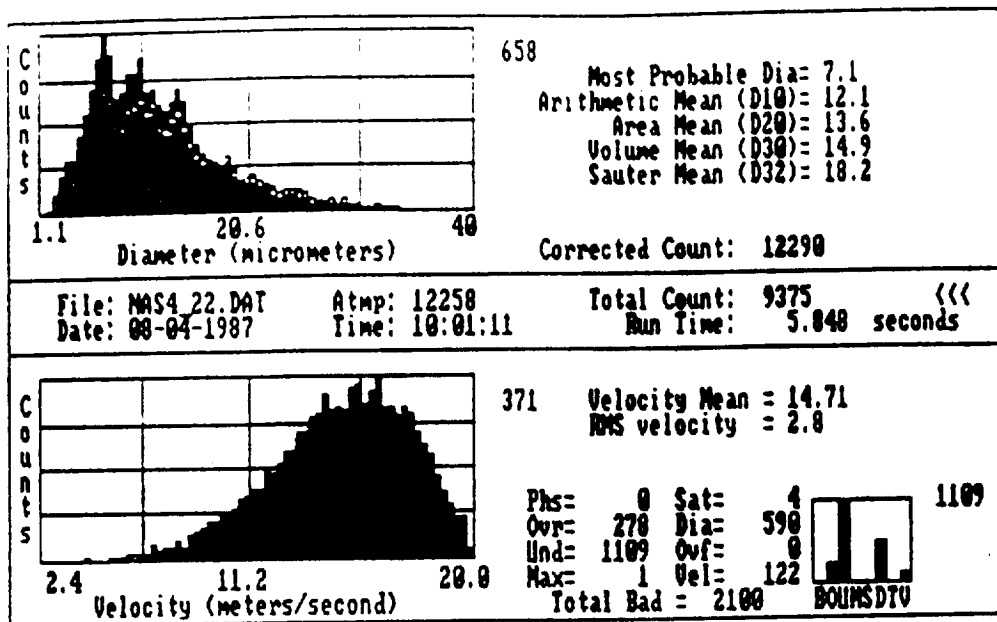
Air Pressure = 65 psia

Water Pressure = 105 psia

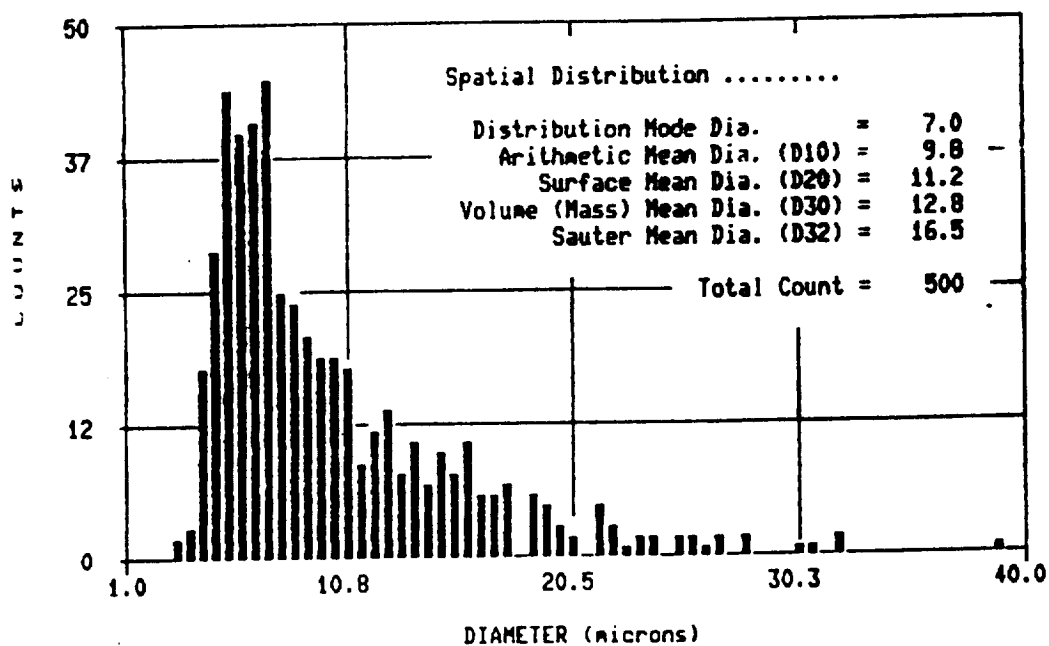
Water Flowrate = 0.038 gal/min.

Axial Position from Nozzle = 2 ft.

Figure 3.25: MOD-1 Nozzle Comparison



a. P/DPA Results



b. LI/VPS Results

(CASE I)

Test Conditions: Radial Position = $\frac{1}{2}$ in.

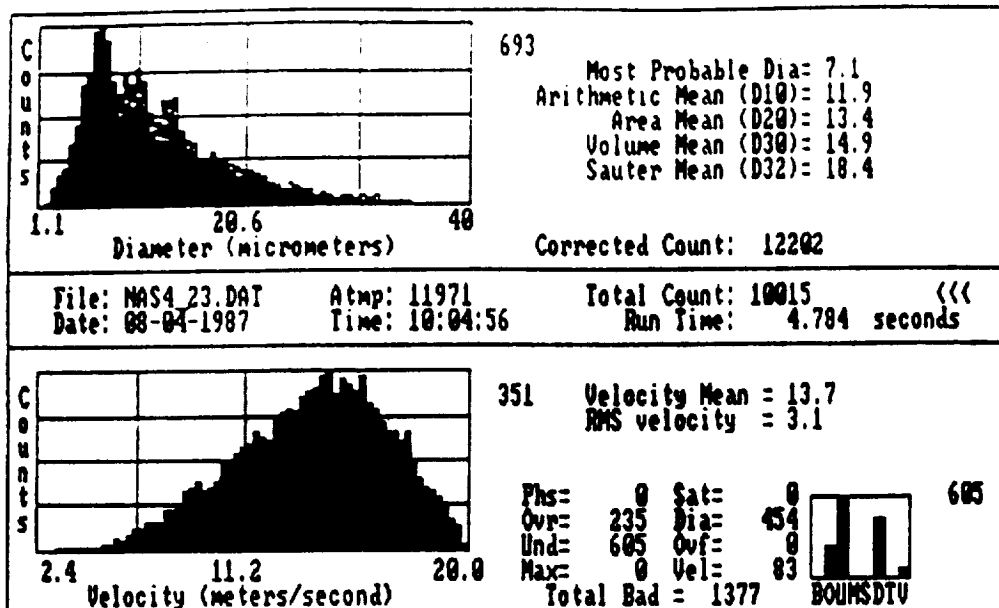
Air Pressure = 65 psia

Water Pressure = 105 psia

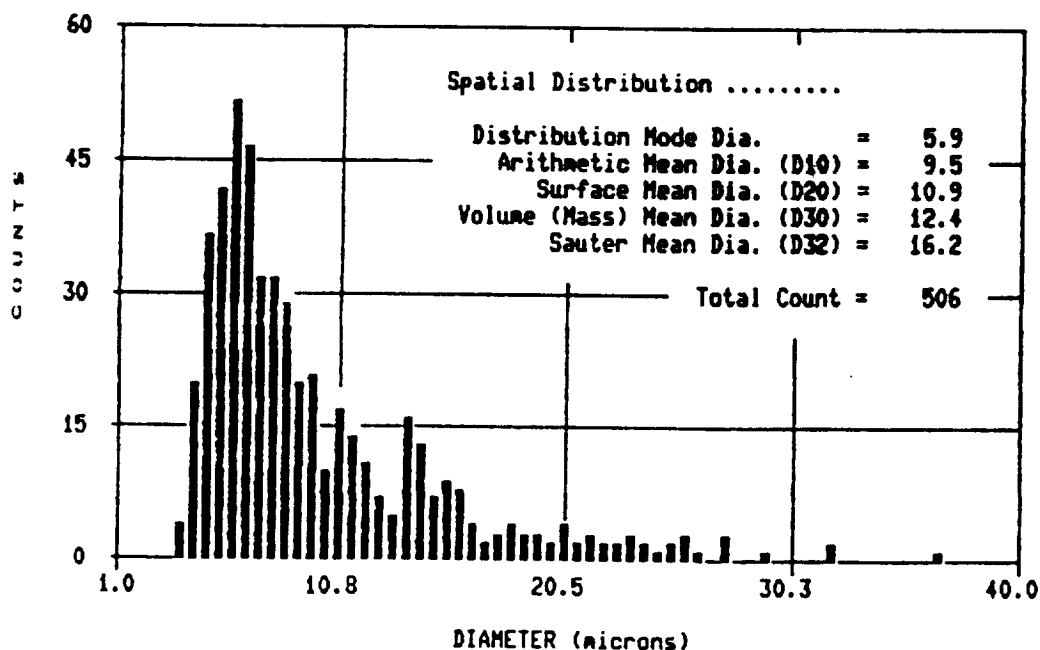
Water Flowrate = 0.038 gal/min.

Axial Position from Nozzle = 2 ft.

Figure 3.26: MOD-1 Nozzle Comparison



a. P/DPA Results



b. LI/VPS Results

(CASE I)

Test Conditions: Radial Position = 1 in.

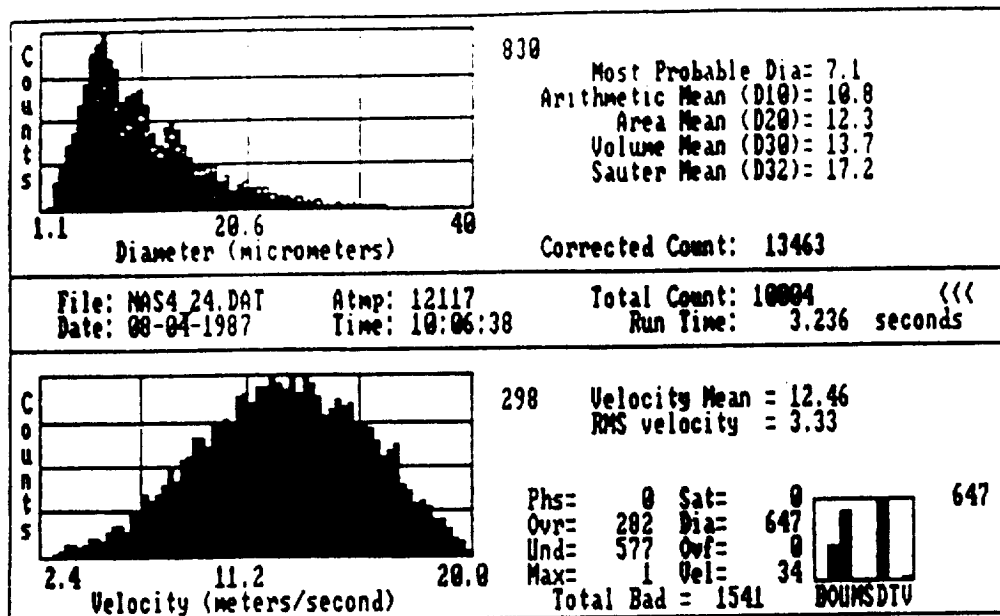
Air Pressure = 65 psia

Water Pressure = 105 psia

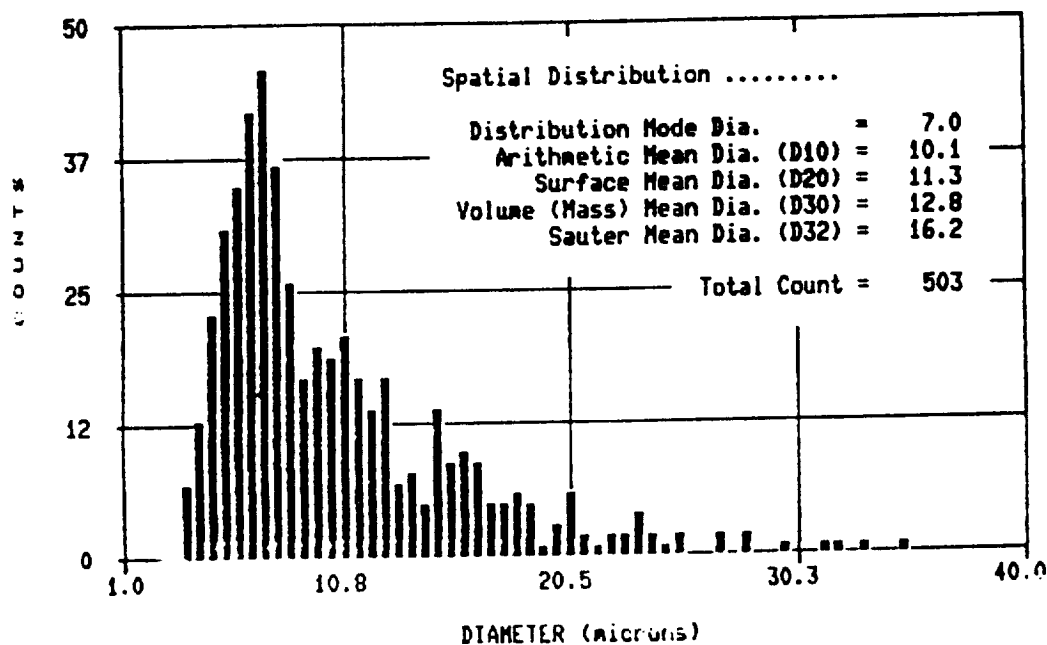
Water Flowrate = 0.038 gal/min.

Axial Position from Nozzle = 2 ft.

Figure 3.27: MOD-1 Nozzle Comparison



a. P/DPA Results



b. LI/VPS Results

(CASE I)

Test Conditions: Radial Position = $1\frac{1}{2}$ in.

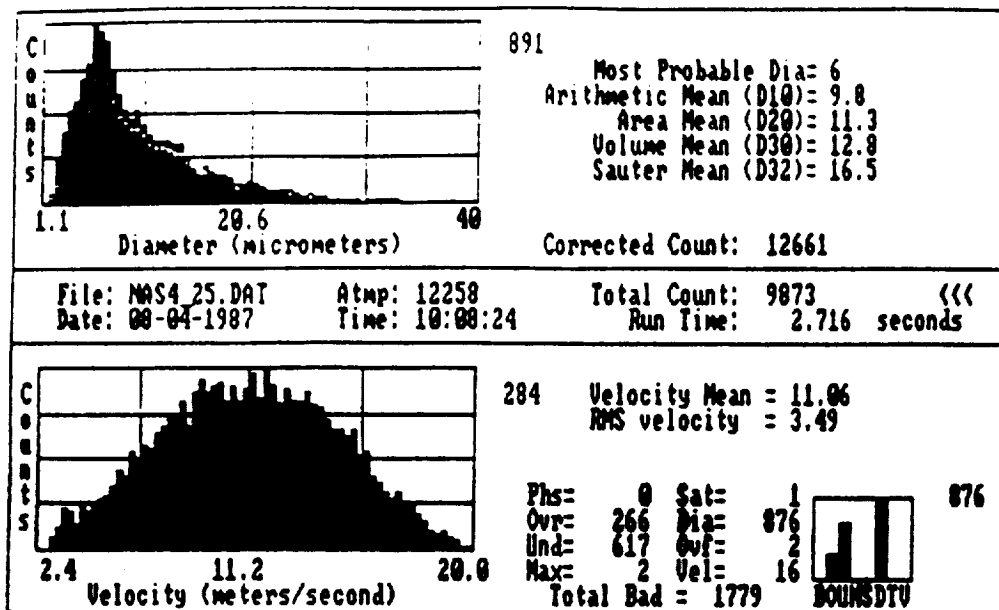
Air Pressure = 65 psia

Water Pressure = 105 psia

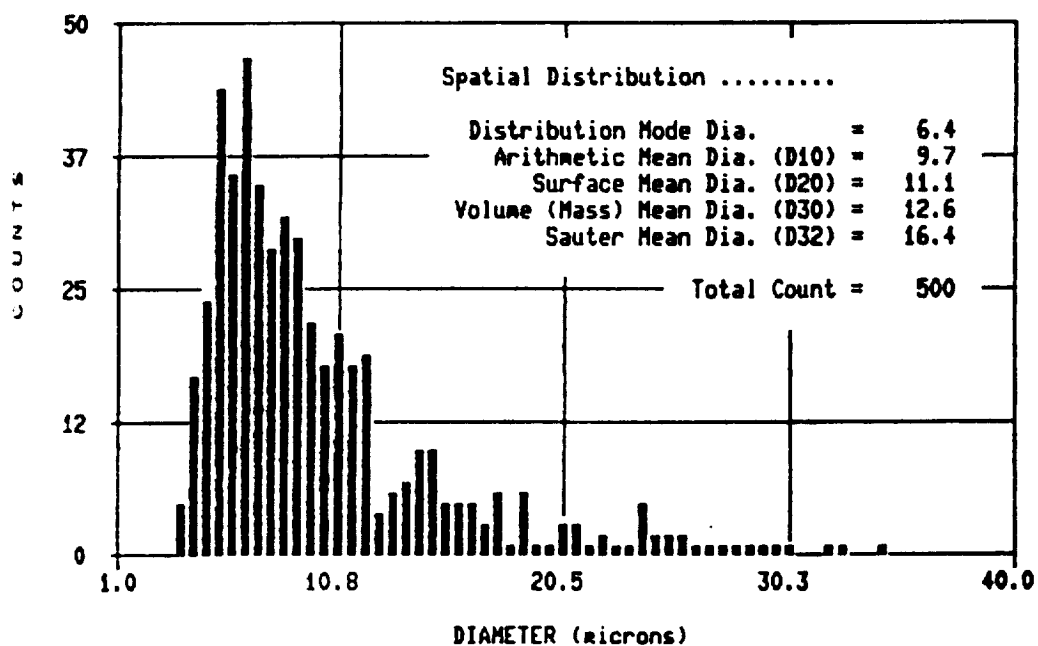
Water Flowrate = 0.038 gal/min.

Axial Position from Nozzle = 2 ft.

Figure 3.28: MOD-1 Nozzle Comparison



a. P/DPA Results



b. LI/VPS Results

(CASE I)

Test Conditions: Radial Position = 2 in.

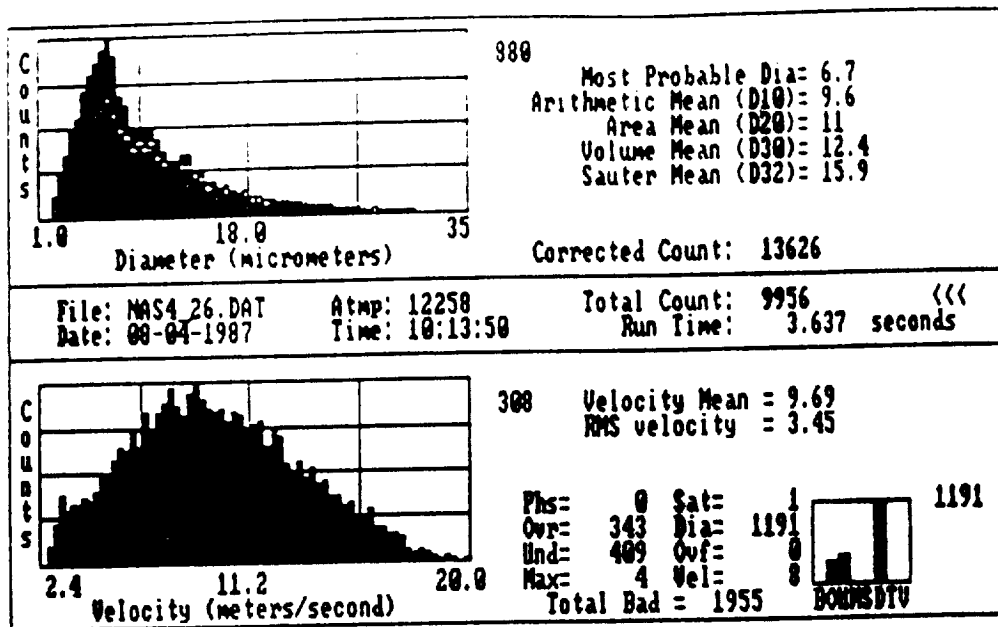
Air Pressure = 65 psia

Water Pressure = 105 psia

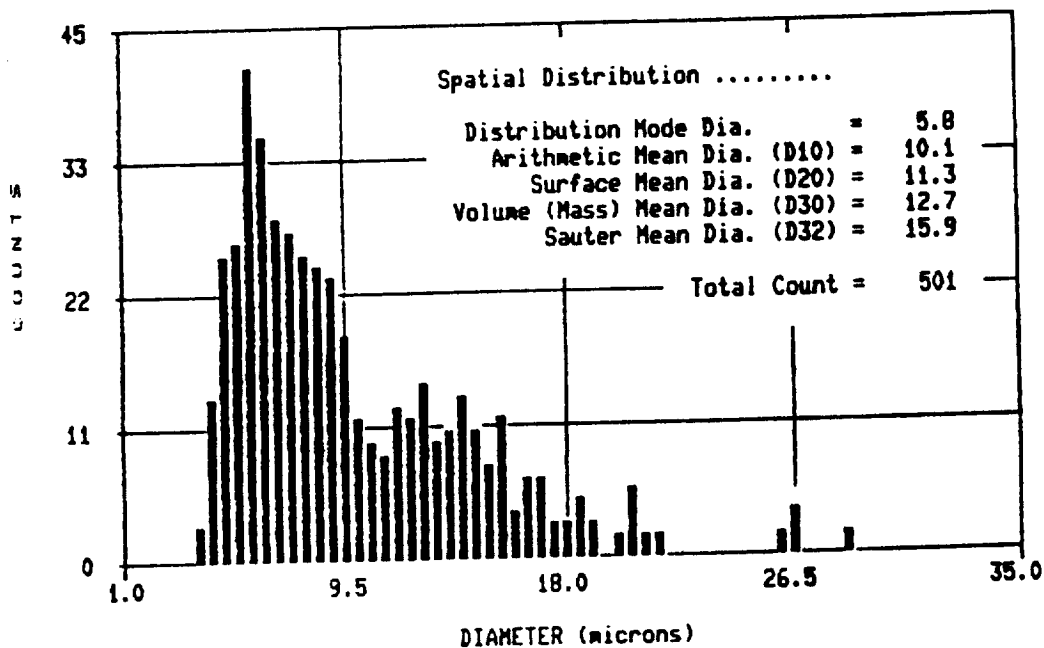
Water Flowrate = 0.038 gal/min.

Axial Position from Nozzle = 2 ft.

Figure 3.29: MOD-1 Nozzle Comparison



a. P/DPA Results



b. LI/VPS Results

(CASE I)

Test Conditions: Radial Position = $2\frac{1}{2}$ in.

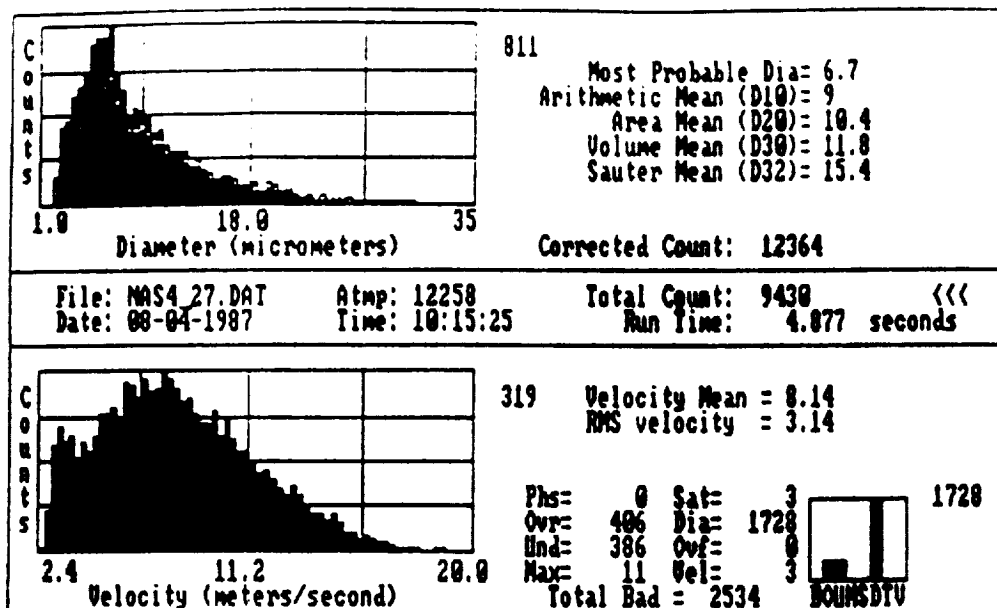
Air Pressure = 65 psia

Water Pressure = 105 psia

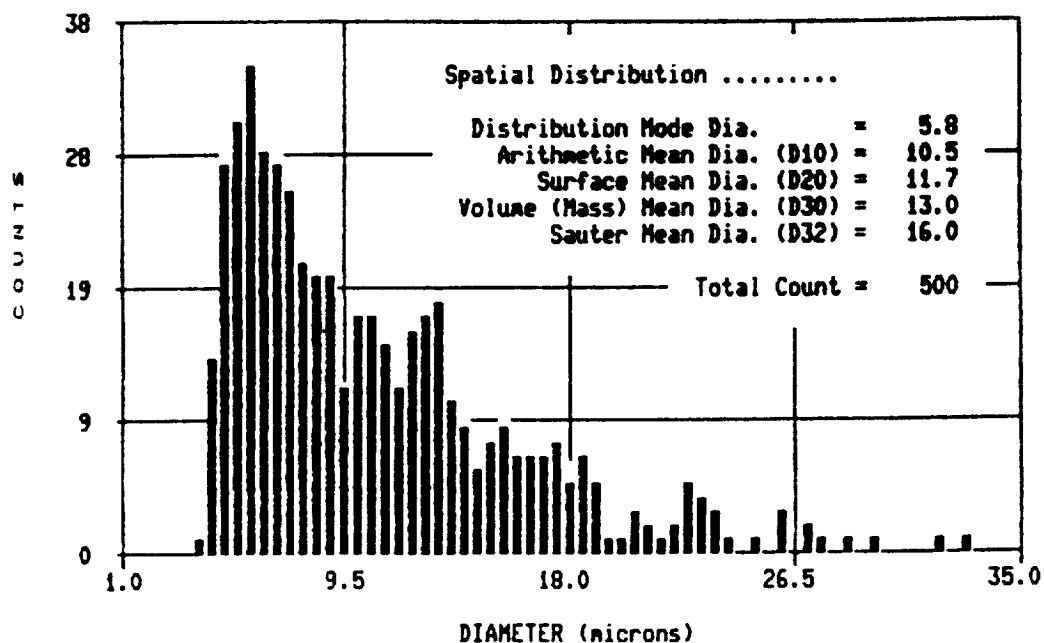
Water Flowrate = 0.038 gal/min.

Axial Position from Nozzle = 2 ft.

Figure 3.30: MOD-1 Nozzle Comparison



a. P/DPA Results



b. LI/VPS Results

(CASE I)

Test Conditions: Radial Position = 3 in.

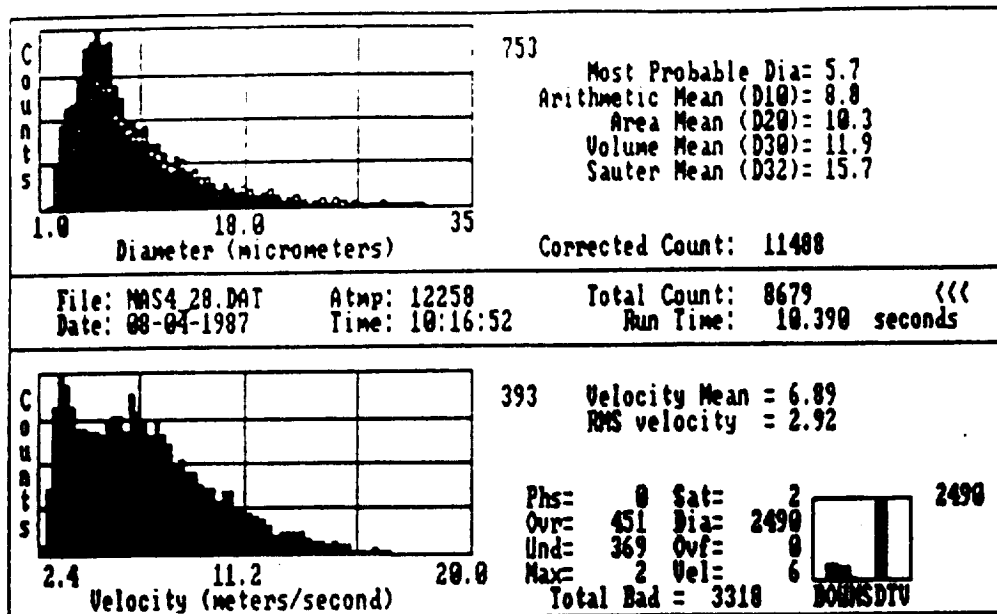
Air Pressure = 65 psia

Water Pressure 105 psia

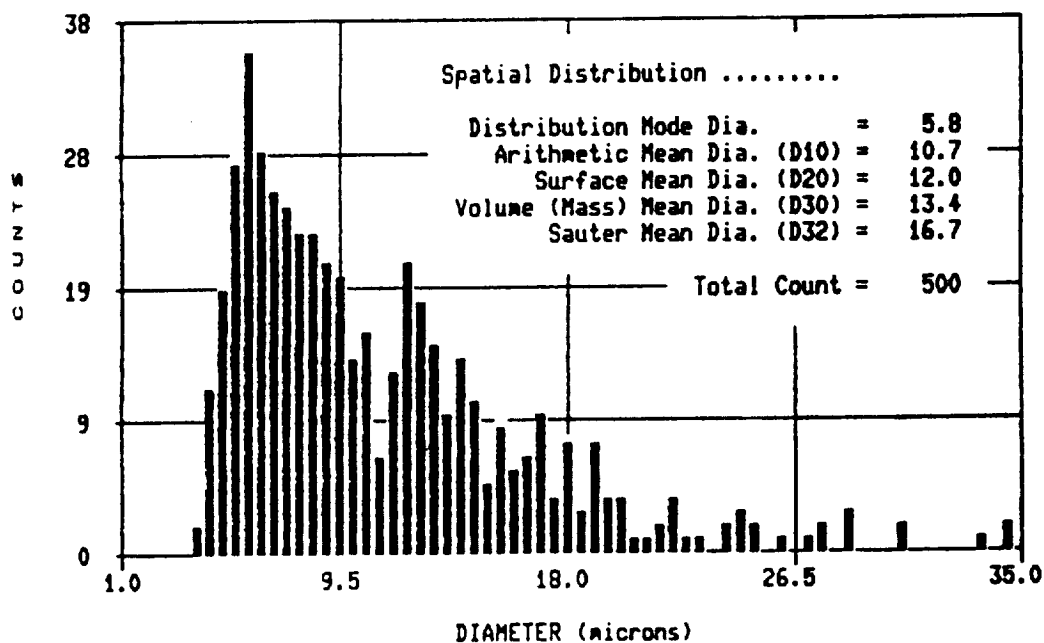
Water Flowrate = 0.038 gal/min.

Axial Position from Nozzle = 2 ft.

Figure 3.31: MOD-1 Nozzle Comparison



a. P/DPA Results



b. LI/VPS Results

(CASE I)

Test Conditions: Radial Position = $3\frac{1}{2}$ in.

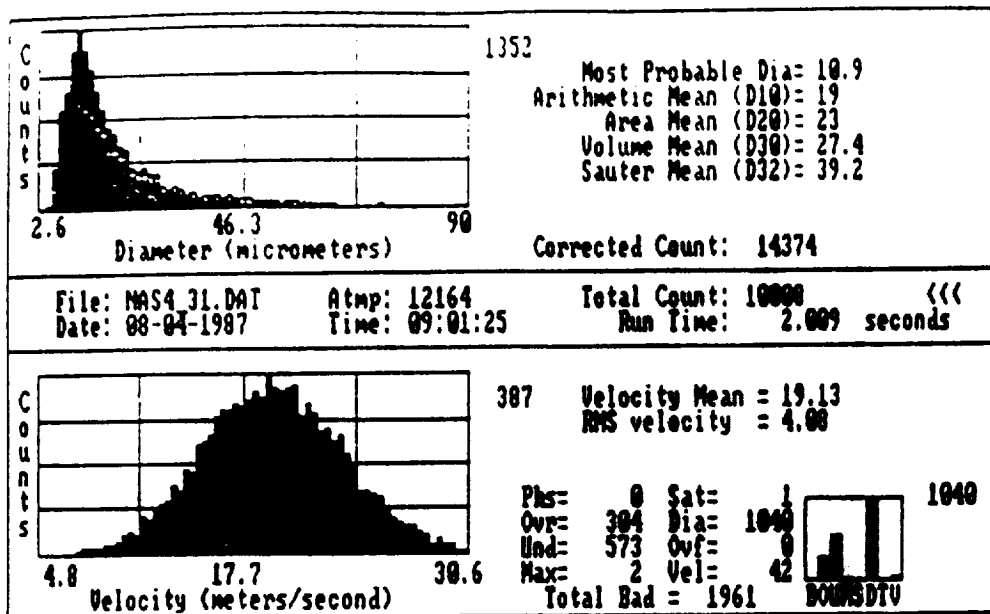
Air Pressure = 65 psia

Water Pressure = 105 psia

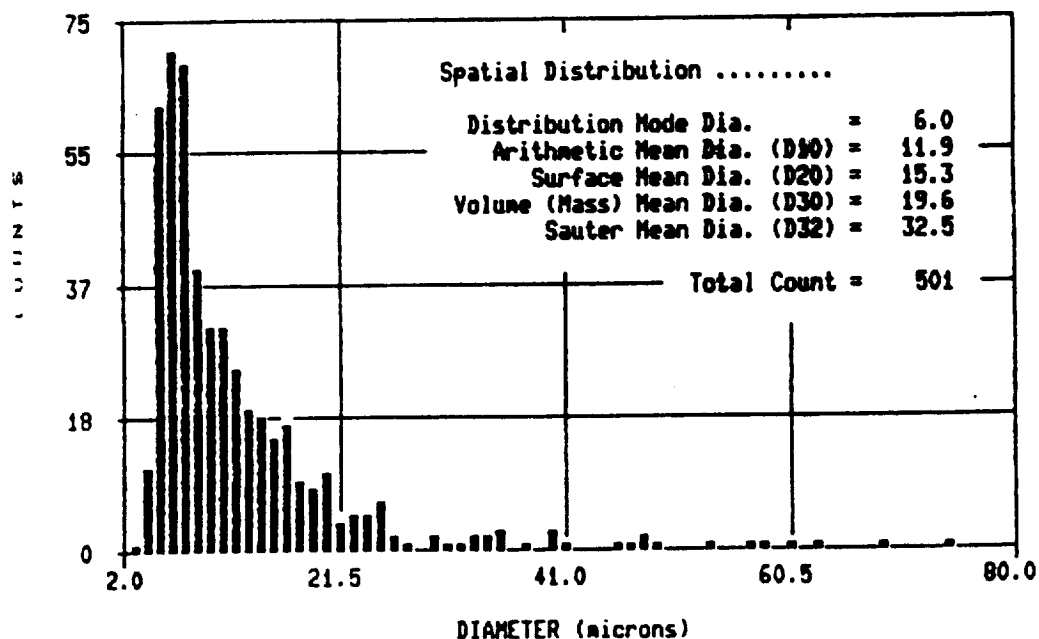
Water Flowrate = 0.038 gal/min.

Axial Position from Nozzle = 2 ft.

Figure 3.32: MOD-1 Nozzle Comparison



a. P/DPA Results



b. LI/VPS Results

(CASE II)

Test Conditions: Radial Position = C_L

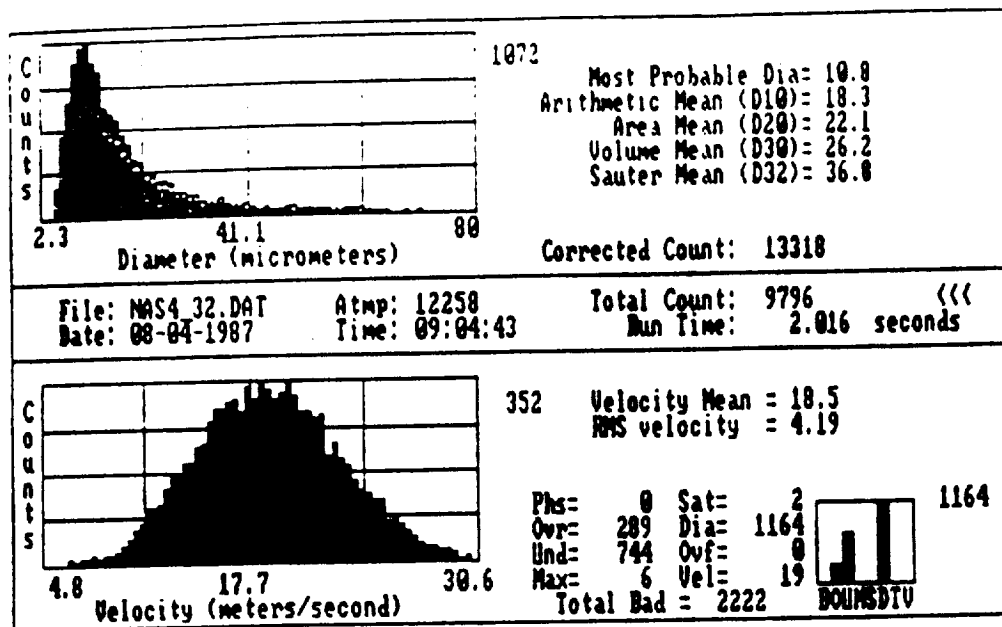
Air Pressure = 45 psia

Water Pressure = 115 psia

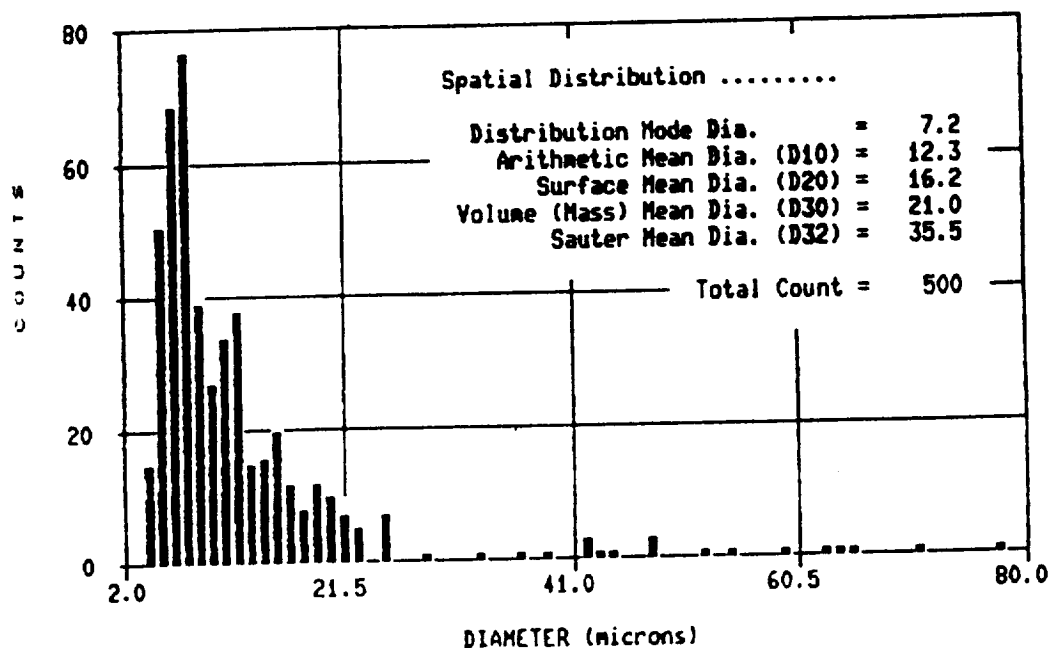
Water Flowrate = 0.06 gal/min.

Axial Position from Nozzle = 2 ft.

Figure 3.33: MOD-1 Nozzle Comparison



a. P/DPA Results



b. LI/VPS Results

(CASE II)

Test Conditions: Radial Position = $\frac{1}{2}$ in.

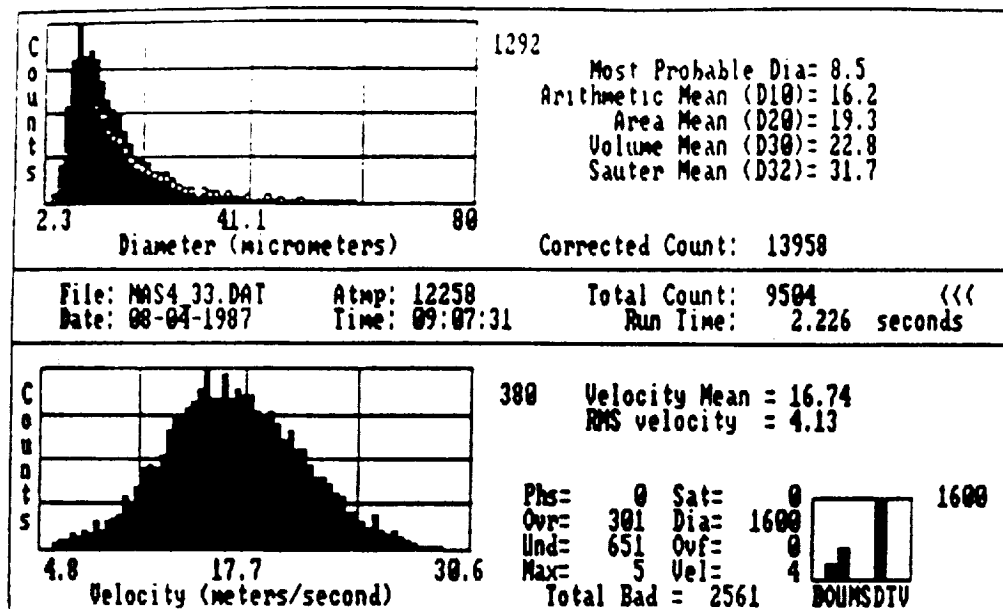
Air Pressure = 45 psia

Water Pressure = 115 psia

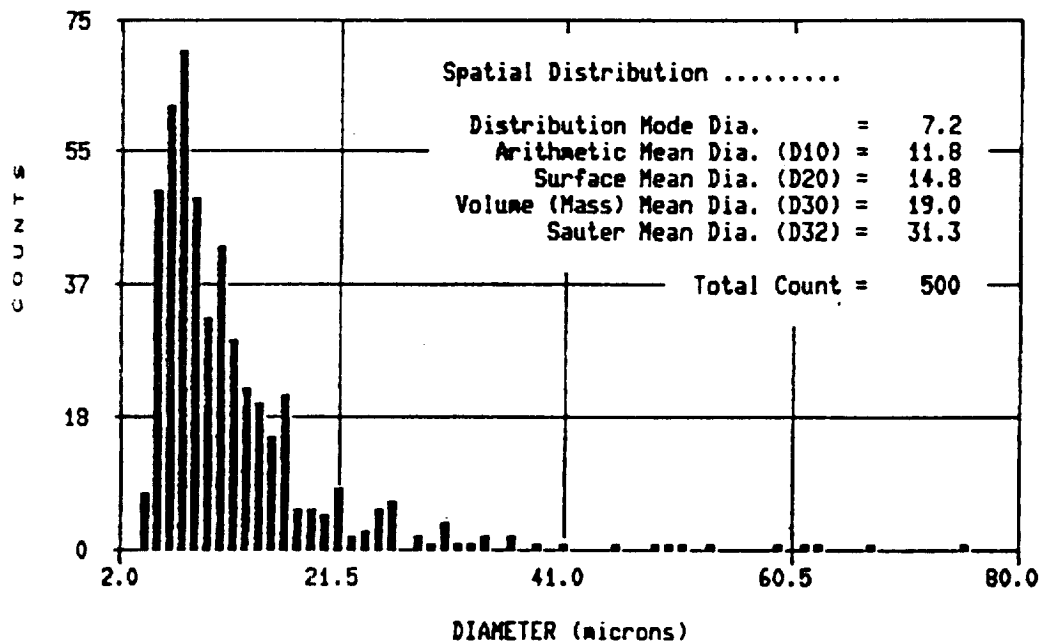
Water Flowrate = 0.06 gal/min.

Axial Position from Nozzle = 2 ft.

Figure 3.34: MOD-1 Nozzle Comparison



a. P/DPA Results



b. LI/VPS Results

(CASE II)

Test Conditions: Radial Position = 1 in.

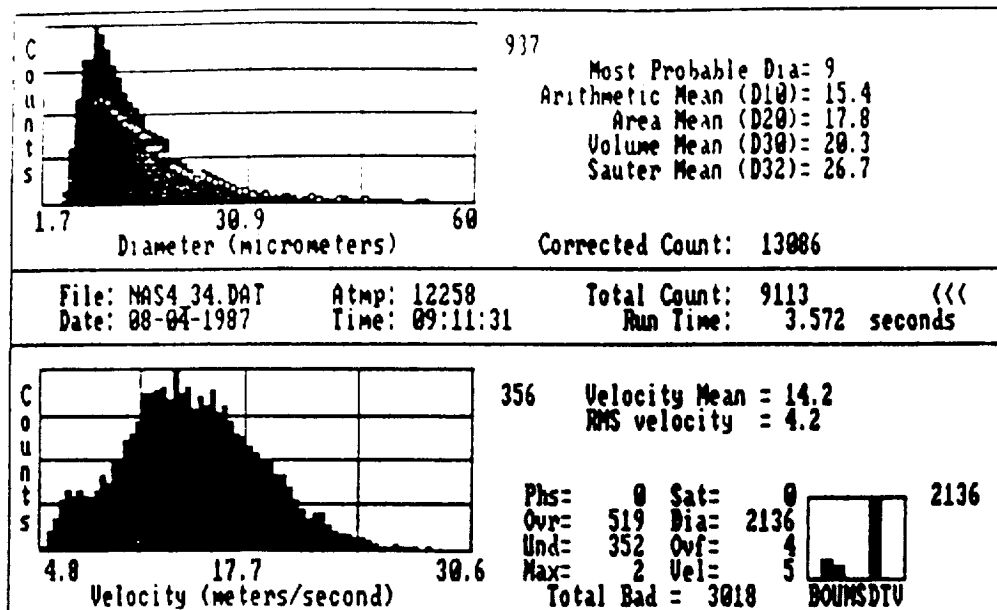
Air Pressure = 45 psia

Water Pressure = 115 psia

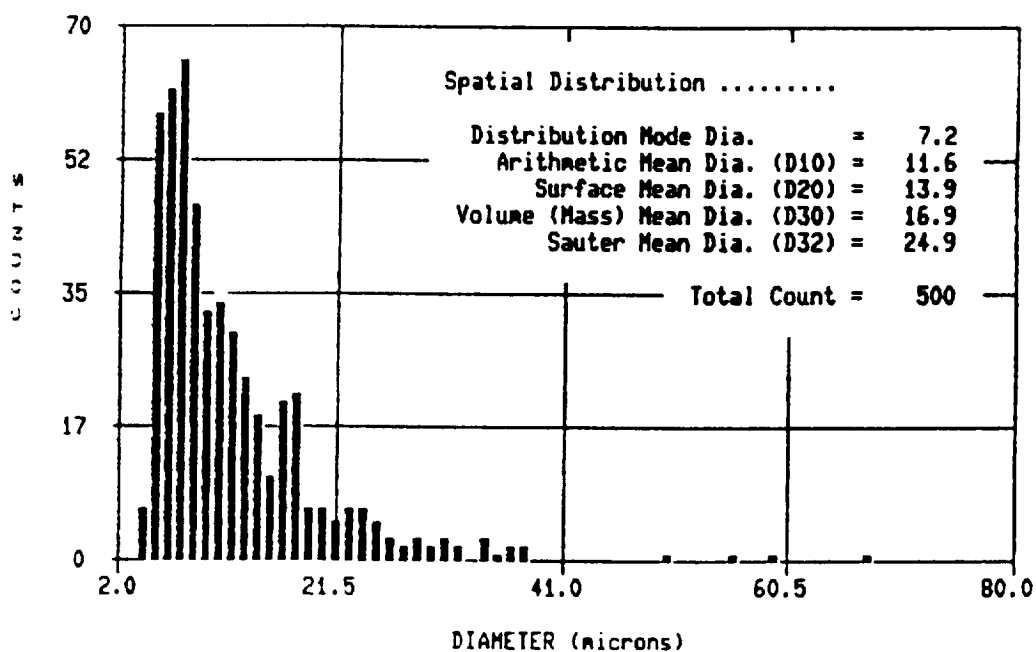
Water Flowrate = 0.06 gal/min.

Axial Position from Nozzle = 2 ft.

Figure 3.35: MOD-1 Nozzle Comparison



a. P/DPA Results

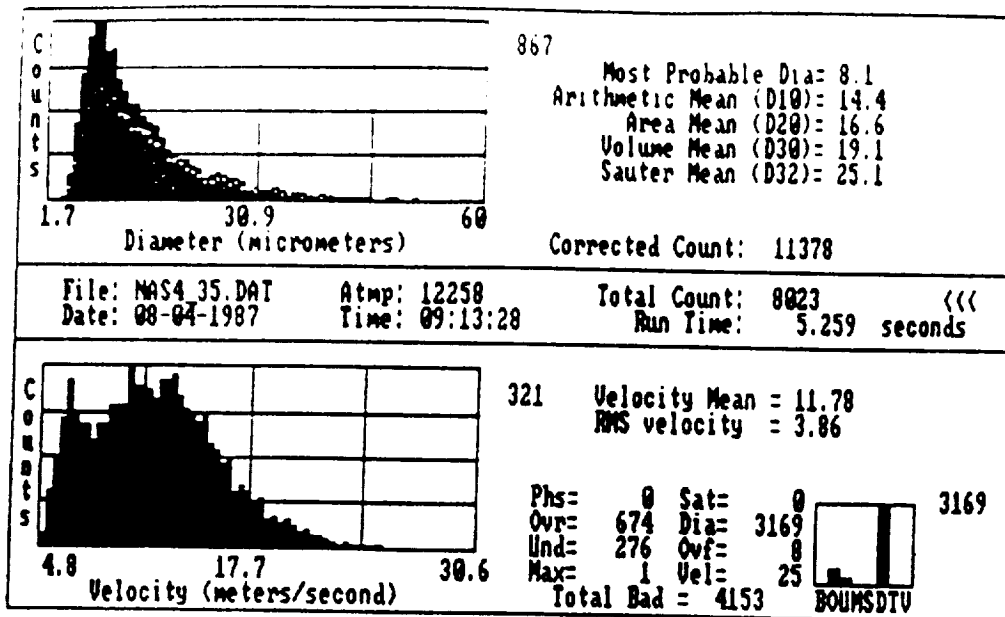


b. LI/VPS Results

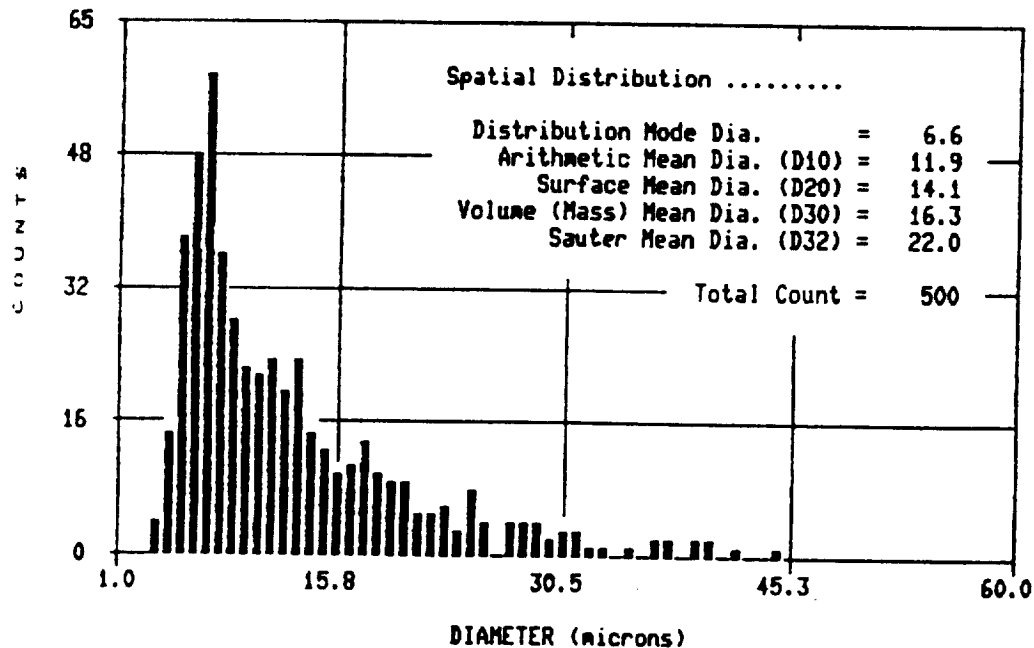
(CASE II)

Test Conditions: Radial Position = $1\frac{1}{2}$ in.
 Air Pressure = 45 psia
 Water Pressure = 115 psia
 Water Flowrate = 0.06 gal/min.
 Axial Position from Nozzle = 2 ft.

Figure 3.36: MOD-1 Nozzle Comparison



a. P/DPA Results



b. LI/VPS Results

(CASE II)

Test Conditions: Radial Position = 2 in.

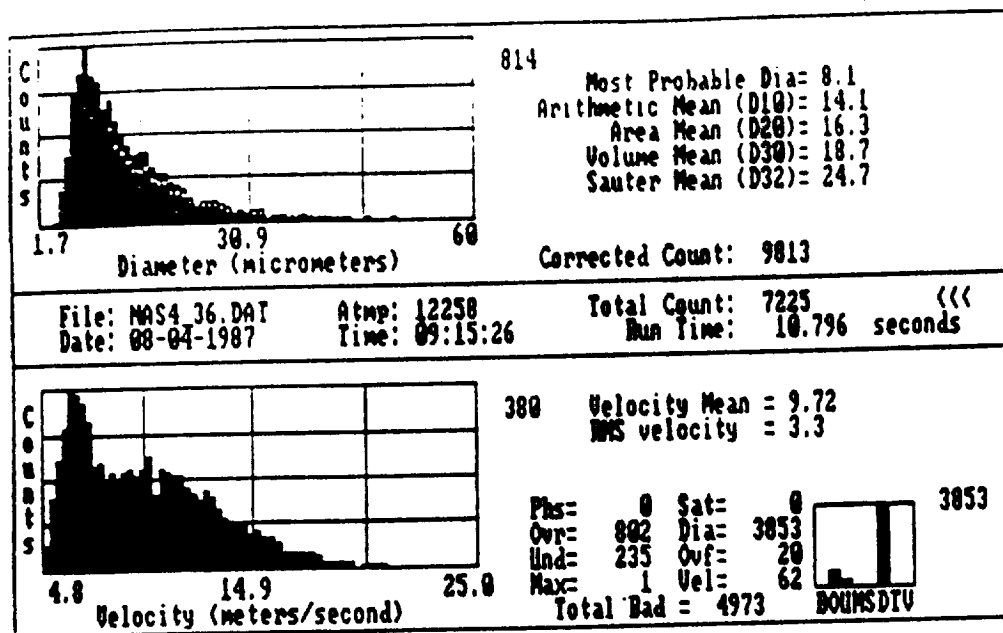
Air Pressure = 45 psia

Water Pressure = 115 psia

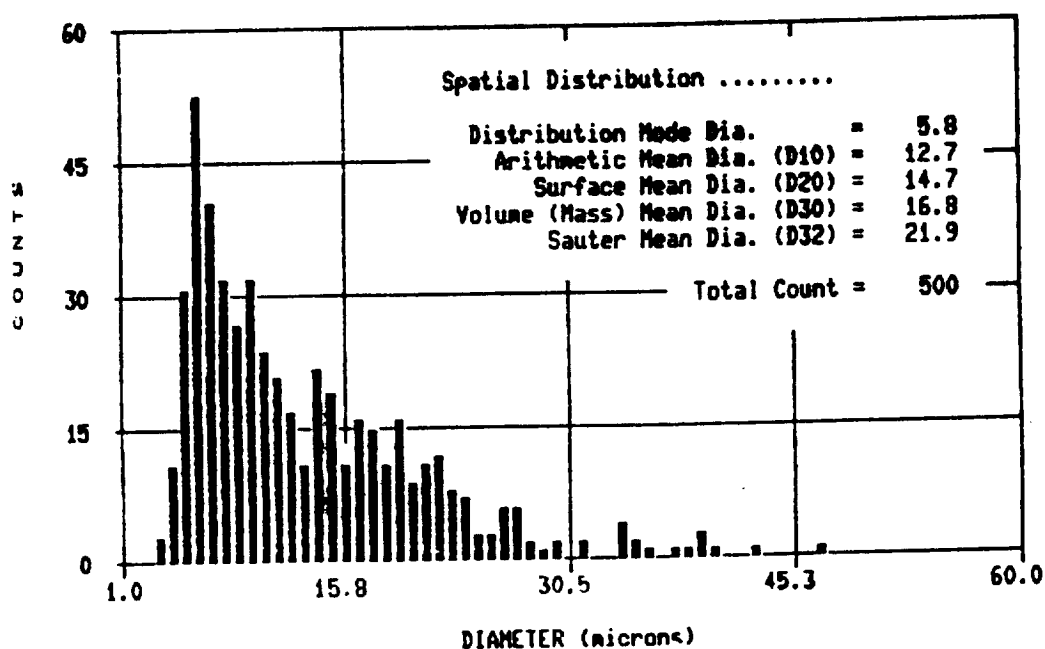
Water Flowrate = 0.06 gal/min.

Axial Position from Nozzle = 2 ft.

Figure 3.37: MOD-1 Nozzle Comparison



a. P/DPA Results

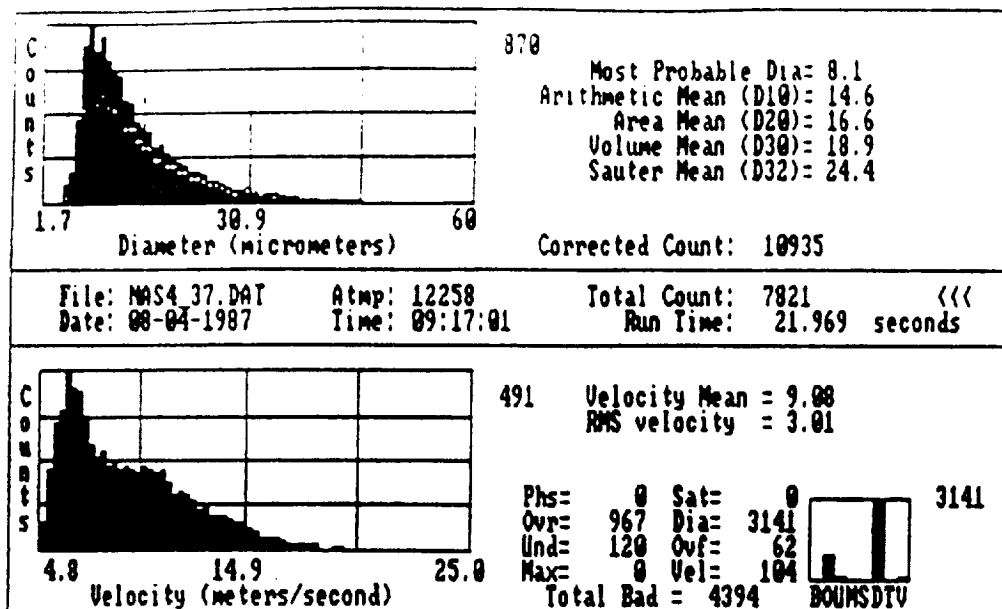


b. LI/VPS Results

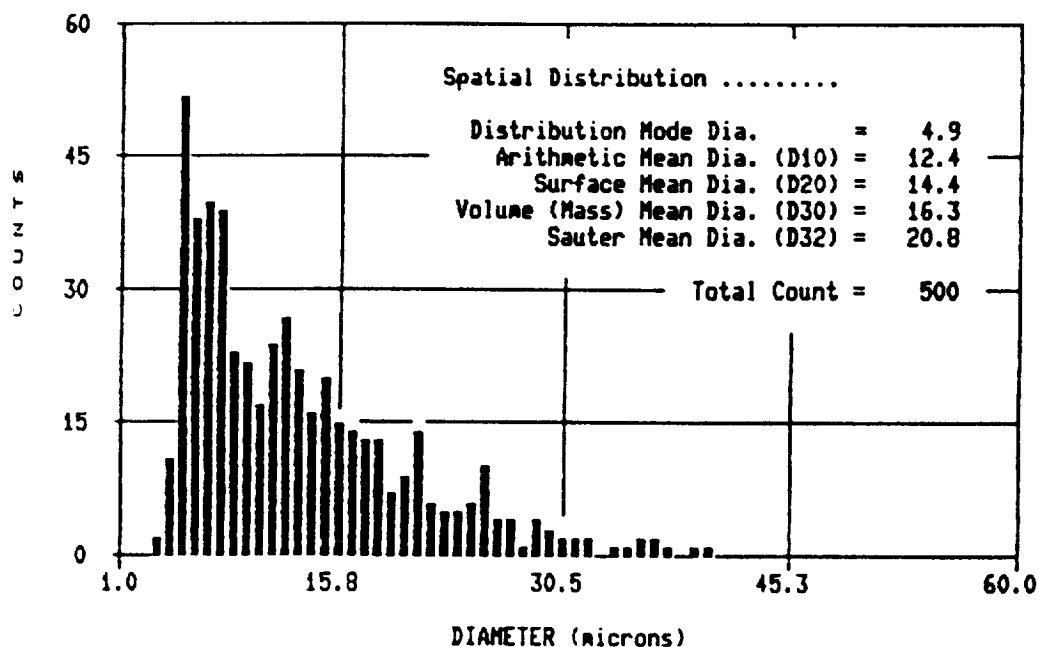
(CASE II)

Test Conditions: Radial Position = $2\frac{1}{2}$ in.
 Air Pressure = 45 psia
 Water Pressure = 115 psia
 Water Flowrate = 0.06 gal/min.
 Axial Position from Nozzle = 2 ft.

Figure 3.38: MOD-1 Nozzle Comparison



a. P/DPA Results



b. LI/VPS Results

(CASE II)

Test Conditions: Radial Position = 3 in.

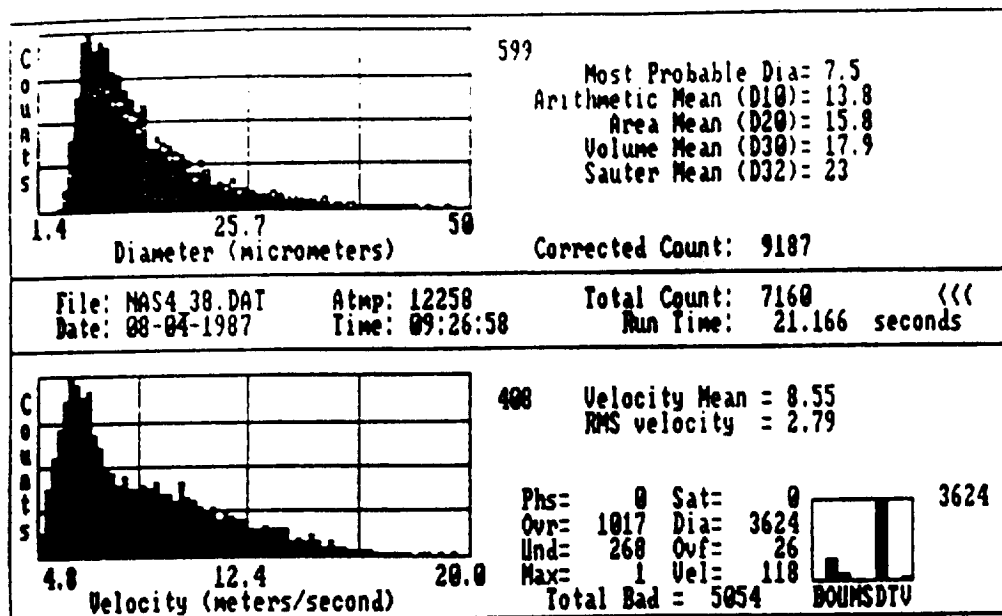
Air Pressure = 45 psia

Water Pressure = 115 psia

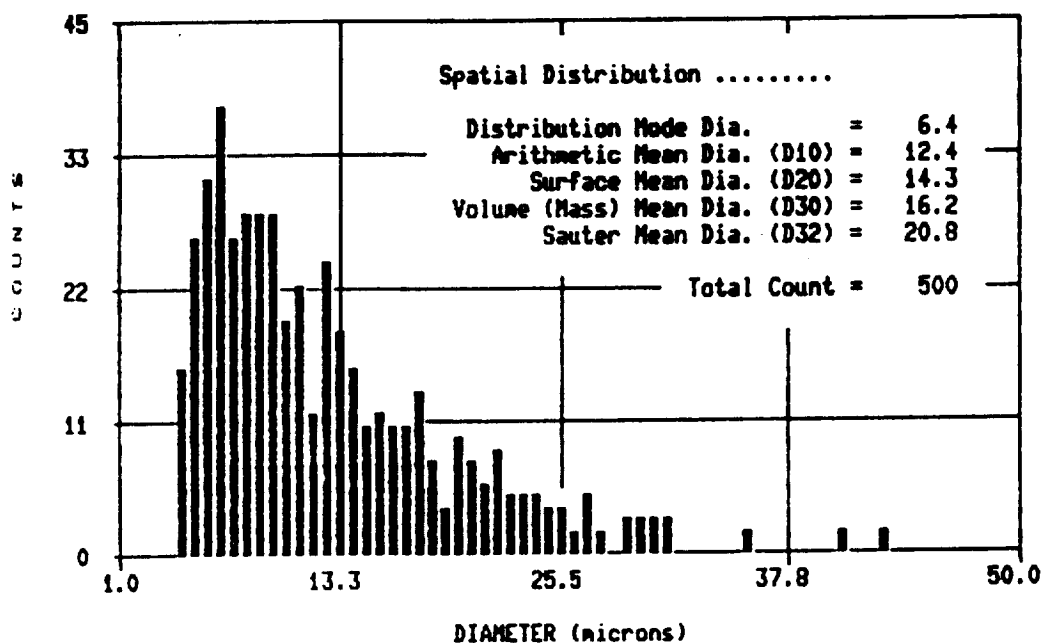
Water Flowrate = 0.06 gal/min.

Axial Position from Nozzle = 2 ft.

Figure 3.39: MOD-1 Nozzle Comparison



a. P/DPA Results



b. LI/VPS Results

(CASE II)

Test Conditions: Radial Position = $3\frac{1}{2}$ in.
 Air Pressure = 45 psia
 Water Pressure = 115 psia
 Water Flowrate = 0.06 gal/min.
 Axial Position from Nozzle = 2 ft.

Figure 3.40: MOD-1 Nozzle Comparison

To study the aforementioned results, the arithmetic mean diameter and Sauter mean diameter from each test were graphed as functions of radial position (Figs. 3.41 and 3.44) for each case. The choice of the arithmetic and Sauter mean diameters in the graphs was made to examine the count vs. particle size distribution. The distribution shape most associated with aerosol spray analysis is similar to a log-normal distribution where the distribution mode leans toward the low side of the distribution and conversely the distribution tail shifts to the high side of the distribution. The distribution is reproduced by the fact, that the arithmetic mean diameter is proportional to the mode of the distribution and the Sauter mean diameter is indicative of the distribution's tail. With the above technique, the comparison of results from the P/DPA and the LI/VPS was performed.

3.2.1 Discussion of Results for Comparison - CASE I

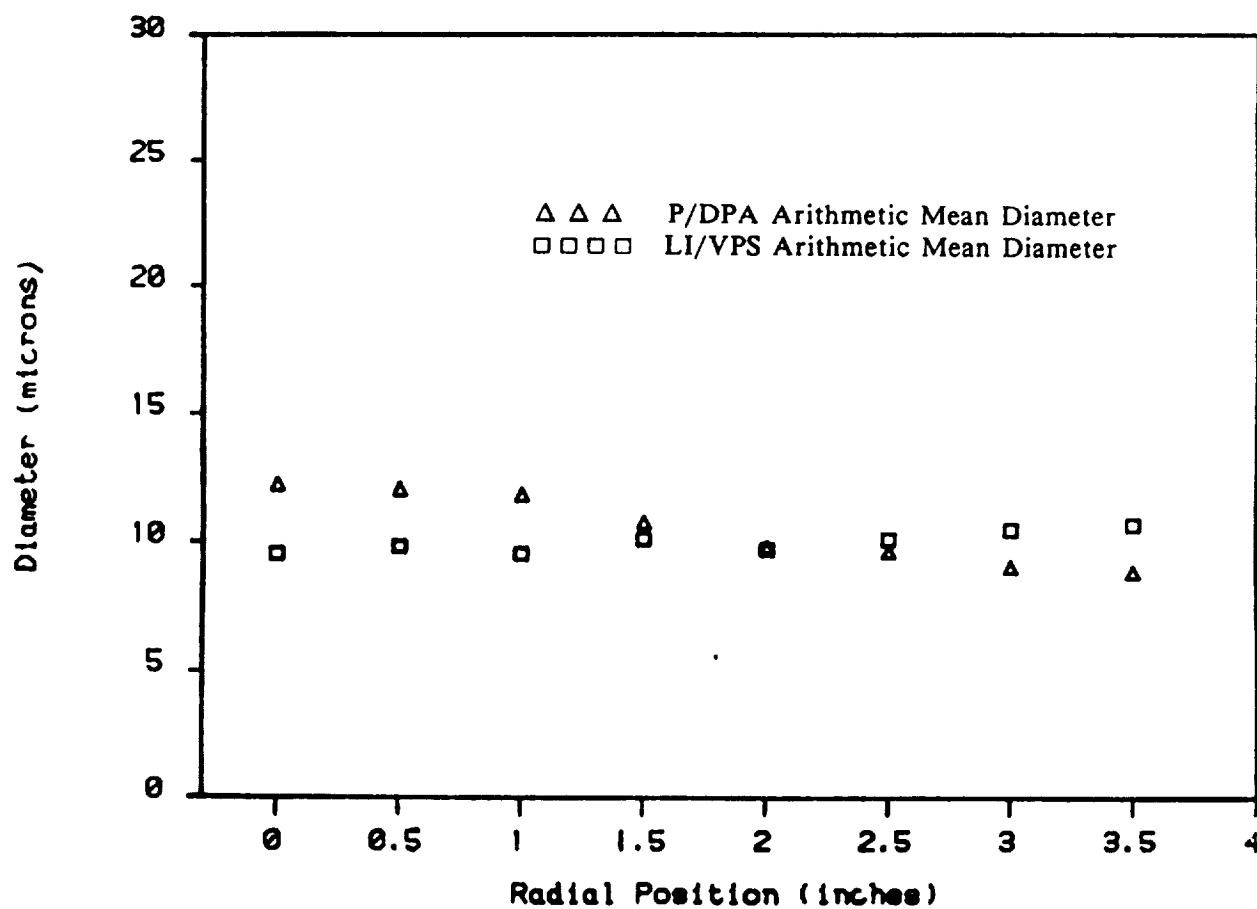
Referring to Table 3.5, the arithmetic mean diameters measured by the LI/VPS remained approximately constant from $9.5\ \mu\text{m}$ at the centerline to $10.7\ \mu\text{m}$ at the edge of the spray, while the P/DPA values varied from $12.3\ \mu\text{m}$ at the centerline to $8.8\ \mu\text{m}$ at the edge of the spray. Figure 3.41 shows the general trend in the LI/VPS and P/DPA arithmetic mean diameter to be very similar with a maximum deviation of $2.8\ \mu\text{m}$ at the centerline and a minimum deviation of $0.1\ \mu\text{m}$ at the 2.0 inch location. Figure 3.42 shows the trend in the Sauter mean diameter to be also similar for both instruments. The maximum deviation is $2.2\ \mu\text{m}$ at the 1.0 inch radial position while the minimum deviation is 0.0 for the 2.5 inch position. The maximum deviation of $2.8\ \mu\text{m}$ for the arithmetic mean diameter, and $2.2\ \mu\text{m}$ for the Sauter mean diameter can be explained as a result of the difference in instrument operation (automatic imaging vs light scattering and spatial vs temporal), the depth of field correction used by the P/DPA and no correction for the LI/VPS system, and to the LI/VPS instrument calibration error calculated to be $\pm 2.6\ \mu\text{m}$ with a standard deviation of $\pm 2.0\ \mu\text{m}$.

3.2.2 Discussion of Results for Comparison - CASE II

Referring to Fig. 3.43 and Table 3.5, the maximum deviation in arithmetic mean diameter of $7.1\ \mu\text{m}$ occurred at the centerline with the minimum deviation of $1.4\ \mu\text{m}$ at the edge of the spray. As in CASE I, the LI/VPS arithmetic mean diameters remained approximately constant from $11.9\ \mu\text{m}$ at the centerline to $12.4\ \mu\text{m}$ at the edge of the spray, and the P/DPA values varied from $19.0\ \mu\text{m}$ at the centerline to $13.8\ \mu\text{m}$ at the outer edge. Figure 3.44 showed a very similar trend in Sauter mean diameters as a function of the radial location for both instruments. A maximum deviation of $6.7\ \mu\text{m}$ occurred at the centerline of the spray and a minimum deviation of $0.4\ \mu\text{m}$ at the 1.0 inch location.

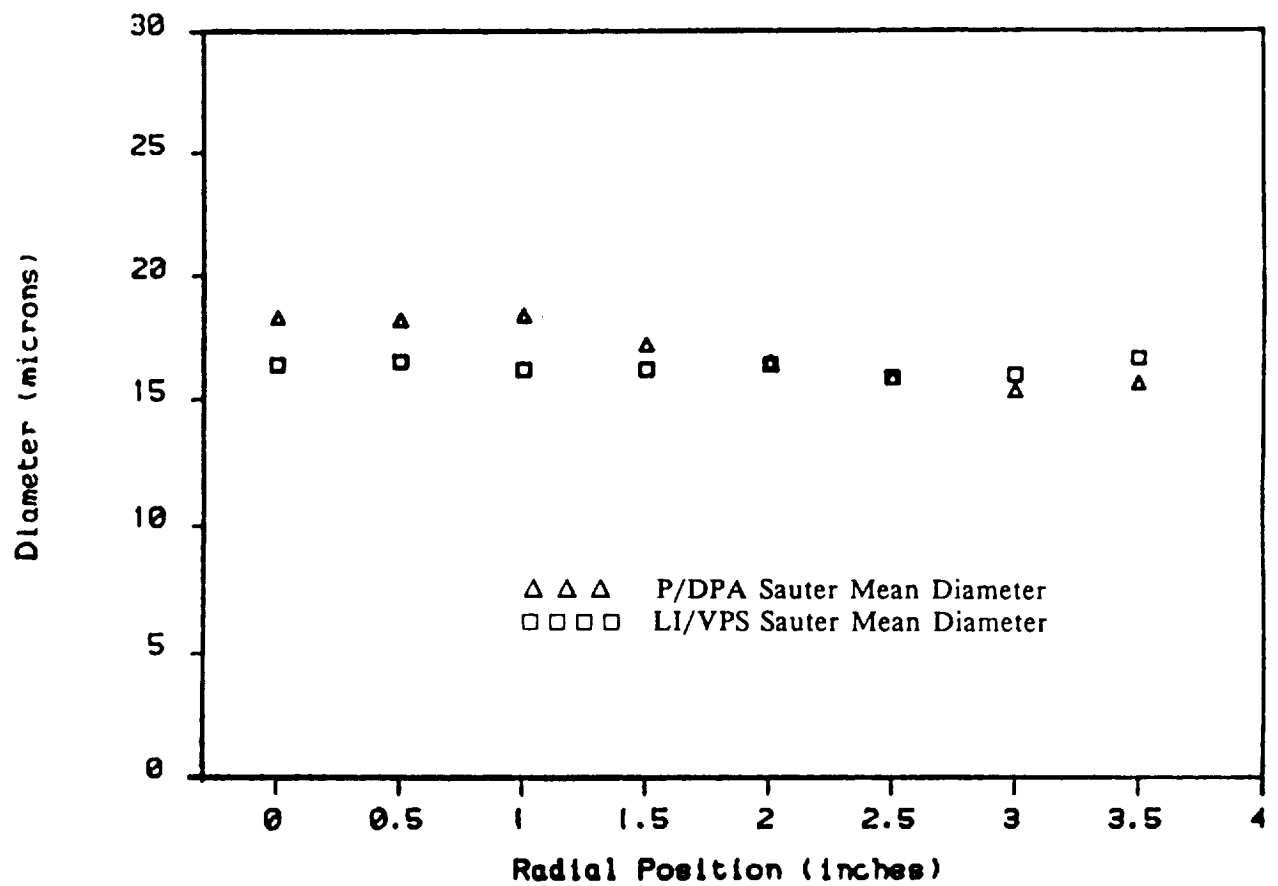
In CASE II, the increase in water pressure may increase the turbulence in the outer region of the spray plume, which in turn caused recirculation of particles through the overlapping probe volumes. In addition to the explanations given in CASE I for the differences in the arithmetic mean diameters we believe that since the trend for both cases is very similar (i.e., LI/VPS values remained approximately constant across the spray plume, while the P/DPA values decreased as the measurements approached the outer edge of the spray), some of the differences is due to the more difficult test conditions of CASE II. As we approach the outer edge of the spray, there is better agreement in the arithmetic mean diameter for both instruments. A possible explanation is the way the P/DPA operates. Recalling from Section 2.1, for proper operation of the P/DPA, the drops must pass through the probe volume perpendicular to Doppler fringes. Drops exactly at the centerline of the spray will almost always be perpendicular to these fringes and as we approach

the outer edge, the drops at these locations will have different directions. The result is an increase in run time which for CASE II varies from 2.0 sec at the centerline to 21.2 sec at the edge of the spray. The increase in time is an indication that more particles were rejected; therefore, the system becomes more selective and perhaps explains the smaller arithmetic mean diameter as the edge of the spray is approached. The difference in arithmetic mean diameters in the inner region of the spray is attributed to the loss of small particles due to the presence of high number of liquid particles per volume of air which produces overlapping signals in the P/DPA. The number density at the center of the spray was 6970 particles/cm³ compared to 1070 particles/cm³ at the edge. According to Dodge et al[22], by comparing the AMD with the SMD for each case, the differences in the shape of the distribution can be observed. Studying Figures 3.41, 3.42, 3.43, and 3.44 it is observed that the Sauter mean diameter compared more closely than the arithmetic mean diameter which suggests a difference in distribution shape for each case.



(CASE I)
Test Conditions:
Air Pressure = 65 psia.
Water Pressure = 105 psia.
Water Flow-rate = 0.069 gal/min.

Figure 3.41: Comparison of Arithmetic Mean Diameters for MOD-1 Nozzle Comparison Test - CASE I



(CASE I)

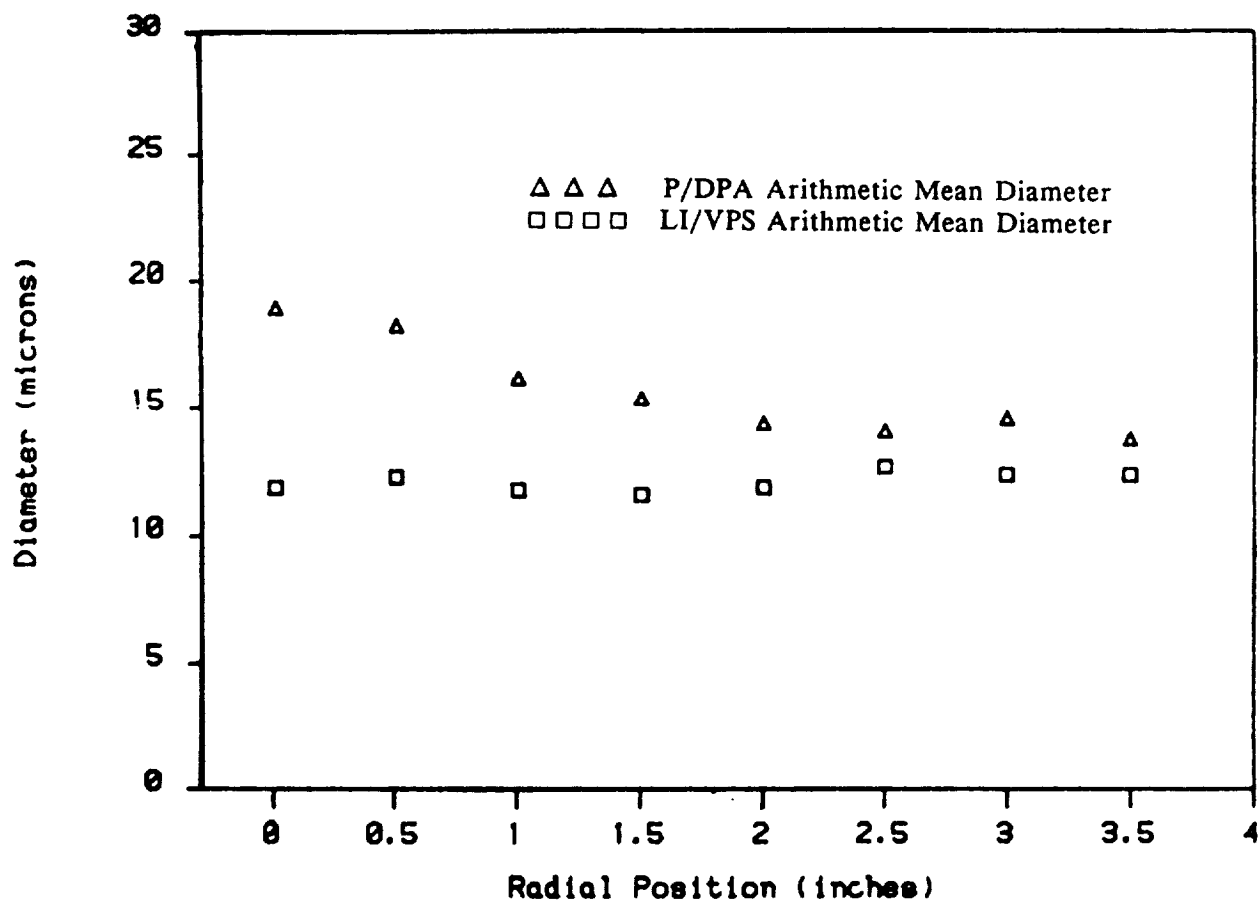
Test Conditions:

Air Pressure = 65 psia.

Water Pressure = 105 psia.

Water Flow-rate = 0.069 gal/min.

Figure 3.42: Comparison of Sauter Mean Diameters for MOD-1 Nozzle Comparison Test - CASE I



(CASE II)

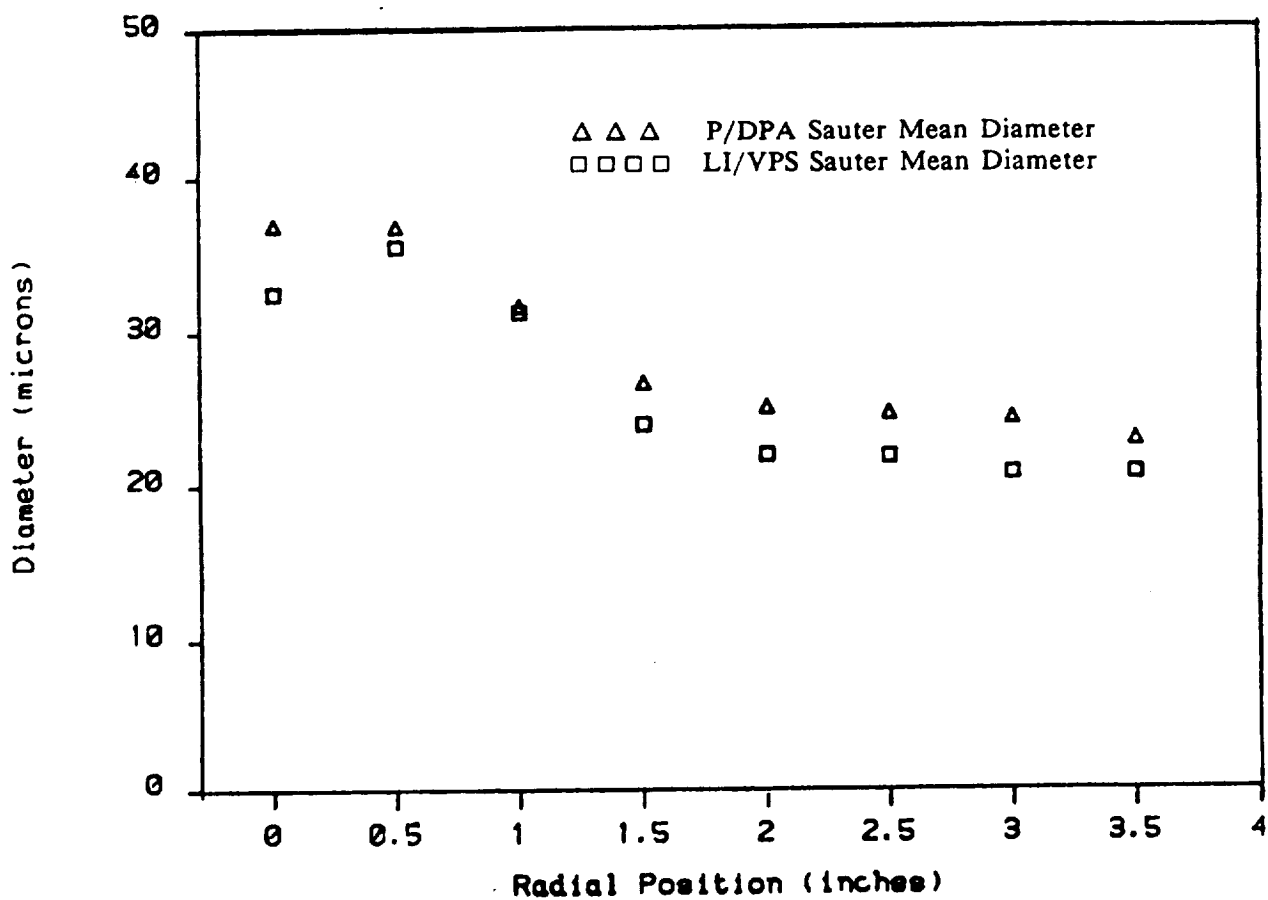
Test Conditions:

Air Pressure = 45 psia.

Water Pressure = 115 psia.

Water Flow-rate = 0.094 gal/min.

Figure 3.43: Comparison of Arithmetic Mean Diameters for MOD-1 Nozzle Comparison Test - CASE II



(CASE II)

Test Conditions:

Air Pressure = 45 psia.
 Water Pressure = 115 psia.
 Water Flow-rate = 0.094 gal/min.

Figure 3.44: Comparison of Sauter Mean Diameters for MOD-1 Nozzle Comparison Test - CASE II

Table 3.5: MOD-1 Nozzle Comparison Results

CASE I

Water Pressure = 105 psia			Air Pressure = 65 psia	
LI/VPS Results			P/DPA Results	
RADIAL POSITION (inches)	ARITHMETIC MEAN DIAMETER (μm)	SAUTER MEAN DIAMETER (μm)	ARITHMETIC MEAN DIAMETER (μm)	SAUTER MEAN DIAMETER (μm)
CL	9.5	16.4	12.3	18.3
0.5	9.8	16.5	12.1	18.2
1.0	9.5	16.2	11.9	18.4
1.5	10.1	16.2	10.8	17.2
2.0	9.7	16.4	9.8	16.5
2.5	10.1	15.9	9.6	15.9
3.0	10.5	16.0	9.0	15.4
3.5	10.7	16.7	8.8	15.7

CASE II

Water Pressure = 115 psia			Air Pressure = 45 psia	
LI/VPS Results			P/DPA Results	
RADIAL POSITION (inches)	ARITHMETIC MEAN DIAMETER (μm)	SAUTER MEAN DIAMETER (μm)	ARITHMETIC MEAN DIAMETER (μm)	SAUTER MEAN DIAMETER (μm)
CL	11.9	32.5	19.0	39.2
0.5	12.3	35.5	18.3	36.8
1.0	11.8	31.3	16.2	31.7
1.5	11.6	24.9	15.4	26.7
2.0	11.9	22.0	14.4	25.1
2.5	12.7	21.9	14.1	24.7
3.0	12.4	20.8	14.6	24.4
3.5	12.4	20.8	13.8	23.0

Section 4

CONCLUSIONS AND RECOMMENDATIONS

This section presents the conclusions of the experimental findings and suggestions for utilizing the experimental apparatus and drop-sizing instrumentation in future studies. The first section deals with the revisions to the LI/VPS, including the upgrade to dynamic particle sizing, the development of the calibration procedure, and the software updates. The second section deals with the comparison of the LI/VPS and the P/DPA, and observations concerning their proper operation, set-up, and limitations. The final section of pertains to the improvement of the LI/VPS to a more complete drop-sizing instrument, the continuation of aerosol spray analysis on the MOD-1 nozzle, and general observations concerning the continuing work in aerosol drop-sizing.

4.1 LI/VPS

The LI/VPS has been upgraded to a system capable of performing drop-sizing analysis on dynamic particles. With the addition of the AD/DA converter board to the control computer, the PSP has shown the capability to distinguish drop-size and focus on dynamic particles in the SPM (i.e., freeze frame analysis). Therefore, the LI/VPS' drop-sizing method and focus criteria, developed prior to this work, remains essentially intact with minor modifications.

A two-dimensional calibration procedure for LI/VPS has been developed which allows for a straight-forward, step-by-step process in determining the micron/pixel correction factors associated with the lens magnification and camera tube non-linearities. With the developed calibration procedure and the availability of a f/8 lens (i.e., approximate LI/VPS magnification of 1000), the lower-limit on the measurable, focus-dependent size-span of the LI/VPS has been reduced from 9 μm to 3 μm .

Included in the LI/VPS upgrade has been the development of the PSP set-up sub-program and a drop-size distribution graphics display package. Due to the variability of conditions in aerosol spray analysis and the flexibility of the LI/VPS, the set-up sub-program was developed to aid the operator in his decision process and allow for utilization of the full capabilities of the LI/VPS. The addition of the graphic package was necessary to further the LI/VPS' ability to characterize aerosol sprays. The graphical representation of the drop-size data was used as a diagnostic tool in specifying the proper drop-size range and a tool in the comparison of the LI/VPS and the P/DPA.

4.2 LI/VPS and P/DPA Comparison

The LI/VPS and the P/DPA compared favorably in tests performed both on the VOAG as well as on the MOD-1 nozzle. Results of calibration runs performed with the VOAG for cases with and without particle dispersion showed agreement between instruments within $\pm 2.6 \mu\text{m}$. The

standard deviation of the calibration test results were all under $2.0\text{ }\mu\text{m}$. The small standard deviation indicates the accuracy of these instruments for similar test conditions. The MOD-1 nozzle experiments also showed similar agreement between instruments. Results from CASE I shows a maximum $2.8\text{ }\mu\text{m}$ difference in AMD and a $2.2\text{ }\mu\text{m}$ difference in SMD. AMD values determined for CASE II show a higher deviation than CASE I ($7.1\text{ }\mu\text{m}$ and $2.8\text{ }\mu\text{m}$ respectively). The AMD values agree quite well for the outer region of the spray where the PDPA system becomes more selective as explained in section 3.3.2. The SMD for both instruments follows the same general trend across the spray with a maximum deviation of $6.7\text{ }\mu\text{m}$. Considering the difference in the basic sizing methods employed by the two instruments and the very difficult test operating conditions, the LI/VPS and the P/DPA comparative measurements were surprisingly close especially for the SMD.

Proper operation and set-up of the LI/VPS and the P/DPA depend highly on the operating conditions specified in each test case. For this discussion, the MOD-1 nozzle is of prime interest. The operating conditions of the MOD-1 nozzle for the aforementioned cases, were not ideal for either instrument. Since the LI/VPS has limited lower size measurement capabilities, the AMD and SMD values determined may be slightly higher than the actual values. On the other hand, turbulence at the outer regions of the spray plume seemed to cause the P/DPA to reject a high number of counts. It is important that the operator monitor each instrument in characterizing any unknown aerosol spray. Even though the LI/VPS and the P/DPA agree remarkably well, each instrument performs better under different test conditions. The LI/VPS performs well in a high density aerosol spray, whereas the P/DPA under similar conditions, appears to have difficulties due to the overlap of signals (multiple particles in probe volume). Particle rejection in the P/DPA appears to limit the capability of this instrument to make liquid water flux measurements for the test conditions considered here. The P/DPA is much faster than the LI/VPS which allows for more versatility especially in sparse sprays. Also, the P/DPA is capable of making velocity measurements concurrently with the drop-size measurement, but as was shown for the MOD-1 comparison, the recirculation of drops associated with the turbulent spray resulted in numerous rejections.

4.3 Suggestions and Recommendation for Future Work

The LI/VPS, as particle sizing instrument, has progressed in stages of development. The next stage of development should be to upgrade the system to off-line analysis (e.g., frame storage on a read-write laser disk recorder), as well as increasing the program speed through hardware and software modifications. A study should be performed to determine the feasibility of frame storage, and if necessary, the error associated with such storage. The control computer, the behavior of imaging laser, and the PSP program structure should be studied to increase the operating speed of the LI/VPS. With the addition of the Micro-VAX computer, the control computer should not be the limiting parameter in program speed. The PSP trigger to the imaging laser doesn't function consistently which makes it necessary to check for appropriate background level before processing. Therefore, with proper operation of the imaging trigger, unnecessary processing time can be avoided. Finally, to increase the speed of the LI/VPS, the PSP should be stream-lined. For example, the double-threshold used to determine BGL parameter for particle focus should be consolidated into a single threshold.

The research on the MOD-1 nozzle and the comparison of the LI/VPS and the P/DPA should be continued. Operating conditions for the current work were specified by NASA. Future work on the MOD-1 nozzle should involve tests performed at lower water and air nozzle pressures. These

operating conditions would produce a larger drop-size and reduce turbulence in the spray. Also, a position closer to the nozzle would produce a higher number density spray which would be ideal for the LI/VPS. The use of the P/DPA 200 mm transmitter lens would reduce the probe volume which, in turn, would reduce the probability of multiple particles in the probe volume produced by the high number density of droplets. The 200 mm transmitter lens was not used in the current work since similar sized probe volumes were needed in making the simultaneous and overlapping probe volume analysis. The above suggestions are included to improve the functionality of the two instruments in future studies.

The current research and other comparison work by Dodge et al. [22] and Jackson et al. [23] improve the understanding of the various types of sizing techniques and assist in the development of accurate sizing instrumentation. The selection of a calibration/verification method or standard should be found for all drop-sizing instruments. The selection should be a priority for researchers and instrument manufacturers.

Section 5

REFERENCES

1. Proceedings - Particle Sizing Instrument Development Group, 1986 Droplet Technology Workshop, NASA Lewis Research Center, Cleveland, Ohio, 1986.
2. Malvern Instruments Limited, Malvern Worcestershire WR14 1AQ, England.
3. Bachalo, W. D., "Method for Measuring the Size and Velocity of Spheres by Dual-Beam Light Scatter Interferometry," *Applied Optics*, Vol. 19, 1980.
4. Bachalo, W. D., and Houser, M. J., "Development of the Phase/Doppler Spray Analyzer for Liquid Drop Size and Velocity Characterizations," *AIAA/SAE/ASME 20th Joint Propulsion Conference*, Cincinnati, Ohio, AIAA paper No. 841199, June 1984.
5. Farmer, W. M., "Measurements of Particle Size, Number Density, and Velocity Using a Laser Interferometer," *Applied Optics*, Vol. 11, No. 11, 1972.
6. Alexander, D. R., and Morrison, M. J., "Particle Concentration Measurements by Laser Imaging for a Turbulent Dispersion," *Particle Science and Technology*, Vol. 2, No. 4, p. 379, 1984.
7. Ahlers, K. D., "A Microcomputer-Based Digital Image Processing System Developed to Count and Size Laser-Generated Small Particle Images," M.S. Thesis, Mechanical Engineering Dept., University of Nebraska-Lincoln, 1984.
8. Alexander, D. R., and Ahlers, K. D., "A Microcomputer-Based Digital Image Processing System Developed to Count and Size Laser-Generated Small Particle Images," *Optical Engineering*, Vol. 24, No. 6, p. 1060, 1985.
9. Ahlers, K. D., and Alexander, D. R., "A Flexible High-Speed Digital Image Processing System," *SPIE 29th Annual Meeting*, Paper No. 573-11, SPIE Proceedings, Vol. 573, San Diego, CA, 1985.
10. Wiles, K. J., "Development of a System for Secondary Liquid Injection into a Mach 2 Supersonic Flow to Study Drop Size Distribution by Video Imaging Techniques," M.S. Thesis, Mechanical Engineering Dept., University of Nebraska-Lincoln, 1985.
11. Weiss, B. A., Derov, P., DeBiase, D., Simmons, H. C., "Fluid Particle Sizing Using a Fully Automated Optical Imaging System," *Optical Engineering*, Vol. 23, No. 5, 1984.
12. Hirleman, E. D., "On-Line Calibration Techniques for Laser Diffraction Droplet Sizing Instruments," *ASME paper No. 83-GT-232*, 1983.

13. Tishkoff, J. M., "Spray Characterization: Practices and Requirements," Optical Engineering, Vol. 23, No. 5, 1984.
14. Alexander, D. R., Wiles, K. J., Schaub, S. A., Seeman, M. P., "Effects of Non-spherical Drops on a Phase Doppler Spray Analyzer," Proceedings of SPIE - The International Society of Optical Engineering, Volume 573, August 21, 1985.
15. ASTM Standard E799-81 (1981).
16. Supplied by NASA Lewis Research Center.
17. Berglund, R. N., and Liu, B. Y. H., "Generation of Monodisperse Aerosol Standards," Environmental Science and Technology, Vol. 7, 1973.
18. Available from TSI Inc., St. Paul, MN.
19. Bachalo, W. D., and Houser, M. J., "Phase/Doppler Particle Analyzer Operation Manual," Aerometrics Inc., Mountain View, CA., Release 1.0, 1985.
20. Interview, Bachalo, W. D., Concerning PMT voltage gain voltage, Dec. 9, 1985.
21. Bachalo, W. D., and Houser, M. J., "Measurements of Drop Dynamics and Mass Flux in Sprays," Presented, 1986 Meeting of the Central States Section/The Combustion Institute, NASA Lewis Research Center, Cleveland, Ohio, May, 1986.
22. Dodge, L. G., Rhodes, D. J., and Reitz, R. D., "Comparison of Drop-size Measurements Techniques in Fuel Sprays: Malvern Laser-Diffraction and Aerometrics Phase/Doppler," Presented, 1986 Meeting of the Central States Section/The Combustion Institute, NASA Lewis Research Center, Cleveland, Ohio, May, 1986.
23. Jackson, T. A., and Samuelson, G. S., "An Evaluation of the Performance of Visibility/Intensity Validation and Phase/Doppler Techniques in Characterizing the Spray of an Air-Assist Nozzle," Presented, 1986 Meeting of the Central States Section/The Combustion Institute, NASA Lewis Research Center, Cleveland, Ohio, May, 1986.

Section 6

APPENDIX A: EQUIPMENT LISTING

Device	Manufacturer	Model #	Serial #
P/DPA Transmitter	Aerometrics Inc.	1100	101
P/DPA Receiver	Aerometrics Inc.	2100	101
P/DPA Signal Processor	Aerometrics Inc.	PDP 3100	103
P/DPA Control Computer	IBM Corp.	AT-5170	01619045170
P/DPA Output Printer	Hewlett Packard Corp.	2225A	2617S31411
LI/VPS Imaging Laser	Energy Systems Inc.	N2-50	
LI/VPS Imaging Laser	Laser Systems Inc.	N2-50	
Power Supply			
LI/VPS Imaging	Laser Holography Inc.	N2-50	
Laser Control Module			
LI/VPS Laser	Laser Holography Inc.	N2-50	
Sync Generator			
LI/VPS (back-up)	Molelectron Corp.	UV-12	198
Imaging Laser			
LI/VPS (back-up) Imaging	Busch Inc.	V-20	116
Laser Vacuum Pump			
LI/VPS Video Camera	COHU Inc.	2006-011	625810
LI/VPS Video Camera	COHU Inc.	7910B-011	112698
Control Unit			
LI/VPS Control Computer	Digital Equipment Corp.	PDP11/73	
LI/VPS Output Printer	Digital Equipment Corp.	LA75-A2	03555
LI/VPS Video Processor	Recognition Concepts Inc.	TRAPIX 55/32Q	134
Computer Terminal	Digital Equipment Corp.	VT-240	HK14705
Computer Terminal	CIE Terminals Inc.	CIT-220+	8471C6916

Video Monitor	Sanyo Corp.	AVM255	55805757
Video Monitor	SONY Corp.	CKV-1900F	204071
Video Cassette Recorder	RCA Corp.	VET650	1032FM243
Video Cassette Recorder	Panasonic Corp.	NV-8950	B5HL00491
Laser/optical	Panasonic Corp.	TQ-2320F(A)	EH4669001
Disk Recorder			
Decwriter	Digital Equipment Corp.	LA120AA	PNE1366
Digital Oscilloscope	Hewlett-Packard Corp.	54200A	2511A-00639
Measurement	Hewlett-Packard Corp.	7090A	2430A00344
Plotting System			
Real-time Oscilloscope	Tektronix Inc.	549	7365
Digital Multimeter	John Fluke Mfg. Co., Inc.	8024B	3715516
Pressure Transducer	OMEGA Eng., Inc.	PX304-150	850502
Pressure Transducer	OMEGA Eng., Inc.	PX304-150	850311
Direct Current	Hewlett-Packard Corp.	6200B	2411A-12365
Power Supply			
Flowmeter-regulator	Cole-Palmer Inc.	PR004	FM044-40G
Monodisperse	TSI Inc.	345000	167
Drop Generator			
Test Nozzle	NASA Lewis Space Center	MOD-1	
Air and Water Supply	University of Nebraska		
Pressure Regulator	WATTS Regulator Co.	2-26A	8305
Water Pressure Vessel	Brunswick Corp.	6121020-024	1003
Isolation Table	Newport Research Corp.		
High-pressure	Yellow Jacket Inc.	WPP0031A	
Charging Hose			
Dead Weight	American Steam Gage Co.		
Pressure Tester			
Balance Scale	HOWE Inc.	3074131	

Section 7

APPENDIX B Design and Implementation of the PSP Laser Trigger

Due to the availability of the existing laser sync circuit (LSC) and the AD/DA converter board, the development of the PSP software generated trigger was simplified. With the aforementioned hardware, the PSP software, utilizing available FORTRAN callable commands, directs a digital value to the AD/DA board. The AD/DA board converts the digital value to the appropriate analog signal. The analog signal is then sent to the LSC. The analog signal from the control computer is paralleled with the sync signal from the CCU, and the resulting signal triggers the imaging laser. The above process was used as the basis for LI/VPS conversion from the CPM to the SPM. Except for cabling, the majority of work in the modification dealt with the LSC. Figure B7.1 shows the overall circuitry of the LSC with special attention given to the source of the LSC laser trigger and the position marked by the Xs. The major addition to the LSC circuitry was the two AND gates (Appendix B, Fig. B7.2. Therefore an analog signal from the control computer must be present at the first AND gate before the imaging laser can be triggered. The above method, therefore, facilitates SPM operation for the LI/VPS.

NEW TB
G. F. L. 1948

COMPOSITE
VIDEO
SYNC IN
(-4V PP)





Section 8

APPENDIX C.1: PSP Set-up Program

```

C
      PROGRAM MENU
C
C*****
***** C
C      PROGRAM DEVELOPED TO SET-UP OPERATING PARAMETERS FOR THE
C      THE PARTICLE SIZING PROGRAM UTILIZING A MENU-TYPE FORMAT.
C
C*****
***** C
      REAL*8 PROCESS(2), YESNO(2), ADVANCE(2), LIMIT(3),
BOUNDRY(2)      REAL*8 MAG(2), A, B, C, D, F, G, H, I, J, V, W
      INTEGER TOD(4), DOY(5)
      CHARACTER*10 NUMBER
      CHARACTER*6 FILE1, FILE2
      CHARACTER*1 L(6), M(6)
      LOGICAL*1 IKEY
      BYTE ESC, LINE(50,4)
      DATA ESC / 27 /
      DATA PROCESS, YESNO / 'STATIC', 'DYNAMC', 'YES  ', 'NO
' /
      DATA ADVANCE, FILE1 / 'SINGLE', 'AUTO  ', 'TEMPO1' /
      DATA LIMIT, FILE2 / 'TIME  ', 'FRAME ', 'PARTCL', 'TEMPO1' /
      DATA BOUNDRY, MAG / 'PROCSS', 'REJECT', 'LOW  ', 'HIGH ' /
      DATA IGPST, WIDTH, NGRPS, ITHRS, LIMVAL / 5, 5.0, 50, 90,
2000 /
      DATA JXSTR, JXDST, JYSTR, JYDST / 50, 400, 50, 400 /
      DATA A, B, C, D / 'DYNAMC', 'YES  ', 'AUTO  ', 'PARTCL' /
      DATA F, G, H, I / 'REJECT', 'YES  ', 'YES  ', 'YES  ' /
      DATA J, V, W / 'NO    ', 'LOW  ', 'NO    ' /
      DATA LINE / 200*' ' /
      DATA NUMBER / '1234567890' /
      EQUIVALENCE(L,FILE1)
      EQUIVALENCE(M,FILE2)
      CALL DATE(DOY)
      CALL TIME(TOD)
      WRITE(7,1) ESC, ESC, ESC, ESC

```

```

1      FORMAT(1X,A1,'[81',A1,'[?251',A1,'[H',A1,'[2J')
C
C*** IF DATE NOT SET, INSERT "NO DATE" INTO DATE FIELD
C
      IF( DOY(1) .EQ. '00' ) DOY(5) = ' '
      IF( DOY(1) .EQ. '00' ) DOY(4) = 'TE'
      IF( DOY(1) .EQ. '00' ) DOY(3) = 'DA'
      IF( DOY(1) .EQ. '00' ) DOY(2) = '0 '
      IF( DOY(1) .EQ. '00' ) DOY(1) = ' N'
C
C
C...   INPUT PREVIOUSLY STORED PSP PARAMETERS.
C
      OPEN(UNIT=1, FILE='SETUP.MNU',STATUS='OLD',ERR= 5)
      READ(1,10) A, B, C, D, LIMVAL, F, G, H, FILE1, I, J, FILE2,
& IGPST, WIDTH, NGRPS, JXSTR, JXDST, JYSTR, JYDST, ITHRSH,
V, W      READ(1,2)
2      FORMAT(2(/))
      DO 4 II=1,4
      READ(1,3) (LINE(JJ,II), JJ=1,50)
3      FORMAT(3X,50A1)
4      CONTINUE
      GOTO 9 5 OPEN(UNIT=1, FILE='SETUP.MNU',STATUS='NEW')
WRITE(1,10) A, B, C, D, LIMVAL, F, G, H, FILE1, I, J, FILE2,
& IGPST, WIDTH, NGRPS, JXSTR, JXDST, JYSTR, JYDST, ITHRSH, V, W
      WRITE(1,2)
      DO 6 II=1,4
      WRITE(1,3) (LINE(JJ,II), JJ=1,50)
6      CONTINUE
9      WRITE(7,10) A, B, C, D, LIMVAL, F, G, H, FILE1, I, J,
FILE2,      & IGPST, WIDTH, NGRPS, JXSTR, JXDST, JYSTR, JYDST,
ITHRSH, V, W      CLOSE(UNIT=1)
10     FORMAT('+',T39,'SETUP'/T26,'PARTICLE SIZING PROGRAM (ver.
4)')//      & 33('-'), ' PROCESSING OPTIONS',T54,25('-')/
& T3,'(A)',T9,A6,T19,'Type of Processing',T49,
& '(STATIC/DYNAMIC)',/
& T3,'(B)',T9,A6,T19,'Focus Criteria',T49,
& '(YES/NO)',/
& T3,'(C)',T9,A6,T19,'Type of Frame Advance',T49,
& '(AUTO/SINGLE)',/
& T3,'(D)',T9,A6,T19,'Processing Limit',T49,
& '(TIME/FRAME/PARTICLE)',/
& T3,'(E) (' ,T9,I6,T15,') Limiting Value',T49,
& '(seconds/frames/particles)',/
& T3,'(F)',T9,A6,T19,'Boundary Particles',T49,
& '(PROCESS/REJECT)',/

```

```

& 36('-'), ' OUTPUT OPTIONS ',26('-')/
& T3,'(G)',T9,A6,T19,'General Results (to PRINTER)
(YES/NO)'/ & T19,'WRITE TO FILE (YES/NO)',T49,
& '(K) FILE HEADER (4 lines)',/
& T3,'(H)',T9,A6,T19,'Average Particle size data -- ',T49,
& '(L) FILE: (' ,A6,').OUT',/
& T3,'(I)',T9,A6,T19,'Group Breakdown data ',9('-'),'/'/
& T3,'(J)',T9,A6,T19,'Per Frame data ',13('-'), '>',T49, &
'(M) FILE: (' ,A6,').DAT',/
& 35('-'), ' GENERAL OPTIONS ',26('-')/
& T3,'(N) Group Start =( ',I3,') '
& T29,'(O) Group Width =( ',F4.1,') '
& T55,'(P) # of Groups =( ',I3,')'/
& T3,'(Q) X Window Start = (' ,I3,')',
& T49,'(R) X Window Width = (' ,I3,')'/
& T3,'(S) Y Window Start = (' ,I3,')',
& T49,'(T) Y Window Width = (' ,I3,')'/
& T3,'(U) Threshold = (' ,I3,')'
& T29,'(V) Lens = ',A6,
& T49,'(W) Markers = ',A6,'(YES/NO)'/78('-'))
WRITE(7,20) ESC, ESC
20 FORMAT('+',A1,'[23;2H',A1,'[OJ', '(X) to exit SETUP menu or
& (Z) to begin Particle Sizing Program .... '/
& T3,'Enter Letter to change specific Parameter ??')

```

C

C

C ... SPECIFY PSP PARAMETER W/ KEY TOGGLE OR KEYBOARD ENTRY.

C

```

30 CALL IPOKE("44","10000 .OR. IPEEK("44))
IKEY = ITTINR()
IF(IKEY.LT.0) GOTO 30
IF(IKEY.EQ.'A') GOTO 100
IF(IKEY.EQ.'B') GOTO 200
IF(IKEY.EQ.'C') GOTO 300
IF(IKEY.EQ.'D') GOTO 400
IF(IKEY.EQ.'E') GOTO 500
IF(IKEY.EQ.'F') GOTO 600
IF(IKEY.EQ.'G') GOTO 700
IF(IKEY.EQ.'H') GOTO 800
IF(IKEY.EQ.'I') GOTO 900
IF(IKEY.EQ.'J') GOTO 1000
IF(IKEY.EQ.'K') GOTO 1100
IF(IKEY.EQ.'L') GOTO 1200
IF(IKEY.EQ.'M') GOTO 1300
IF(IKEY.EQ.'N') GOTO 1400
IF(IKEY.EQ.'O') GOTO 1500

```

```

        IF(IKEY.EQ.'P')    GOTO 1600
        IF(IKEY.EQ.'Q')    GOTO 1700
        IF(IKEY.EQ.'R')    GOTO 1800
        IF(IKEY.EQ.'S')    GOTO 1900
        IF(IKEY.EQ.'T')    GOTO 2000
        IF(IKEY.EQ.'U')    GOTO 2100
        IF(IKEY.EQ.'V')    GOTO 2200
        IF(IKEY.EQ.'W')    GOTO 2400
        IF(IKEY.EQ.'X')    GOTO 2600
C      IF(IKEY.EQ.'Y') GOTO 2500
        IF(IKEY.EQ.'Z')    GOTO 2600
        GO TO 30
90     FORMAT('+',A1,'[23;2H',A1,'[0J',
& 'Enter new value for (' ,A1,') here ==>',$)
C
C...  (A) SPECIFY PROCESS TYPE (DYNAMIC/STATIC)
C
100    CALL IPOKE("44","167777 .AND.  IPEEK("44))
        IF(A.EQ.PROCESS(1)) GOTO 150
        A = PROCESS(1)
        GOTO 180
150    A = PROCESS(2)
180    WRITE(7,190) ESC, A
190    FORMAT('+',A1,'[5;8H',A6)
        GOTO 30 C
C...  (B) SPECIFY FOCUS (YES/NO)
C
200    CALL IPOKE("44","167777 .AND.  IPEEK("44))
        IF(B.EQ.YESNO(1)) GOTO 250
        B = YESNO(1)
        GOTO 280
250    B = YESNO(2)
280    WRITE(7,290) ESC, B
290    FORMAT('+',A1,'[6;8H',A6)
        GOTO 30
C
C...  (C) TYPE OF FRAME ADVANCE (SINGLE/AUTO)
C
300    CALL IPOKE("44","167777 .AND.  IPEEK("44))
        IF(C.EQ.ADVANCE(1)) GOTO 350
        C = ADVANCE(1)
        GOTO 380
350    C = ADVANCE(2)
380    WRITE(7,390) ESC, C
390    FORMAT('+',A1,'[7;8H',A6)
        GOTO 30

```



```

C
C... (D) PROCESSING LIMIT (TIME/PARTICLE/FRAME)
C... NOTE: DUE TO COMPUTER LIMITATIONS TIME IS NOT INCLUDED C
400 CALL IPOKE("44","167777 .AND. IPEEK("44))
    IF(D.EQ.LIMIT(1).OR.D.EQ.LIMIT(2)) GOTO 450
    D = LIMIT(1)
    GOTO 480
450 IF(D.EQ.LIMIT(2)) GOTO 470
    D = LIMIT(2)
    GOTO 480
470 D = LIMIT(3)
480 WRITE(7,490) ESC, D
490 FORMAT('+',A1,'[8;8H',A6)
    GOTO 30

C
C... (E) SPECIFY LIMITING VALUE
C
500 CALL IPOKE("44","167777 .AND. IPEEK("44))
    WRITE(7,90) ESC, ESC, 'E'
    READ(5,*) LIMVAL
580 WRITE(7,590) ESC, LIMVAL
590 FORMAT('+',A1,'[9;8H',I6)
    WRITE(7,20) ESC, ESC
    GOTO 30

C
C... (F) BOUNDARY ANALYSIS
C... NOTE: UNAVAILABLE
C
600 CALL IPOKE("44","167777 .AND. IPEEK("44))
    IF(F.EQ.BOUNDARY(1)) GOTO 650
    F = BOUNDARY(1)
    GOTO 680
650 F = BOUNDARY(2)
680 WRITE(7,690) ESC, F
690 FORMAT('+',A1,'[10;8H',A6)
    GOTO 30

C
C... (G) OUTPUT GENERAL RESULTS TO PRINTER
C
700 CALL IPOKE("44","167777 .AND. IPEEK("44))
    IF(G.EQ.YESNO(1)) GOTO 750
    G = YESNO(1)
    GOTO 780
750 G = YESNO(2)
780 WRITE(7,790) ESC, G
790 FORMAT('+',A1,'[12;8H',A6)

```

```

        GOTO 30
C
C... (H) WRITE TO FILE: ANALYSIS SUMMARY (YES/NO)
C
800  CALL IPOKE("44","167777 .AND. IPEEK("44))
      IF(H.EQ.YESNO(1)) GOTO 850
      H = YESNO(1)
      GOTO 880
850  H = YESNO(2)
880  WRITE(7,890) ESC, H
890  FORMAT('+',A1,'[14;8H',A6)
      GOTO 30
C
C... (I) WRITE TO FILE: GROUP BREAKDOWN (YES/NO)
C
900  CALL IPOKE("44","167777 .AND. IPEEK("44))
      IF(I.EQ.YESNO(1)) GOTO 950
      I = YESNO(1)
      GOTO 980
950  I = YESNO(2)
980  WRITE(7,990) ESC, I
990  FORMAT('+',A1,'[15;8H',A6)
      GOTO 30
C
C... (J) WRITE TO FILE: PER FRAME DATA (YES/NO)
C
1000 CALL IPOKE("44","167777 .AND. IPEEK("44))
      IF(J.EQ.YESNO(1)) GOTO 1050
      J = YESNO(1)
      GOTO 1080
1050 J = YESNO(2)
1080 WRITE(7,1090) ESC, J
1090 FORMAT('+',A1,'[16;8H',A6)
      GOTO 30
C
C... (K) SPECIFY FILE HEADER
C
1100 CALL IPOKE("44","167777 .AND. IPEEK("44))
      WRITE(7,1110) ESC, ESC, ESC, ESC
1110  FORMAT(1X,A1,'[81',A1,'[?251',A1,'[H',A1,'[2J')
      WRITE(7,1111) ((LINE(JJ,II), JJ=1,50), II=1,4)
1111  FORMAT('+',T39,'SETUP'/T35,'FOR FILE HEADER'//
      & T36,'CHANGE (Y/N)'///T16,54('*'),/T16,'*',T69,'*',
      & 4(/,T16,'* '50A1,' *'),/T16,'*',T69,'*',
      & /T16,54('*')//T31,'(4 LINES/50 SPACES each)')
      CALL IPOKE("44","10000 .OR. IPEEK("44))

```

```

1115 IKEY = ITTINR()
      IF(IKEY.LT.0) GOTO 1115
      IF(IKEY.EQ.'Y') GOTO 1120
      IF(IKEY.EQ.'N') GOTO 1190
      GOTO 1115
1120 CALL IPOKE("44","167777 .AND. IPEEK("44))
      DO 1140 II=1,4
      WRITE(7,1125) ESC, ESC, II
1125 FORMAT('+',A1,'[17;3H',A1,'[OJ',
      & 'Change Line (' ,I1,')', (Y/N)')
      CALL IPOKE("44","10000 .OR. IPEEK("44))
1126 IKEY = ITTINR()
      IF(IKEY.LT.0) GOTO 1126
      IF(IKEY.EQ.'Y') GOTO 1127
      IF(IKEY.EQ.'N') GOTO 1140
      GOTO 1126
1127 CALL IPOKE("44","167777 .AND. IPEEK("44))
      WRITE(7,1130) ESC, ESC, ESC, II
1130 FORMAT('+',A1,'[22;1H',A1,'[OJ',A1,'[?8h',
      & ' Line (' ,I1,') ==>', $)
      IF(II.EQ.1) GOTO 1141
      IF(II.EQ.2) GOTO 1143
      IF(II.EQ.3) GOTO 1145
      IF(II.EQ.4) GOTO 1147
1140 CONTINUE
      GOTO 1180
1141 READ(5,1170) (LINE(JJ,1), JJ=1,50)
      WRITE(7,1142) ESC, (LINE(JJ,1), JJ=1,50)
1142 FORMAT('+',A1,'[9;15H','* ',50A1,' *')
      GOTO 1140
1143 READ(5,1170) (LINE(JJ,2), JJ=1,50)
      WRITE(7,1144) ESC, (LINE(JJ,2), JJ=1,50)
1144 FORMAT('+',A1,'[10;15H','* ',50A1,' *')
      GOTO 1140
1145 READ(5,1170) (LINE(JJ,3), JJ=1,50)
      WRITE(7,1146) ESC, (LINE(JJ,3), JJ=1,50)
1146 FORMAT('+',A1,'[11;15H','* ',50A1,' *')
      GOTO 1140
1147 READ(5,1170) (LINE(JJ,4), JJ=1,50)
      WRITE(7,1148) ESC, (LINE(JJ,4), JJ=1,50)
1148 FORMAT('+',A1,'[12;15H','* ',50A1,' *')
      GOTO 1140
1170 FORMAT(50A1)
1180 GOTO 1100
1190 WRITE(7,1) ESC, ESC, ESC, ESC
      GOTO 9

```

```

C
C... (L) FILE SPECIFICATION: GENERAL & GROUP DATA
C
1200 CALL IPOKE("44,"167777 .AND. IPEEK("44))
      WRITE(7,1220) ESC, ESC, 'L'
1220 FORMAT('+',A1,'[23;2H',A1,'[OJ',
      & 'File Name (' ,A1,') (4 letters) here ==>',$)
      READ(5,1230) (L(II), II=1,4)
1230 FORMAT(4A1)
      WRITE(7,1240) ESC, (L(II), II=1,4)
1240 FORMAT('+',A1,'[14;60H',4A1)
      WRITE(7,1250) ESC, ESC, 'L'
1250 FORMAT('+',A1,'[23;2H',A1,'[OJ',
      & 'File Number (' ,A1,') (2 numbers) here ==>',$)
      READ(5,1260) L1
1260 FORMAT(I2)
      I1 = L1/10
      IO = L1-I1*10
      IF(L1.LT.10) I1=10
      IF(IO .EQ. 0) IO=10
      L(5) = NUMBER(I1:I1)
      L(6) = NUMBER(IO:IO)
      IF(L1.LT.10) GOTO 1280
      WRITE(7,1270) ESC, L1
1270 FORMAT('+',A1,'[14;64H',I2)
      WRITE(7,20) ESC, ESC
      GOTO 30
1280 WRITE(7,1290) ESC, L1
1290 FORMAT('+',A1,'[14;64H0',I1)
      WRITE(7,20) ESC, ESC
      GOTO 30

```

```

C
C... (M) FILE SPECIFICATION: PER FRAME DATA
C
1300 CALL IPOKE("44,"167777 .AND. IPEEK("44))
      WRITE(7,1320) ESC, ESC, 'M'
1320 FORMAT('+',A1,'[23;2H',A1,'[OJ',
      & 'File Name (' ,A1,') (4 letters) here ==>',$)
      READ(5,1330) (M(II), II=1,4)
1330 FORMAT(4A1)
      WRITE(7,1340) ESC, (M(II), II=1,4)
1340 FORMAT('+',A1,'[16;60H',4A1)
      WRITE(7,1350) ESC, ESC, 'M'
1350 FORMAT('+',A1,'[23;2H',A1,'[OJ',
      & 'File Number (' ,A1,') (2 numbers) here ==>',$)
      READ(5,1360) M1

```

```

1360  FORMAT(I2)
      I1 = M1/10
      IO = M1-I1*10
      IF(M1.LT.10) I1=10
      IF(IO .EQ. 0) IO=10
      M(5) = NUMBER(I1:I1)
      M(6) = NUMBER(IO:IO)
      IF(M1.LT.10) GOTO 1380
      WRITE(7,1370) ESC, M1
1370  FORMAT('+',A1,'[16;64H',I2)
      WRITE(7,20) ESC, ESC
      GOTO 30
1380  WRITE(7,1390) ESC, M1
1390  FORMAT('+',A1,'[16;64H0',I1)
      WRITE(7,20) ESC, ESC
      GOTO 30

C
C... (N) DROP-SIZE GROUP BREAKDOWN: STARTING VALUE
C
1400  CALL IPOKE("44","167777 .AND. IPEEK("44))
      WRITE(7,90) ESC, ESC, 'N'
      READ(5,*) IGPST
1480  WRITE(7,1490) ESC, IGPST
1490  FORMAT('+',A1,'[18;21H',I3)
      WRITE(7,20) ESC, ESC
      GOTO 30

C
C... (O) DROP-SIZE GROUP BREAKDOWN: INTERVAL WIDTH
C
1500  CALL IPOKE("44","167777 .AND. IPEEK("44))
      WRITE(7,90) ESC, ESC, 'O'
      READ(5,*) WIDTH
1580  WRITE(7,1590) ESC, WIDTH
1590  FORMAT('+',A1,'[18;46H',F4.1)
      WRITE(7,20) ESC, ESC
      GOTO 30

C
C... (P) DROP-SIZE GROUP BREAKDOWN: # OF GROUPS
C
1600  CALL IPOKE("44","167777 .AND. IPEEK("44))
      WRITE(7,90) ESC, ESC, 'P'
      READ(5,*) NGRPS
1680  WRITE(7,1690) ESC, NGRPS
1690  FORMAT('+',A1,'[18;73H',I3)
      WRITE(7,20) ESC, ESC
      GOTO 30

```

```

C
C... (Q) SIZING WINDOW (PIXEL SPEC): X STARTING VALUE
C
1700 CALL IPOKE("44","167777 .AND. IPEEK("44))
      WRITE(7,90) ESC, ESC, 'Q'
      READ(5,*) JXSTR
1780 WRITE(7,1790) ESC, JXSTR
1790 FORMAT('+',A1,'[19;24H',I3)
      WRITE(7,20) ESC, ESC
      GOTO 30

C
C... (R) SIZING WINDOW (PIXEL SPEC): X SCREEN WIDTH
C
1800 CALL IPOKE("44","167777 .AND. IPEEK("44))
      WRITE(7,90) ESC, ESC, 'R'
      READ(5,*) JXDST
1880 WRITE(7,1890) ESC, JXDST
1890 FORMAT('+',A1,'[19;72H',I3)
      WRITE(7,20) ESC, ESC
      GOTO 30

C
C... (S) SIZING WINDOW (PIXEL SPEC): Y STARTING VALUE
C
1900 CALL IPOKE("44","167777 .AND. IPEEK("44))
      WRITE(7,90) ESC, ESC, 'S'
      READ(5,*) JYSTR
1980 WRITE(7,1990) ESC, JYSTR
1990 FORMAT('+',A1,'[20;26H',I3)
      WRITE(7,20) ESC, ESC
      GOTO 30

C
C... (T) SIZING WINDOW (PIXEL SPEC): Y SCREEN WIDTH
C
2000 CALL IPOKE("44","167777 .AND. IPEEK("44))
      WRITE(7,90) ESC, ESC, 'T'
      READ(5,*) JYDST
2080 WRITE(7,2090) ESC, JYDST
2090 FORMAT('+',A1,'[20;70H',I3)
      WRITE(7,20) ESC, ESC
      GOTO 30

C
C... (U) INPUT SIZING THRESHOLD
C
2100 CALL IPOKE("44","167777 .AND. IPEEK("44))
      WRITE(7,90) ESC, ESC, 'U'
      READ(5,*) ITHRS

```

```

2180 WRITE(7,2190) ESC, ITHRSH
2190 FORMAT('+',A1,'[21;19H',I3)
      WRITE(7,20) ESC, ESC
      GOTO 30

C
C... (V) INPUT SYSTEM MAGNIFICATION (HIGH/LOW)
C
2200 CALL IPOKE("44","167777 .AND. IPEEK("44))
      IF(V.EQ.MAG(1)) GOTO 2250
      V = MAG(1)
      GOTO 2280
2250 V = MAG(2)
2280 WRITE(7,2290) ESC, V
2290 FORMAT('+',A1,'[21;39H',A6)
      GOTO 30

C
C... (W) DIAGNOSTIC MARKERS PLACED ON COUNTED PARTICLES
C
2300 CALL IPOKE("44","167777 .AND. IPEEK("44))
      IF(W.EQ.YESNO(1)) GOTO 2350
      W = YESNO(1)
      GOTO 2380
2350 W = YESNO(2)
2380 WRITE(7,2390) ESC, W
2390 FORMAT('+',A1,'[21;62H',A6)
      GOTO 30

C
C... (Z) STORE SET-UP PARAMETERS AND START PSP
C
2600 CALL IPOKE("44","167777 .AND. IPEEK("44))
      OPEN(UNIT=1, FILE='SETUP.MNU',STATUS='NEW')
      WRITE(1,10) A, B, C, D, LIMVAL, F, G, H, FILE1, I, J,
FILE2,      & IGPST, WIDTH, NGRPS, JXSTR, JXDST, JYSTR, JYDST,
ITHRSH, V, W      WRITE(1,2605)
2605 FORMAT(2(/))
      DO 2650 II=1,4
      WRITE(1,2610) (LINE(JJ,II), JJ=1,50)
2610 FORMAT(3X,50A1)
2650 CONTINUE
      CLOSE(UNIT=1)
      WRITE(7,2690) ESC, ESC, ESC, ESC
2690 FORMAT(1X,A1,'[8h',A1,'[?25h',A1,'[H',A1,'[2J')
      IF(IKEY.EQ.'Z') CALL SETCMD('RUN PSP1')
      CALL EXIT
2700 STOP
      END

```

Section 9

APPENDIX C.2: PSP Graphical Presentation of Results

```

C
    PROGRAM GRAPH
C+++++
+++++ C
C    PROGRAM DEVELOPED FOR THE PSP TO GRAPHICALLY REPRESENT C
    THE GROUP BREAK-DOWN DATA ON A DEC COMPATIBLE TERMINAL. C
C+++++
+++++ C
    DIMENSION X(1000), Y(1000), Y1(70), X1(70)
    BYTE ESC, CSI, TIM(9), DAY(9)
    CHARACTER*1 A, B, C, H, II, NUMX0, NUMY0, NUMX1, NUMY1
CHARACTER*11 CO
    CHARACTER*1 NAME(7), JUNK
    CHARACTER*10 NUMBER, FILE
    DATA A, ESC, CSI /'*', 27, 155 /
    DATA B, C, H /'[', ';', 'f'/
    DATA NUMBER / '1234567890' /
    DATA CO, PI / ' ', 3.1415926 /
    EQUIVALENCE (NAME(1),B)
    EQUIVALENCE (NAME(2),NUMX1)
    EQUIVALENCE (NAME(3),NUMX0)
    EQUIVALENCE (NAME(4),C)
    EQUIVALENCE (NAME(5),NUMY1)
    EQUIVALENCE (NAME(6),NUMY0)
    EQUIVALENCE (NAME(7),H)
1    DO 5 I=1,1000
        X(I)=0.0
        Y(I)=0.0
5    CONTINUE
    DAVSUM = 0.0
    DSSUM = 0.0
    DVSUM = 0.0
    DWSUM = 0.0
    SUMN = 0.0
    SUM = 0.0

```



```

        WEIGHT = 0.0
        COUNT  = 0.0
        DO 6 I=1,70
            X1(I)=0.0
            Y1(I)=0.0
6        CONTINUE
C
C...    INPUT DATA FILE NAME.
C
        WRITE(7,10)
10       FORMAT(1X,'INPUT DATA FILE ==> ', $)
        READ(5,20,ERR=200)FILE
20       FORMAT(A10)
        OPEN(UNIT=2,NAME=FILE,STATUS='OLD')
        DO 30 I=1,1000
            READ(2,*,END=40) X(I),Y(I)
30       CONTINUE
40       INDEX = I-1
            IF(INDEX.EQ.68) GO TO 94
            YMAX = -1.0E+30
            XMIN = 1.0E+30
            XMAX = -1.0E+30
            DO 50 K=1,INDEX
                XMIN = AMIN1(XMIN,Y(K))
50         XMAX = AMAX1(XMAX,Y(K))
            XCEN = (XMIN+XMAX)/2.0
            XSCALE = (XMAX-XMIN)/67.0
            DO 60 J=1,67
                X1(J)=XMIN+XSCALE*FLOAT(J)
60       CONTINUE
            DO 90 L=1,INDEX
                DO 70 M=1,67
                    IF(Y(L).GT.X1(M)) GO TO 70
                GO TO 80
70       CONTINUE
            M=68
80       Y1(M)=Y1(M)+1.0
90       CONTINUE
C
C...    STATISTICAL MEAN DIAMETERS DETERMINED
C
        DO 93 I=1,67
            IF(I.EQ.1) GRPAVG = X1(I)/2.0
            IF(I.NE.1) GRPAVG = (X1(I)+X1(I-1))/2.0
            DIAMAX = YMAX
            DAVSUM = DAVSUM + Y1(I)*GRPAVG

```

```

DSSUM = DSSUM + Y1(I)*GRPAVG**2
DVSUM = DVSUM + Y1(I)*GRPAVG**3
DWSUM = DWSUM + Y1(I)*GRPAVG**4
SUMN  = SUMN  + Y1(I)
SUM   = SUM   + Y1(I)
WEIGHT = WEIGHT + (4./3.*PI*(GRPAVG/2.))**3)*Y1(I)
93  CONTINUE
    DAV = DAVSUM/SUMN
    DS  = SQRT(DSSUM/SUM)
    DV  = (DVSUM/SUMN)**(1./3.)
    DVS = DVSUM/DSSUM
    DW  = DWSUM/DVSUM
    NSUM = IFIX(SUM)
    GOTO 97
94  REWIND (2)
    READ(2,*) GCD,DAV,DS,DV,DVS,DW
    DO 95 K=1,67
    X1(K) = X(K+1)
    Y1(K) = Y(K+1)
95  CONTINUE
    XMAX = X1(67)
    XMIN = X1(1)-(X1(67)-X1(66))
    XCEN = (XMIN+XMAX)/2.0
    XQUA = (XCEN-XMIN)/2.0
    X14  = XMIN + XQUA
    X34  = XCEN + XQUA
    COUNT=0.0
97  DO 100 K=1,67
    COUNT=COUNT + Y1(K)
    YMAX = AMAX1(YMAX,Y1(K))
100 CONTINUE
    NSUM = IFIX(COUNT)
    YSCALE = YMAX/21.0
    YSCAL1 = YMAX/199.0
    IYMAX = IFIX(YMAX)
    IYCEN = IFIX(.50*YMAX)
    IY14  = IYCEN/2
    IY34  = IYCEN + IY14
C
C... UTILIZING THE PSEUDO-GRAPHIC CAPABILITIES OF
C... DEC COMPATIBLE TERMINALS: INITIATE GRID.
C
    CALL CHARGR
    WRITE(7,105) ESC, ESC
105  FORMAT('+',A1,'*0',A1,'n')
    WRITE(7,110) ESC, ESC, ESC, ESC

```

```

110    FORMAT(1X,A1,'[H',A1,'[2J',A1,'[?3h',A1,'[?251')
      WRITE(7,115) CO(1:1),IYMAX
115    FORMAT('+',1X,A1,2X,I4,2X,'w',16('q'),'w',16('q'),'w',
      & 16('q'),'w',16('q'),'k')
117    FORMAT(2X,A1,2X,I4,2X,'n',16('q'),'n',16('q'),'n',      &
16('q'),'n',16('q'),'u')
120    FORMAT(2X,A1,8X,'n',16('q'),'n',16('q'),'n',
      & 16('q'),'n',16('q'),'u')
      DO 130 M=1,19
      M1=M
      IF(M.EQ. 5)WRITE(7,117) CO(M1:M1), IY34
      IF(M.EQ. 5) GOTO 130
      IF(M.GT. 5) GOTO 122
      GOTO 128
122    IF(M.EQ.10)WRITE(7,117) CO(M1:M1), IYCEN
      IF(M.EQ.10) GOTO 130
      IF(M.GT.10) GOTO 124
      GOTO 128
124    M1=1
      IF(M.EQ.15)WRITE(7,117) CO(M1:M1), IY14
      IF(M.EQ.15) GOTO 130
128    WRITE(7,140) CO(M1:M1)
130    CONTINUE
140    FORMAT(2X,A1,8X,'x',16X,'x',16X,'x',
      & 16X,'x',16X,'x')
      WRITE(7,120) CO(1:1)
      WRITE(7,145) ESC, ESC, ESC
145    FORMAT('+',A1,'*B',A1,'n',A1,'[Om')
      WRITE(7,146) XMIN, X14, XCEN, X34, XMAX
146    FORMAT(8X,F5.1,12X,F5.1,12X,F5.1,12X,F5.1,12X,F5.1,
      & //37X,'DIAMETER [microns]')
      WRITE(7,161) ESC, ESC
      WRITE(7,147) ESC, ESC, ESC, ESC, ESC, ESC
147    FORMAT('+',A1,'[7;2f 5',
      & A1,'[8;2f 6',
      & A1,'[9;2f 7',
      & A1,'[10;2f 8',
      & A1,'[11;2f 9',
      & A1,'[12;2f :')
161    FORMAT('+',A1,'* @',A1,'n')
      DO 168 J = 12,78
      J1 = J/10
      J0 = J - J1*10
      IF(J.LT.10)J1=10
      IF(J0.EQ.0)J0=10
      NUMYO = NUMBER(J0:J0)

```

```

        NUMY1 = NUMBER(J1:J1)
C
C... HISTOGRAM SCREEN PLOT
C
        J2 = J-11
        IF(Y1(J2).LE.0.0) GOTO 168
        NN2 = 4
        NN1 = IFIX(Y1(J2)/YSCAL1)
        I1 = 2
        IO = 1
        NUMX0 = NUMBER(IO:IO)
        NUMX1 = NUMBER(I1:I1)
        IF(NN1.GT.4) GOTO 162
        IF(NN1.EQ.1) WRITE(7,163) ESC, (NAME(K),K=1,7)
        IF(NN1.EQ.2) WRITE(7,164) ESC, (NAME(K),K=1,7)
        IF(NN1.EQ.3) WRITE(7,165) ESC, (NAME(K),K=1,7)
        GOTO 168
162  WRITE(7,166) ESC, (NAME(K),K=1,7)
163  FORMAT('+',A1,7A1,'1')
164  FORMAT('+',A1,7A1,'2')
165  FORMAT('+',A1,7A1,'3')
166  FORMAT('+',A1,7A1,'4')
        DO 167 I = 20,1,-1
        NN2 = NN2 + 10
        IF(NN2.GT.NN1) GOTO 250
        I1 = I/10
        IO = I - I1*10
        IF(I.LT.10)I1=10
        IF(IO.EQ.0)IO=10
        NUMX0 = NUMBER(IO:IO)
        NUMX1 = NUMBER(I1:I1)
        WRITE(7,169) ESC, (NAME(K),K=1,7)
167  CONTINUE
250  NN2 = NN2 - 10
        NN2 = NN1 - NN2
        I1 = I/10
        IO = I - I1*10
        IF(I.LT.10)I1=10
        IF(IO.EQ.0)IO=10
        NUMX0 = NUMBER(IO:IO)
        NUMX1 = NUMBER(I1:I1)
        IF(NN2.EQ.1) WRITE(7,301) ESC, (NAME(K),K=1,7)
        IF(NN2.EQ.2) WRITE(7,302) ESC, (NAME(K),K=1,7)
        IF(NN2.EQ.3) WRITE(7,303) ESC, (NAME(K),K=1,7)
        IF(NN2.EQ.4) WRITE(7,304) ESC, (NAME(K),K=1,7)
        IF(NN2.EQ.5) WRITE(7,305) ESC, (NAME(K),K=1,7)

```

```

      IF(NN2.EQ.6)    WRITE(7,306) ESC, (NAME(K),K=1,7)
      IF(NN2.EQ.7)    WRITE(7,307) ESC, (NAME(K),K=1,7)
      IF(NN2.EQ.8)    WRITE(7,308) ESC, (NAME(K),K=1,7)
      IF(NN2.EQ.9)    WRITE(7,309) ESC, (NAME(K),K=1,7)
168    CONTINUE
301    FORMAT('+',A1,7A1,'A')
302    FORMAT('+',A1,7A1,'B')
303    FORMAT('+',A1,7A1,'C')
304    FORMAT('+',A1,7A1,'D')
305    FORMAT('+',A1,7A1,'E')
306    FORMAT('+',A1,7A1,'F')
307    FORMAT('+',A1,7A1,'G')
308    FORMAT('+',A1,7A1,'H')
309    FORMAT('+',A1,7A1,'I')
169    FORMAT('+',A1,7A1,'J')
C
C...  OUTPUT MEAN DIAMETERS TO SCREEN
C
      WRITE(7,145) ESC, ESC, ESC
      CALL DATE(DAY)
      CALL TIME(TIM)
      WRITE(7,170) ESC
170    FORMAT('+',A1,'[3;85f','Spatial Distribution .....
      WRITE(7,171) ESC, GCD
171    FORMAT('+',A1,'[5;85f','Most Probable Dia.
      WRITE(7,172) ESC, DAV
      =',F7.1)
172    FORMAT('+',A1,'[6;85f','Arithmetic Mean Dia. (D10)
      WRITE(7,173) ESC, DS
      =',F7.1)
173    FORMAT('+',A1,'[7;85f','Surface Mean Dia. (D20)
      WRITE(7,174) ESC, DV
      =',F7.1)
174    FORMAT('+',A1,'[8;85f','Volume (Mass) Mean Dia. (D30)
      WRITE(7,175) ESC, DVS
      =',F7.1)
175    FORMAT('+',A1,'[9;85f','Sauter Mean Dia. (D32)
      WRITE(7,176) ESC, NSUM
      =',F7.1)
176    FORMAT('+',A1,'[11;85f','Total Count
      WRITE(7,177) ESC, FILE
      =',I7)
177    FORMAT('+',A1,'[16;85f','File: ',A10)
      WRITE(7,178) ESC, DAY
178    FORMAT('+',A1,'[17;85f','Date: ',9A1)
      WRITE(7,179) ESC, TIM
179    FORMAT('+',A1,'[18;85f','Time: ',9A1)
      READ(7,198) JUNK
198    FORMAT(A1)
      WRITE(7,199) ESC, ESC, ESC, ESC, ESC
199    FORMAT(1X,A1,'[0m',A1,'[H',A1,'[?3l',A1,'[2J',A1,'[?25h')
      CLOSE(2)

```

```

        CALL SETCMD('RUN GRAPH')
        CALL EXIT
200      STOP
        END

C
C...  SUBROUTINE UTILIZED TO SET-UP HISTOGRAM SYMBOLS
C
        SUBROUTINE CHARGR
        BYTE ESC
        DATA ESC / 27 /
        WRITE(7,147) ESC, ESC
147      FORMAT('+',A1,'PO;33;1;0;0;0{ @???????/GGGGGGG',A1,'\')
        WRITE(7,148) ESC, ESC
148      FORMAT('+',A1,'PO;34;1;0;0;0{ @???????/KKKKKKK',A1,'\')
        WRITE(7,149) ESC, ESC
149      FORMAT('+',A1,'PO;35;1;0;0;0{ @???????/MMMMMMM',A1,'\')
        WRITE(7,150) ESC, ESC
150      FORMAT('+',A1,'PO;36;1;0;0;0{ @???????/NNNNNNN',A1,'\')
        WRITE(7,151) ESC, ESC
151      FORMAT('+',A1,'PO;37;1;0;0;0{ @_____/NNNNNNN',A1,'\')
        WRITE(7,152) ESC, ESC
152      FORMAT('+',A1,'PO;38;1;0;0;0{ @oooooooo/NNNNNNN',A1,'\')
        WRITE(7,153) ESC, ESC
153      FORMAT('+',A1,'PO;39;1;0;0;0{ @wwwwwww/NNNNNNN',A1,'\')
        WRITE(7,154) ESC, ESC
154      FORMAT('+',A1,'PO;40;1;0;0;0{ @{{{{{{{{/NNNNNNN',A1,'\')
        WRITE(7,155) ESC, ESC
155      FORMAT('+',A1,'PO;41;1;0;0;0{ @}}}}}}}/NNNNNNN',A1,'\')
        WRITE(7,156) ESC, ESC
156      FORMAT('+',A1,'PO;42;1;0;0;0{ @~~~~~/NNNNNNN',A1,'\')
        WRITE(7,157) ESC, ESC
157      FORMAT('+',A1,'PO;17;1;0;0;0{ @wwwwwww/???????'',A1,'\')
        WRITE(7,158) ESC, ESC
158      FORMAT('+',A1,'PO;18;1;0;0;0{ @[[[[[[[/???????'',A1,'\')
        WRITE(7,159) ESC, ESC
159      FORMAT('+',A1,'PO;19;1;0;0;0{ @]]]]]]]/???????'',A1,'\')
        WRITE(7,160) ESC, ESC
160      FORMAT('+',A1,'PO;20;1;0;0;0{ @~~~~~/???????'',A1,'\')
        WRITE(7,161) ESC, ESC
161      FORMAT('+',A1,'PO;21;1;0;0;0{ @NOOM@]/???????'',A1,'\')
        WRITE(7,162) ESC, ESC
162      FORMAT('+',A1,'PO;22;1;0;0;0{ @~CCCCC/???????'',A1,'\')
        WRITE(7,163) ESC, ESC
163      FORMAT('+',A1,'PO;23;1;0;0;0{ @PXTTTRP/???????'',A1,'\')
        WRITE(7,164) ESC, ESC
164      FORMAT('+',A1,'PO;24;1;0;0;0{ @PPPPPPM/???????'',A1,'\')

```

```
WRITE(7,165) ESC, ESC
165   FORMAT('+',A1,'P0;25;1;0;0;0{ 0MPPPPPM/???????'',A1,'\')
WRITE(7,166) ESC, ESC
166   FORMAT('+',A1,'P0;26;1;0;0;0{ 0MP000PM/???????'',A1,'\')
CALL EXIT
STOP
END
```

Section 10

APPENDIX C.3: MOD-1 Nozzle Input Pressure Determination

```
C
      SUBROUTINE PRESSURE(NCHCK)
C+++++
+++++ C
C      SUBROUTINE TO DETERMINE WATER AND AIR PRESSURE FROM C
      THE OMEGA TRANSDUCERS USING THE AXV11-C A-D BOARD. C
C+++++
+++++ LOGICAL*1 IKEY
      BYTE ESC
      DATA ESC / 27 /
      CALL IPOKE("44","10000.0R.IPEEK("44))
C
C...   THE FOLLOWING ARE THE APPROPRIATE OCTAL VALUES TO
C...   BE STORED IN THE CSRs OF CH. 1 & 2 TO START AN
C...   A TO D CONVERSION OF THE PRESSURE TRANSDUCERS.
C
      ISTRT1 = "415
      ISTRT2 = "1015
C
      IF(NCHCK.EQ.1) GOTO 12
      WRITE(7,10) ESC, ESC, ESC
10     FORMAT('+',A1,'[2J',A1,'[?251',A1,'[H')
      WRITE(7,11) ESC
11     FORMAT(1X,A1,'#6', ' PRESS "C" to continue')
C
C...   17770400 IS THE CSR (CONTROL STATUS REGISTER) FOR CH. 1
C
12     CALL IPOKE("17770400,ISTRT1)
13     ICHK = IPEEK("17770400)
      IF(ICHK.NE."614) GOTO 13
C
C...   17770402 IS THE DBR (DATA BUFFER REGISTER) FOR CH. 1
C...   AND IPW IS THE WATER PRESSURE (DIGITAL VOLTS).
C
      IPW = IPEEK("17770402)
```



```

CALL IPOKE("17770400,ISTRT2)
14  ICHK = IPEEK("17770400)
    IF(ICHK.NE."1214) GOTO 14
    IPA = IPEEK("17770402)
    IPA = -1.189 + 0.4598*IPA
    IPW = -1.95 + 0.4598*IPW

C
C... OUTPUT PRESSURE VALUES TO TERMINAL SCREEN
C
    WRITE(7,18) ESC, ESC, IPW, IPA
    WRITE(7,19) ESC, ESC, IPW, IPA
    IF(NCHCK.EQ.1) GOTO 25
    IKEY = ITTINR()
    IF(IKEY.EQ.'C') GOTO 20
    GOTO 12
18  FORMAT('+',A1,'[22;1f',A1,'#3','WATER PRESSURE = ',
& I3,' AIR PRESSURE = ',I3)
19  FORMAT('+',A1,'[23;1f',A1,'#4','WATER PRESSURE = ',
& I3,' AIR PRESSURE = ',I3)
20  CALL IPOKE("44,"167777.AND.IPEEK("44))
    WRITE(7,21) ESC,ESC
21  FORMAT('+',A1,'[H',A1,'[2J')
25  RETURN
    END

```

Section 11

APPENDIX C.4: PSP Magnification Correction Factor Determination

```

C
C+++++-----
C***** C
C      FUNCTIONS TO DETERMINE CORRECTION FACTORS FOR
C      MICRON TO PIXEL FACTORS WHICH DEPEND ON X AND Y.
C
C+++++-----
C*****      FUNCTION      XFACT(MAG,XPOS,YPOS)
C              IF(MAG.EQ.500) GOTO 100
C
C...      HIGH MAGNIFICATION X-CORRECTION
C
C              IF(XPOS.LE.100.0) XFACT=0.977+YPOS*8.09E-05
C              IF(XPOS.GT.100.0.AND.XPOS.LE.150.0)
XFACT=0.974+YPOS*2.60E-05
C              IF(XPOS.GT.150.0.AND.XPOS.LE.200.0) XFACT=0.967-YPOS*8.12E-07
C              IF(XPOS.GT.200.0.AND.XPOS.LE.250.0) XFACT=0.961+YPOS*4.73E-06
C              IF(XPOS.GT.250.0.AND.XPOS.LE.300.0) XFACT=0.961-
YPOS*5.46E-05      IF(XPOS.GT.300.0.AND.XPOS.LE.350.0)
XFACT=0.948-YPOS*3.72E-05
C              IF(XPOS.GT.350.0.AND.XPOS.LE.400.0) XFACT=0.943-YPOS*6.80E-05
C              IF(XPOS.GT.400.0) XFACT=0.920-YPOS*2.58E-05
C              RETURN
100      IF(XPOS.LE.100.0) XFACT=2.21+YPOS*0.290E-04
C
C...      LOW MAGNIFICATION X-CORRECTION
C
C              IF(XPOS.GT.100.0.AND.XPOS.LE.150.0)
XFACT=2.22+YPOS*0.803E-04
C              IF(XPOS.GT.150.0.AND.XPOS.LE.200.0) XFACT=2.16+YPOS*0.679E-04
C              IF(XPOS.GT.200.0.AND.XPOS.LE.250.0) XFACT=2.16+YPOS*0.442E-07
C              IF(XPOS.GT.250.0.AND.XPOS.LE.300.0) XFACT=2.16-
YPOS*0.947E-04      IF(XPOS.GT.300.0.AND.XPOS.LE.350.0)
XFACT=2.11-YPOS*0.306E-07
C              IF(XPOS.GT.350.0.AND.XPOS.LE.400.0) XFACT=2.10-YPOS*0.124E-03

```

```

      IF(XPOS.GT.400.0) XFACT=2.07-YPOS*0.135E-03
      RETURN
      END

C
      FUNCTION YFACT(MAG,XPOS,YPOS)
      IF(MAG.EQ.500) GOTO 100

C
C... HIGH MAGNIFICATION Y-CORRECTION
C
      IF(XPOS.LE.100.0) YFACT=0.977-YPOS*9.17E-05
      IF(XPOS.GT.100.0.AND.XPOS.LE.150.0) YFACT=0.981-
YPOS*1.24E-04      IF(XPOS.GT.150.0.AND.XPOS.LE.200.0)
YFACT=0.981-YPOS*1.19E-04
      IF(XPOS.GT.200.0.AND.XPOS.LE.250.0) YFACT=0.990-YPOS*1.63E-04
      IF(XPOS.GT.250.0.AND.XPOS.LE.300.0) YFACT=1.000-YPOS*1.96E-04
      IF(XPOS.GT.300.0.AND.XPOS.LE.350.0) YFACT=1.014-
YPOS*2.19E-04      IF(XPOS.GT.350.0.AND.XPOS.LE.400.0)
YFACT=1.027-YPOS*2.63E-04      IF(XPOS.GT.400.0) YFACT=1.029-
YPOS*2.69E-04
      RETURN

100      IF(XPOS.LE.100.0) YFACT=2.10-YPOS*0.183E-03
C
C... LOW MAGNIFICATION Y-CORRECTION
C
      IF(XPOS.GT.100.0.AND.XPOS.LE.150.0) YFACT=2.15-
YPOS*0.268E-03      IF(XPOS.GT.150.0.AND.XPOS.LE.200.0)
YFACT=2.12-YPOS*0.315E-03
      IF(XPOS.GT.200.0.AND.XPOS.LE.250.0) YFACT=2.13-YPOS*0.313E-03
      IF(XPOS.GT.250.0.AND.XPOS.LE.300.0) YFACT=2.15-YPOS*0.397E-03
      IF(XPOS.GT.300.0.AND.XPOS.LE.350.0) YFACT=2.18-
YPOS*0.484E-03      IF(XPOS.GT.350.0.AND.XPOS.LE.400.0)
YFACT=2.19-YPOS*0.505E-03      IF(XPOS.GT.400.0) YFACT=2.18-
YPOS*0.509E-03
      RETURN
      END

```

APPENDIX D: Mean Diameter Calculations

Arithmetic Mean Diameter (AMD)

$$D(10) = \frac{\sum_{i=1}^N n_i d_i}{\sum_{i=1}^N n_i}$$

Area Mean Diameter (ArMD)

$$D(20) = \sqrt{\frac{\sum_{i=1}^N n_i d_i^2}{\sum_{i=1}^N n_i}} \quad (12.1)$$

Volume Mean Diameter (VMD)

$$D(30) = \sqrt[3]{\frac{\sum_{i=1}^N n_i d_i^3}{\sum_{i=1}^N n_i}} \quad (12.2)$$

Sauter Mean Diameter (SMD)

$$D(32) = \frac{\sum_{i=1}^N n_i d_i^3}{\sum_{i=1}^N n_i d_i^2} \quad (12.3)$$

where

N = total number of bins

n_i = counts per bin

d_i = diameter for size class i

Section 13

APPENDIX E: Cole-Palmer Flowmeter Calibration Data

Scale Reading	Flow-rate (gpm) ¹
30	0.022
40	0.031
50	0.040
60	0.050
70	0.059
80	0.069
90	0.078
100	0.090
110	0.100
120	0.110
130	0.120
140	0.130

*Calibration values were verified by replication.

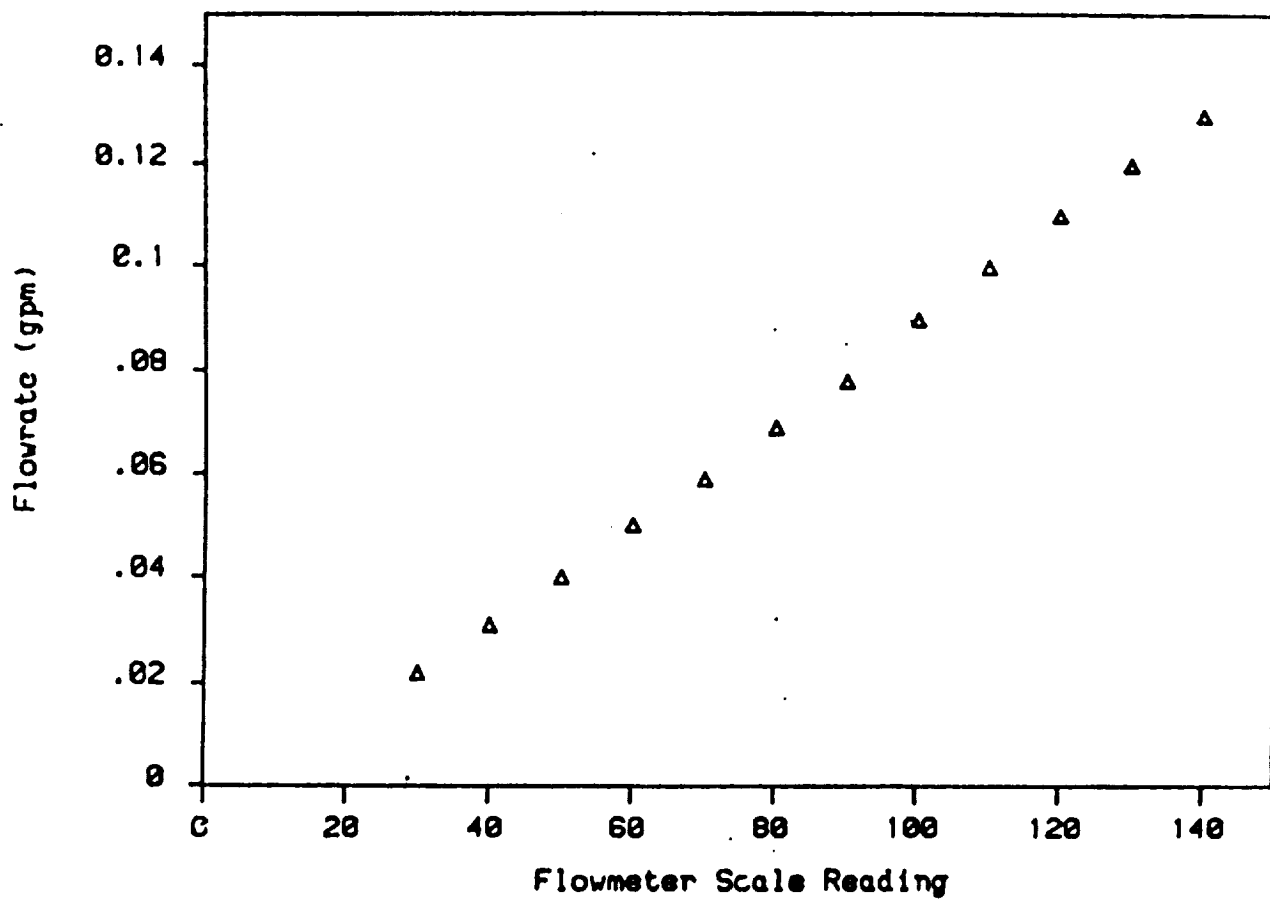


Figure 13.1: Cole-Palmer Flowmeter Calibration

Section 14

APPENDIX F: OMEGA Pressure Transducer Calibration Data

Table 14.1: S/N: 850502

Standard Pressure Corrected to psia	Output Voltage (millivolts)
0	9.20
10	15.00
20	21.70
30	28.30
40	34.80
50	41.45
60	47.95
70	55.20
80	61.70
90	68.60
100	75.20
110	80.70

Table 14.2: OMEGA S/N: 850311

Standard Pressure Corrected to psia	Output Voltage (millivolts)
0	9.80
10	16.00
20	22.90
30	29.10
40	35.75
50	42.60
60	49.10
70	56.20
80	62.60
90	69.40
100	75.80
110	81.50

*Calibration values were verified by replication.

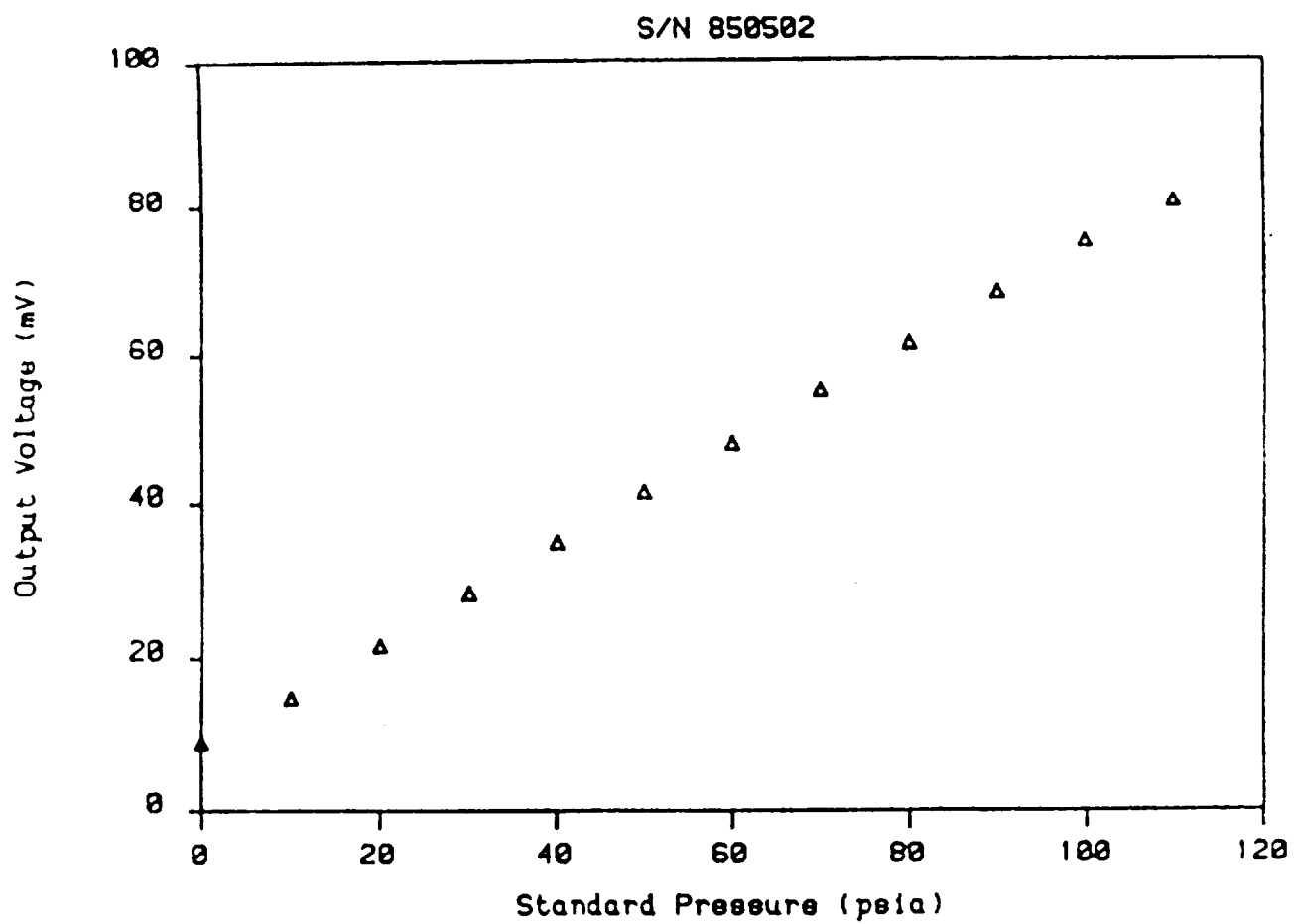


Figure 14.1: OMEGA Pressure Transducer Calibration

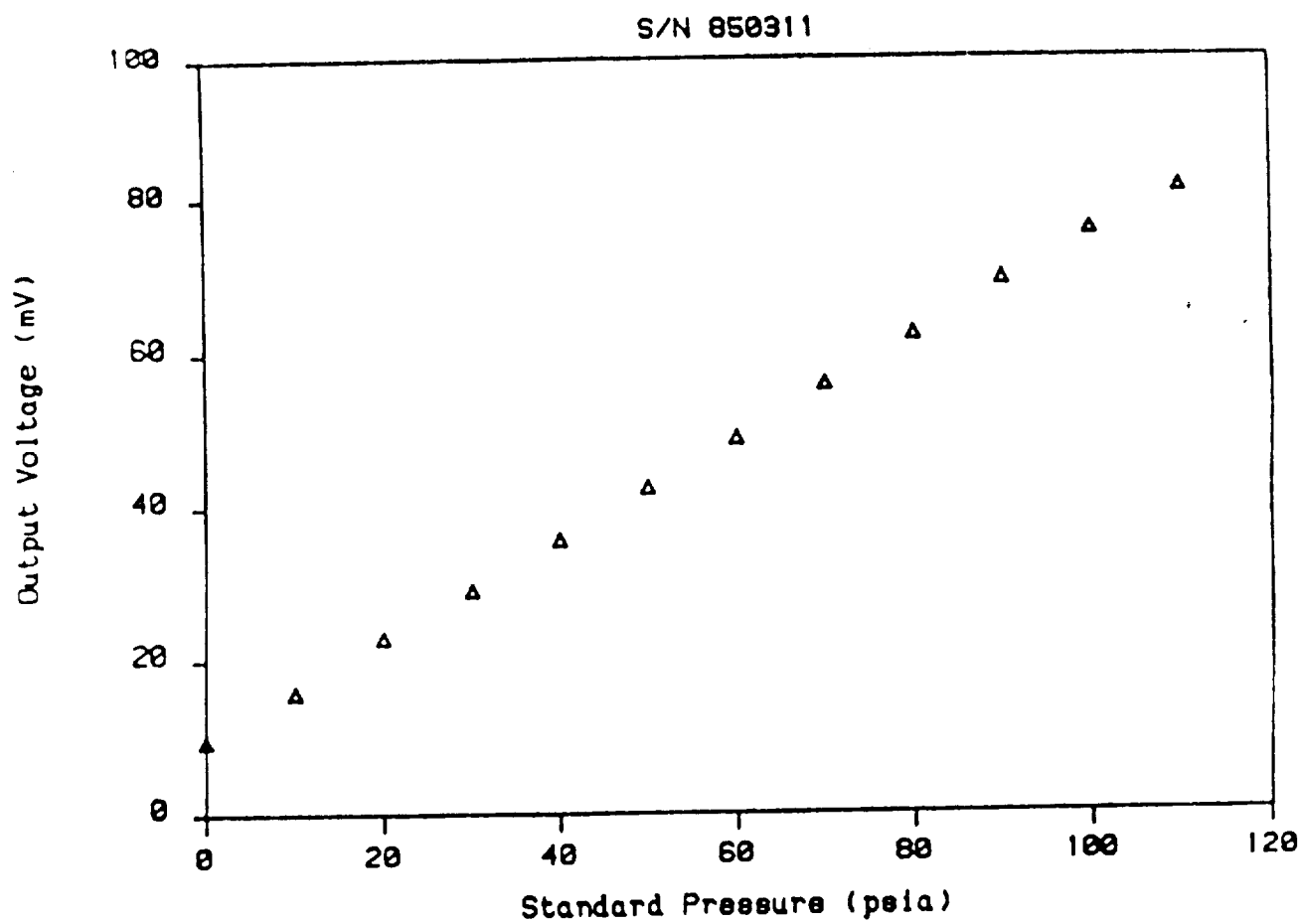


Figure 14.2: OMEGA Pressure Transducer Calibration

Report Documentation Page

1. Report No. NASA CR-185239		2. Government Accession No.		3. Recipient's Catalog No.	
4. Title and Subtitle Comparison of UNL Laser Imaging and Sizing System and a Phase Doppler System for Analyzing Sprays From a NASA Nozzle				5. Report Date March 1990	
				6. Performing Organization Code	
7. Author(s) Dennis R. Alexander				8. Performing Organization Report No. None	
				10. Work Unit No. 505-68-11	
9. Performing Organization Name and Address University of Nebraska-Lincoln Lincoln, Nebraska 68588-0525				11. Contract or Grant No. NAG3-634	
				13. Type of Report and Period Covered Contractor Report Final	
12. Sponsoring Agency Name and Address National Aeronautics and Space Administration Lewis Research Center Cleveland, Ohio 44135-3191				14. Sponsoring Agency Code	
15. Supplementary Notes Project Manager, John R. Oldenburg, Propulsion Systems Division, NASA Lewis Research Center.					
16. Abstract Research was conducted on aerosol spray characterization using a P/DPA and a laser imaging/video processing system on a NASA MOD-1 air-assist nozzle being evaluated for use in aircraft icing research. Benchmark tests were performed on monodispersed particles and on the NASA MOD-1 nozzle under identical laboratory operating conditions. The laser imaging/video processing system and the P/DPA showed agreement on a calibration tests in monodispersed aerosol sprays of $\pm 2.6 \mu\text{m}$ with a standard deviation of $\pm 2.6 \mu\text{m}$. Benchmark tests were performed on the NASA MOD-1 nozzle on the centerline and radially at 0.5-inch increments to the outer edge of the spray plume at a distance 2 feet (0.61 m) downstream from the exit of the nozzle. Comparative results at two operating conditions of the nozzle are presented for the two instruments. For the first case studied, the deviation in arithmetic mean diameters determined by the two instruments was in a range of 0.1 to 2.8 μm , and the deviation in Sauter mean diameters varied from 0 to 2.2 μm . Operating conditions in the second case were more severe which resulted in the arithmetic mean diameter deviating from 1.4 to 7.1 μm and the deviation in the Sauter mean diameters ranging from 0.4 to 6.7 μm .					
17. Key Words (Suggested by Author(s)) Particle sizing; Droplet sizing; Spray characterization; Laser imaging; Aerosol sizing instrumentation; Instrument comparison				18. Distribution Statement Unclassified—Unlimited Subject Category 35	
19. Security Classif. (of this report) Unclassified		20. Security Classif. (of this page) Unclassified		21. No. of pages 135	
				22. Price* A07	

National Aeronautics and
Space Administration

Lewis Research Center
Cleveland, Ohio 44135

Official Business
Penalty for Private Use \$300

FOURTH CLASS MAIL

ADDRESS CORRECTION REQUESTED



Postage and Fees Paid
National Aeronautics and
Space Administration
NASA-451

NASA
